The evolution of the Greenland Ice Sheet from the Last Glacial Maximum to present-day: An assessment using glaciological and Glacial Isostatic Adjustment modelling

SIMPSON, MATTHEW,JAMES,ROSS

The evolution of the Greenland Ice Sheet from the Last Glacial Maximum to present-day: An assessment using glaciological and Glacial Isostatic Adjustment modelling.

By Matthew James Ross Simpson

Submitted for the award of Doctor of Philosophy

Durham University

2009

Declaration

No part of this thesis has previously been submitted for a degree at this or any other university. The work described in this thesis is entirely that of the author, except where reference is made to previously published or unpublished work.

Matthew Simpson

Department of Earth Sciences,

Durham University,

Science Labs,

Durham,

DH1 3LE

22nd September 2009

Acknowledgements

First and foremost I would like to thank my supervisor Glenn Milne for guiding me over the course of my PhD and the writing of this thesis. Glenn, you have taught me to have an ever meticulous approach to my research and you have always been available to discuss the science (albeit the often long distances between us!). I wish you, Sylvie and the children well and look forward to our future work together. Secondly, I thank my supervisor Antony Long, you made time for me despite an often busy schedule and your infectious enthusiasm for the subject often spurs me on. I also thank Philippe Huybrechts for introducing me to the rigors of ice sheet modelling and for looking after me during my visits to Brussels. Others involved in the 'Greenland project' and help I am also grateful for are Sarah Woodroffe, Dave Roberts and, naturally, my fellow PhD accomplice Leanne. I am always glad of your company, be it in the office or on trips abroad. For help with computing I thank Jim, Sarah, Gary and Chris and also Pippa for getting me through the GPS work.

Of course, it is unlikely any of this would have happened without the support of my dear old Ma and Pa. I simply say thank you for giving me the foundations on which I could build. To all my friends outside of science, scattered as you are, thanks for reminding me there is an outside world (especially over the last few months). Lastly, Therese - I am so grateful for the wonderful life we have together and I hope I make you proud.

Abstract

In this thesis we constrain a three-dimensional thermomechanical model of Greenland ice sheet (GrIS) evolution from the Last Glacial Maximum (LGM, 21 ka BP) to the present-day using, primarily, observations of relative sea level (RSL) as well as field data on past ice extent. The new model (Huy2) fits a majority of the observations and is characterised by a number of key features: (i) the ice sheet had an excess volume (relative to present) of 4.1 m ice-equivalent sea level at the LGM, which increased to reach a maximum value of 4.6 m at 16.5 ka BP; (ii) retreat from the continental shelf was not continuous around the entire margin, as there was a Younger Dryas readvance in some areas. The final episode of marine retreat was rapid and relatively late (c. 12 ka BP), leaving the ice sheet land based by 10 ka BP; (iii) in response to the Holocene Thermal Maximum (HTM) the ice margin retreated behind its present-day position by up to 80 km in the southwest, 20 km in the south and 80 km in a small area of the northeast. As a result of this retreat the modelled ice sheet reaches a minimum extent between 5 and 4 ka BP, which corresponds to a deficit volume (relative to present) of 0.17 m ice-equivalent sea level. The results suggest that remaining discrepancies between the model and the observations are likely associated with non-Greenland ice load, differences between modelled and observed present-day ice elevation around the margin, lateral variations in Earth structure and/or the pattern of ice margin retreat.

Predictions of present-day vertical land motion generated using the new Huy2 model are highly sensitive to variations of upper mantle viscosity. Depending on the Earth model adopted, different periods of post-LGM ice loading change dominate the present-day response in particular regions of Greenland. These results will be a useful resource when interpreting existing and future observations of vertical land motion in Greenland. In comparison to the sparse number of GPS

observations available, predictions from the Huy2 model are in good agreement to the absolute measurements from south and southwest Greenland. This suggests that the response of the ice sheet to the HTM is reasonably well produced by the Huy2 model and, thus, corroborates our earlier findings. Uplift predictions generated using a surface mass balance reconstruction of the GrIS (Wake et al., 2009), which covers the period 1866-2005, show that decadal-scale ice mass variability over the last c. 140 years plays a small role in determining the present-day viscous response (it is as large as ±0.2 mm/yr). Results from the same reconstruction show that high rates of peripheral thinning in west and southwest Greenland from 1995 to 2005 (due to surface mass balance changes) generate elastic uplift rates over 6 mm/yr.

In the final part of the thesis, we examine how non-Greenland ice mass loss influenced vertical land motion and sea-level change around Greenland over the last deglaciation and consider the implications for GrIS evolution. Results from this analysis suggest non-Greenland solid Earth deformation had little impact on the evolution ice sheet. Sea-level change around Greenland which is driven by non-Greenland ice mass loss departs from the associated eustatic signal; largely because of the close proximity of the late North American ice sheets (NAIS). Non-Greenland RSL change is also spatially non-uniform and is characterised by a distinct east-west gradient. For example, we find that from 16 to 14 ka BP rates of sea-level rise remained relatively low in the west (0-2 m/ka), whereas, those in the east reach values between 6 and 8 m/ka (although these results are sensitive to the source of meltwater, in particular, the relative partitioning of meltwater pulse 1A (mwp-1A, 14.2 ka BP) between the North American and Antarctic ice sheets). If the marine breakup of the GrIS was forced by non-Greenland RSL change, then we would expect the retreat of the ice sheet to reflect the sea-level changes described. A preliminary modelling study suggests that, assuming a conventional ice sheet model calving treatment, a more realistic sea-level forcing results in a pattern of ice margin retreat which is at least partly due to spatial variations in non-Greenland RSL change.

Thus, the modelled marine retreat is generally earlier in east Greenland and later in the west than for when non-Greenland RSL change is not accounted for - this pattern of ice margin retreat is generally consistent with observations from the continental shelf.

Contents

List of Figures and Tables

Chapter 1:

Introduction.

1.1. Background

1.1.1. Quaternary glacial history: A brief overview

The onset of extensive glaciations in the Northern Hemisphere, including the inception of the Greenland ice sheet (GrIS), began around 3 million years ago (Maslin et al., 1998; Bartoli et al., 2005; Lunt et al., 2008). Since that time, Greenland has experienced large fluctuations in ice mass as the Earth has passed through successive glacial cycles. Glacial cycles can largely be explained using Milankovitch theory; this describes the orbital changes of the Earth and how they result in variations in solar forcing, which drives long-term climate change (e.g. see Berger and Loutre, 1991). Observations from deep-ocean cores (e.g. Hays et al., 1976) and, more recently, cores drilled in ice sheets (e.g. Dansgaard et al., 1993; Petit et al., 1999; Andersen et al., 2004) have shown that records of palaeoclimate are in good agreement with this theory, which has led to its wide acceptance.

Data derived from drilled ice cores, in particular, has been a very valuable source of information on Late Quaternary climate change. Ice cores contain a number of proxy data but it is the composition of air bubbles trapped within the ice (and the measurement of oxygen and hydrogen isotope values) that has provided some of most valuable palaeoclimate data. Cores drilled in Antarctica have provided the longest time series; Figure 1 shows a temperature reconstruction based on isotope

measurements from the Vostok ice core, which covers the last c. 420 ka. A stack of benthic $\delta^{18}O$ records from 57 globally distributed sites is also plotted for comparison (Lisiecki and Raymo, 2005). These data show that global climate change (and Late Quaternary glaciation) has been characterised by a 100 ka cycle. We can also see that climate (and ice volume) change follows a sawtooth wave pattern; during glacial-interglacial cycles the build up of ice volume is relatively gradual whilst deglaciation (sometimes called a glacial termination) occurs far more rapidly.

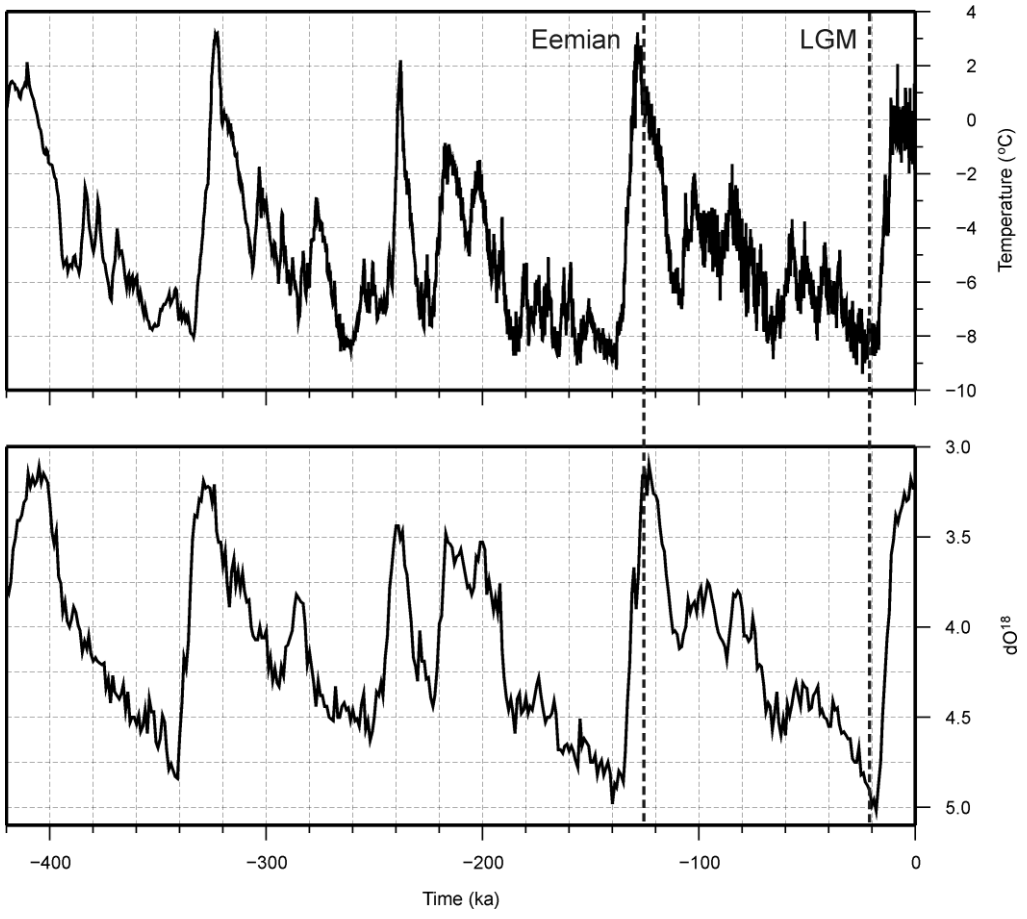

Fig. 1. Upper panel shows temperature reconstruction from the Vostok ice core drilled in Antarctica (Petit et al., 1999). Values shown are relative to modern mean temperatures. No correction for ice elevation changes was applied. Lower panel shows a stack of benthic $\delta^{18}O$ records from 57 globally distributed sites (Lisiecki and Raymo, 2005). Dashed lines mark the Eemian period (125 ka BP) and the Last Glacial Maximum (21 ka BP).

The last interglacial period, commonly referred to as the Eemian, is dated to around 125 ka BP. At this time global mean sea level was 4 to >6 m higher than today (e.g. Stirling et al., 1998) and the GrIS is thought to have been considerably smaller than it is at present (Cuffey and Marshall, 2000; Tarasov and Peltier, 2003). After the Eemian interglacial period, there was the onset of a new glacial cycle which culminated in the Last Glacial Maximum (LGM, 21 ka BP). At the LGM there was extensive glaciation and large parts of the northern hemisphere were ice covered. The GrIS is thought to have extended to cover parts of the continental shelf (Funder and Hansen, 1996) and reached an excess volume (compared to present) of 2-3 m ice-equivalent sea level (Clark and Mix, 2002).

The focus of this thesis is the behaviour of the GrIS from the LGM up until present-day. Since the LGM, the Earth has seen the decay of the great ice sheets covering North America and Eurasia, ice mass loss in Greenland and Antarctica and the reduction of mountain glaciers. Over this time, global mean sea level has risen c. 120 m (e.g. Fairbanks, 1989; Yokoyama et al., 2000). This large ice-ocean mass exchange together with rapid climate change in Greenland (e.g. Cuffey et al., 1995; Cuffey and Clow, 1997) has played a part in the evolution of the GrIS over this period. The last 10 ka (the Holocene) has been characterised by relatively stable climatic conditions which have continued up until present-day (see Fig. 1).

1.1.2. The Greenland ice sheet at present-day

At present, the GrIS covers an area of approximately 1.71 million km^2 and holds enough ice volume to raise mean global sea level by c. 7 m (Bamber et al., 2001). Accumulation largely occurs in the interior of the ice sheet where snowfall undergoes compaction and forms ice. The ice sheet flows outward from its central region through a combination of internal deformation and basal sliding,

mass is lost through surface melting and calving of icebergs. Generally speaking, the pattern of ice mass change shows that the GrIS is thickening or near balance in the interior (elevations above 2000 m) (e.g. Thomas et al., 2000, 2008) whilst on the flanks and at the margin of the ice sheet rapid mass loss has been observed. Indeed, recent mass balance estimates generally indicate an accelerated mass loss from Greenland over the last decade (Fig. 2) (Lemke et al., 2007).

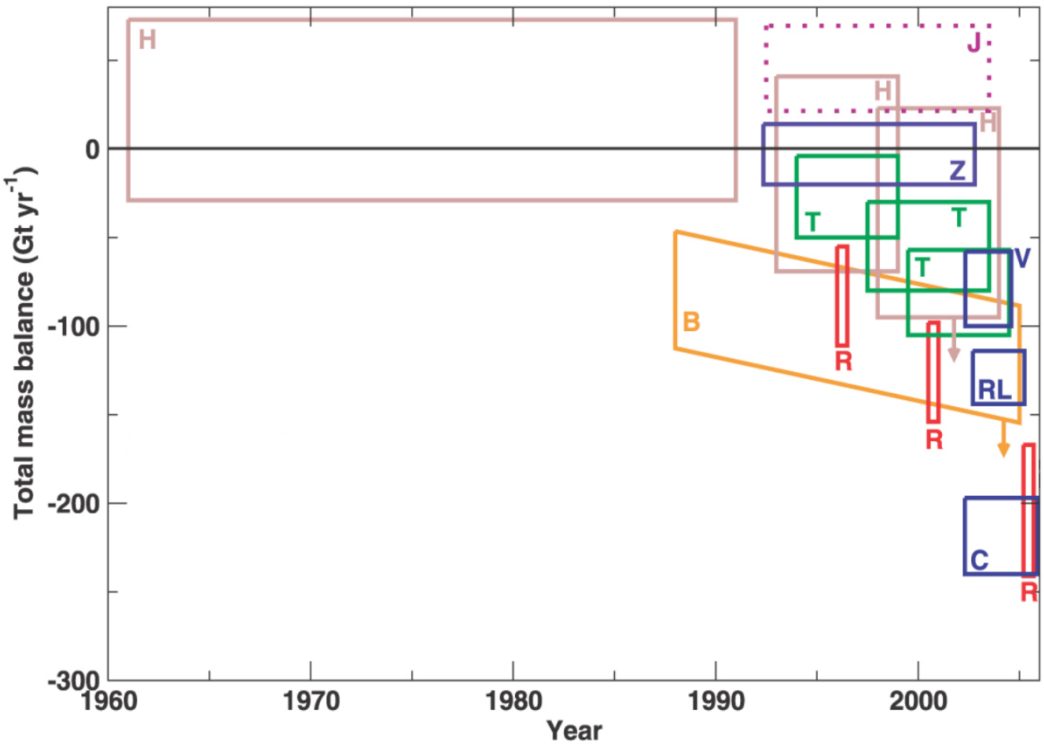

Fig. 2. Mass balance estimates for the GrIS – taken from Lemke et al. (2007). The coloured boxes indicate the time over which the observations were taken and the uncertainty in the mass balance measurement. Letters and colours correspond to the following publications: B Orange – Box et al., 2006, H brown – Hanna et al., 2005, T dark green – Thomas et al., 2006 and including new results and revisions of Krabill et al., 2004, Z violet – Zwally et al., 2005, R red – Rignot and Kanagaratnam, 2006, V blue – Velicogna and Wahr, 2005, RL blue – Ramillien et al., 2006, J magenta dashed – Johannessen et al., 2005. Arrows indicate additional mass loss from ice flow acceleration.

The latest work suggests it is variations in ice sheet flow that dominate the overall mass balance of the GrIS (Rignot et al., 2008). Across most of Greenland ice flow has been observed to have

accelerated over the last decade (Rignot and Kanagaratnam, 2006) and many of the ice sheet's major outlet glaciers are thinning and/or in retreat (e.g. Joughin et al., 2004, 2008; Krabill et al., 2004; Howat et al., 2005; Stearns and Hamilton, 2007). Investigations examining surface ice mass changes (snowfall minus meltwater runoff) have shown increased melting over the last few decades (Hanna et al., 2005, 2008; Box et al., 2006). The seasonal ablation area has also become more extensive over this time (Krabill et al., 2000; Abdalati and Steffen, 2001; Paterson and Reeh, 2001). Recently, attention has been focussed on meltwater that pools on the surface of the ice sheet. Observations have shown that in some circumstances this meltwater propagates to the ice-bedrock interface which has led to increased ice sheet flow (Zwally et al., 2002; Das et al., 2008). In summary, almost all investigations of the GrIS indicate that it is in a state of negative mass balance and in some areas (notably the southeast, e.g. Wouter et al. (2008)) very rapid mass loss has been observed. However, due to the short time span of these observations it remains contested if these changes are the beginning of a sustained response of the ice sheet to recent warming.

1.1.3. The Greenland ice sheet in the future?

Greenland will likely make a positive contribution to future sea-level rise because increased ablation will outweigh increases in accumulation as temperatures get higher (e.g. Van de Wal et al., 2001; Huybrechts et al., 2004). Ice sheet model predictions of the future evolution of the GrIS suggest that, depending on different greenhouse gas emission scenarios, it will contribute between 1 to 12 cm ice-equivalent sea-level by the end of the 21st century (Meehl et al., 2007). This is a relatively modest contribution to predicted global sea-level rise. Thermal expansion is predicted to dominate the sea-level budget over the next hundred years but contributions from ice sheets are expected to become increasingly important. However, it is important to note that future predictions are limited because the current generation of ice sheet models do not take into account processes driving the contemporary rapid changes observed at the ice margin (see above Sub-Section) (e.g. Alley et al.,

2005). Recent work has aimed to address this issue; Pfeffer et al. (2008) indicate that with high increases in ice sheet flow the GrIS could contribute as much as 54 cm to sea-level rise by 2100, a figure considerably higher than the estimates of Meehl et al. (2007). Long-term predictions suggest that for the ice sheet to be eliminated completely would require sustained warming in Greenland exceeding 4.5 ± 0.9 ^{o}C (relative to preindustrial temperatures) (Gregory and Huybrechts, 2006). Ridley et al. (2005) found that it would take around 3000 years for most of the ice sheet to disappear if carbon dioxide levels were increased to 4 times the preindustrial level (a high CO_2 climate) and held constant.

1.2. Aims and outline of this thesis

In this thesis I examine the evolution of the GrIS from the LGM up until present-day. To achieve this aim, use is made of glaciological and glacial isostatic adjustment (GIA) models. The output of these numerical models is constrained by and compared to a number of datasets and observations. A description of the methodology and models used is given below (see Section 1.4), modelling work features in all subsequent Chapters of the thesis. The data is introduced in the relevant chapters; the relative sea level (RSL) data and ice extent data at the beginning of Chapter 2 and GPS data at the start of Chapter 3.

The core of the work comprising this thesis is contained in Chapter 2; the aim of which is to calibrate a glaciological model of GrIS evolution since the LGM using inferences of RSL and past ice extent from field data. A key aspect of this work is a detailed modelling sensitivity analysis and the comparison of our results to other modelling studies and independent observations of the ice sheet's past behaviour. The reader should note that Chapter 2 is now published material (see Simpson et al., 2009) and that this work was conducted largely by the author of this thesis – co-

authors provided guidance and useful comments on the written manuscript before submission. Using the new ice model developed in Chapter 2, I then go on in Chapter 3 to generate predictions of present-day vertical land motion in Greenland. The main aim of this chapter is the examination of different aspects of the loading history (in both time and space) and how they contribute to the present-day pattern of uplift. The uplift predictions generated using the new ice model are also compared to some of the published GPS data. The results presented in Chapter 4 examine how non-Greenland (i.e. outside of Greenland) ice mass loss influenced vertical land motion and sea-level change around Greenland over the last deglaciation and consider the implications for GrIS evolution. In Chapter 5 I summarise the overall findings and discuss future work that would build upon the research presented in this thesis.

1.3. Applications of the research

There are three primary applications of the research presented in the following chapters:

(i) The development of a post-LGM model of GrIS evolution can provide important insights into how the ice sheet reacted to past sea-level and climate change - thus informing us how the ice sheet might behave in the future. In that regard, a particular focus of Chapter 2 is the reaction of the ice sheet to the peak warming period known as the Holocene Thermal Maximum (HTM), during which mid-Holocene temperatures were c. 2.5 ^{o}C higher than at present (Dahl Jensen et al., 1998). Climate model predictions suggest that global mean temperatures could well exceed such an increase by 2100 (see Meehl et al., 2007).

(ii) As stated above, one application of our model is to predict the pattern of present-day solid Earth deformation in Greenland (Chapter 3). Contemporary geodetic measurements require a correction for the ongoing vertical motion of the Earth which comes from GIA models (e.g. Velicogna and Wahr,

2005; Thomas et al., 2006; Zwally et al., 2005). Measurements of the Earth's gravity field are particularly sensitive to contamination by this solid surface signal due to the relatively high density of the Earth (c. 3300 kg/m^3) when compared to the overlying ice (c. 910 kg/m^3). Furthermore, predictions of present-day solid Earth deformation can also assist in the interpretation of GPS data (e.g. Khan et al., 2008) by providing information to aid in separating the signal due to past (viscous component) and present (elastic component) ice thickness changes. It is clear that a good understanding of past GrIS evolution is required if present-day observations are to be interpreted correctly.

(iii) Calibrating a model to field data will highlight any particular weaknesses in the ice and Earth model adopted and can therefore guide future research into model development. Some examples highlighted in this thesis are the inclusion of lateral structure in GIA Earth models and a more accurate treatment of sea-level change in modelling the retreat of marine-based ice.

1.4. Methodology

Three approaches can be employed to reconstruct the deglaciation history of ice sheets:

(1) Three-dimensional ice sheet models that are forced by prescribed climatic conditions and freely simulate past ice sheet evolution (e.g. Huybrechts, 1990, 2002; Letréguilly et al., 1991; Siegert et al., 2001; Charbit et al., 2002; Forsström and Greve, 2004; Zweck and Huybrechts, 2005). The workings of three-dimensional ice sheet models are briefly described in Sub-Section 1.4.1 (see below). These ice sheet models are typically forced in two ways; by time series of past climate change derived from ice cores (e.g. Dansgaard et al., 1993) and by records of past sea-level change. For sea level it is usual

that a record pertaining to eustatic changes is prescribed (e.g. see Fairbanks, 1989). The outputs of the model are the three-dimensional geometry of ice sheet and other physical characteristics (e.g. ice velocity and temperature) as a function of time.

(2) Observations of GIA-induced sea-level change in the near-field of past or presently glaciated regions that are used to quantitatively infer the loading history of grounded ice sheets (e.g. Tushingham and Peltier, 1991; Peltier, 1994; Lambeck et al., 2006). In the near-field RSL change is significantly influenced by isostatic adjustment (so reflects ice loading changes over time). The sea level and Earth model components of such GIA models are described below (see Sub-Section 1.4.1). Note that, in most cases, this method involves the application of ice models that contain little glaciology (i.e. no treatment of surface mass balance or ice flow; at best simplistic parabolic equations are used to determine the geometry of the past ice load). The resulting ice sheet reconstructions have also been used to study Earth structure and dynamics (e.g. Kaufmann and Lambeck, 2002).

(3) Directly constraining the lateral and/or height extent of past ice from field observations made on land and adjacent continental shelves (e.g. Dyke and Prest, 1987; Evans et al., 2002; Bentley et al., 2006). For example, glacial landforms (such as moraines) and stratigraphical data provide evidence of past ice sheet extent and flow. Other features, such as trimlines, mark the former altitude of the ice sheet surface and constrain ice height. If these geomorphological landforms can be dated then they give us a valuable understanding of past ice sheet evolution.

Previous studies have, in general, combined only two of these approaches; normally (1) and (3) (e.g. Marshall et al., 2002) or (2) and (3) (e.g. Tushingham and Peltier, 1991). The Greenland GrB model of Tarasov and Peltier (2002) first demonstrated that by adopting (1) a 3-D ice sheet model with (2) a GIA forward model is a powerful tool that reduces the uncertainty of past ice sheet evolution. In Chapter 2, we combine and apply all three methods (e.g. Tarasov and Peltier, 2004) to the Greenland ice sheet. Using, primarily, observations of relative sea level (RSL) complemented by geological and geomorphological data we constrain the millennial-scale spatial changes of a 3-D thermomechanical ice sheet model (Huybrechts, 2002) from the LGM to the present-day.

1.4.1. Description of the glacial isostatic adjustment model

The GIA forward model is comprised of an ice sheet model, a sea-level model and a model of Earth rheology. The first two model components define the ice-ocean mass exchange which represents the forcing, whilst the isostatic response is governed by the prescribed Earth structure and rheology. Each component is described, in turn, below.

We adopt the three-dimensional thermomechanical ice sheet model of Huybrechts (2002) as a starting Greenland ice load (hereafter referred to as 'Huy1'). The Huy1 model simulates the evolution of the Greenland ice sheet over the last two glacial cycles in response to changes in past climate and eustatic sea level. The model is comprised of three parts; calculating ice-dynamics, solid Earth (isostatic) response and surface mass balance (see Huybrechts and de Wolde (1999) for a full description). There are 31 layers in the vertical and a horizontal grid resolution of 20 km, which corresponds to 83 × 141 horizontal grid cells for Greenland. Ice-dynamics are simplified to the shallow ice approximation for large ice masses (Hutter, 1983). Grounded ice flows through internal deformation and basal sliding. Longitudinal stress is ignored and grounding-line dynamics are not

modelled. The Earth model of Huy1 should not be confused with the one employed in this thesis; Huy1 has an asthenosphere with a single relaxation time (3000 years) overlain by an elastic lithosphere. Overall mass balance is considered as the net contribution of the input (snowfall accumulation) and outputs (meltwater runoff and calved ice) to the ice sheet system. Meltwater runoff is calculated using the positive degree day method (e.g. Braithwaite, 1995) which takes the melt rate to be proportional to the surface air temperature. Huy1 uses the recalibrated runoff model of Janssens and Huybrechts (2000). The sea-level and climate forcing are outlined in Sub-Sections 3.2.2 and 3.2.3, respectively. The non-Greenland component of the ice load is represented by the global ice sheet model ICE-5G (Peltier, 2004).

Farrell and Clark (1976) presented the seminal work on sea-level change as a result of Earth glaciation. Their theory is encompassed by the 'sea-level equation', which has undergone a number of developments over the last 30 years that have improved the method of solution and/or extended the theoretical basis (e.g. Nakada and Lambeck, 1987; Mitrovica and Peltier, 1991; Johnston, 1993; Milne and Mitrovica, 1996; Milne et al., 1999; Mitrovica and Milne, 2003). We do not go into theoretical detail in this study; the most recent advances and a review of the sea-level equation (as applied in this analysis) are described by Mitrovica and Milne (2003) and Kendall et al. (2005). In general terms, the sea-level model predicts the vertical deflection of both the ocean surface and the Earth's solid surface due to changes in ice-ocean mass configuration. Height shifts of the ocean surface are determined by computing perturbations to the geopotential. Changes to this field can be split into: (i) the direct effect – the gravitational effect caused by changes in ice-ocean mass configuration and GIA-induced changes in the rotational potential and (ii) the indirect effect – the gravitational effect caused by internal mass flux of the solid Earth driven be the ice-ocean loading and GIA-induced changes in the rotational potential. Note that these terms will be used at various points throughout this thesis. Perturbations to the rotation vector and the resulting feedback of this

forcing on sea level and land motion are computed as described in Milne and Mitrovica (1998) and Mitrovica et al. (2001a). Global ice/water mass is conserved in the model.

To model the Earth's response to changes in surface load the impulse response formalism of Peltier (1974) is applied. The impulse response formalism requires three relations to be satisfied; the momentum equation, the continuity equation (i.e. conservation of mass) and Poisson's equation (which describes the influence of mass changes on the potential field). A Maxwell visco-elastic rheology is used and the Earth model is spherically symmetric, self-gravitating and compressible. The procedure to calculate the Earth's response is very briefly described here: The unknown perturbations of the density and stress fields as described by the momentum equation are expressed, respectively, in terms of displacement using the continuity equation and strain using the constitutive equation for the rheology. Poisson's equation must be solved simultaneously to ensure that the solution is gravitationally consistent. The time domain form of the solutions to the visco-elastic problem are then expressed as a series of Legendre polynomials. These give solutions to the radial and tangential components of Earth displacement and also to perturbation of the geopotential. Instead of using these, however, solutions are given in terms of surface load Love numbers. These describe the temporal response in terms of an instantaneous elastic component and a slower viscous response which is represented by a series of exponential functions with a number of decay times. Finally, the GIA ice-ocean forcings are convolved, in space and time, with the impulse response Love numbers to give solution for a generalised surface load.

The elastic and density structure are taken from seismic constraints (Dziewonski and Anderson, 1981) and depth parameterised with a resolution of 15-25 km. The radial viscosity structure is depth parameterised to give an elastic lithosphere (i.e. very high viscosity values are assigned), an

isoviscous upper mantle bounded by the base of the lithosphere and the 670 km deep seismic discontinuity, and an isoviscous lower mantle continuing below this depth to the core-mantle boundary. For convenience we define a reference Earth model with a lithospheric thickness of 96 km and upper and lower mantle viscosities of 5×10^{20} Pa s and 10^{22} Pa s, respectively. These parameters fall near the middle of the range of values inferred in recent GIA modelling studies (e.g. Mitrovica and Peltier, 1993, 1995; Peltier, 1996; Peltier and Jiang, 1996; Mitrovica and Forte, 1997, 2004; Lambeck et al., 1998; Kaufmann and Lambeck, 2000, 2002) and so our reference model can be considered as a useful intermediate model for comparison purposes.

For the GIA loading computations, the ice-ocean loading increments are every 6000 years from 122 to 32 ka BP, every 1000 years from 32 to 17 ka BP and every 500 years from 17 to 0.5 ka BP. The final loading step before present is 100 years BP. Note that the timing of the loading increments are the same as with the ICE-5G model (Peltier, 2004).

Chapter 2:

Calibrating a glaciological model of the Greenland ice sheet from the Last Glacial Maximum to present-day using field observations of relative sea level and ice extent.

2.1. Introduction

At the LGM (as previously briefly discussed), the GrIS is thought to have extended to cover parts of the continental shelf (Funder and Hansen, 1996) and reached an excess volume (compared to present) of 2–3 m ice-equivalent sea level (Clark and Mix, 2002). The retreat of the GrIS is hypothesised to have occurred in two key stages (Funder, 1989); initial retreat was driven by sea-level rise, causing the calving of ice grounded below sea-level and breakup of the marine portions of the ice sheet. By c. 10 ka BP (all dates given are in calibrated years) the GrIS was essentially at or inland of the present-day coastline (Funder and Hansen, 1996; Bennike and Björck, 2002). The second phase of retreat during the Holocene (10 ka BP to present) was slower and driven, primarily, by surface melting. As mentioned, of particular interest is the reaction of the GrIS to peak warming during the HTM. The response of the ice sheet to this forcing may be a useful analogue for its future behaviour in a warming climate. The HTM occurred, broadly, between 9 and 5 ka BP in Greenland (Kaufman et al., 2004) causing the ice sheet to retreat behind its present-day position and reach a minimum post-LGM volume. It is not clear where and how far the ice margin retreated inland of its current position, as subsequent to reaching this minima the GrIS experienced a neoglacial readvance

(Kelly, 1980), and so all geological and geomorphological evidence of the minimum configuration was overridden by advancing ice.

Two previous studies have constrained the evolution (LGM to present-day) of the GrIS using RSL data. First, as mentioned above, Tarasov and Peltier (2002) presented their GrB model which forms the Greenland component of the global ice sheet reconstruction ICE-5G (Peltier, 2004). Second, Fleming and Lambeck (2004) presented their GREEN1 model which has a deglaciation history based on several stages of linear interpolation between an LGM reconstruction (Denton and Hughes, 1981) and the observed present-day ice sheet (Ekholm, 1996). We extend these previous studies in two main respects: (i) we make use of an RSL and ice extent dataset that is significantly improved over those used in these past two analyses. In particular, previous models were constrained primarily using sea-level observations derived from molluscan assemblages which have a large altitude uncertainty. We focus on the growing number of RSL observations reconstructed from isolation basins (e.g. Long et al., 2006, 2008, 2009; Sparrenbom et al., 2006a, b) which are more precise and consequently provide a more powerful model constraint (see Section 2.2); (ii) we provide a more detailed sensitivity analysis which targets key Earth and ice model parameters.

The overall aim of this work is to calibrate a glaciological model of GrIS evolution since the LGM using inferences of relative sea level (RSL) and past ice extent from field data. The work is structured as follows; in Section 2.2 we describe the nature of the data employed to calibrate the ice model and provide an overview of the observed sea-level history of Greenland. We start our modelling (Section 2.3) by comparing predictions generated using the ice model published by Huybrechts (2002). Adopting this as our preliminary ice model, we consider the sensitivity of sea-level predictions to wide ranges in the more important Earth model parameters and identify an optimal set of values.

Based on this Earth model sensitivity study, we are able to isolate data-model misfits that are due to limitations in the ice model. We then explore key aspects of the ice history that might explain the misfits of our starting ice model (Sub-Section 2.3.2). A central element of our analysis is the careful examination of trade-offs between ice and Earth model parameters. In Sub-Section 2.3.3 we show fits to the RSL data for our new calibrated ice model, before discussing the key aspects of our new model (Sub-Section 2.4.1) and possible sources for any remaining data-model residuals (Sub-Section 2.4.2). The conclusions are listed in Section 2.5. The reader should note that a version of this chapter has been published (see Simpson et al., 2009).

2.2. Nature of the data

In our modelling analysis we use data on past RSL and past ice extent. The primary focus is upon RSL data, the locations and source references of which are shown in Fig. 3 and Table 1, respectively. In total there are 214 observations used for RSL reconstruction; 73 of which have a well defined height and age relationship to former sea level and a further 141 that provide limiting constraints. Sea-level index points are derived from field evidence that has a defined (c. ±50 cm) vertical relationship to past mean sea level. This height relationship is referred to as the 'indicative meaning' (e.g. Shennan, 1986). In Greenland, the most precise sea-level index points are derived from dating the sediments preserved in isolation basins (e.g. Bennike, 1995; Long et al., 1999; Sparrenbom et al., 2006a) and thus provide a precise measure of past sea level in both time and height. By analysing a staircase of basins that occur below the marine limit, a well constrained RSL reconstruction can be produced (e.g. Fig. 4).

A variety of other field evidence lack an indicative meaning (a defined height relationship to a former tidal datum) and so provide a less precise height constraint on past sea level; these are referred to as

limiting dates. Radiocarbon dates from marine shells within raised beaches or deltas are typical examples of limiting dates. It is often uncertain how far below past sea level the shells lived and in most instances they provide only a lower height limit for RSL reconstructions (Gotfredsen and Møberg (2004) detail the height relationship to mean sea level for specific molluscan species).

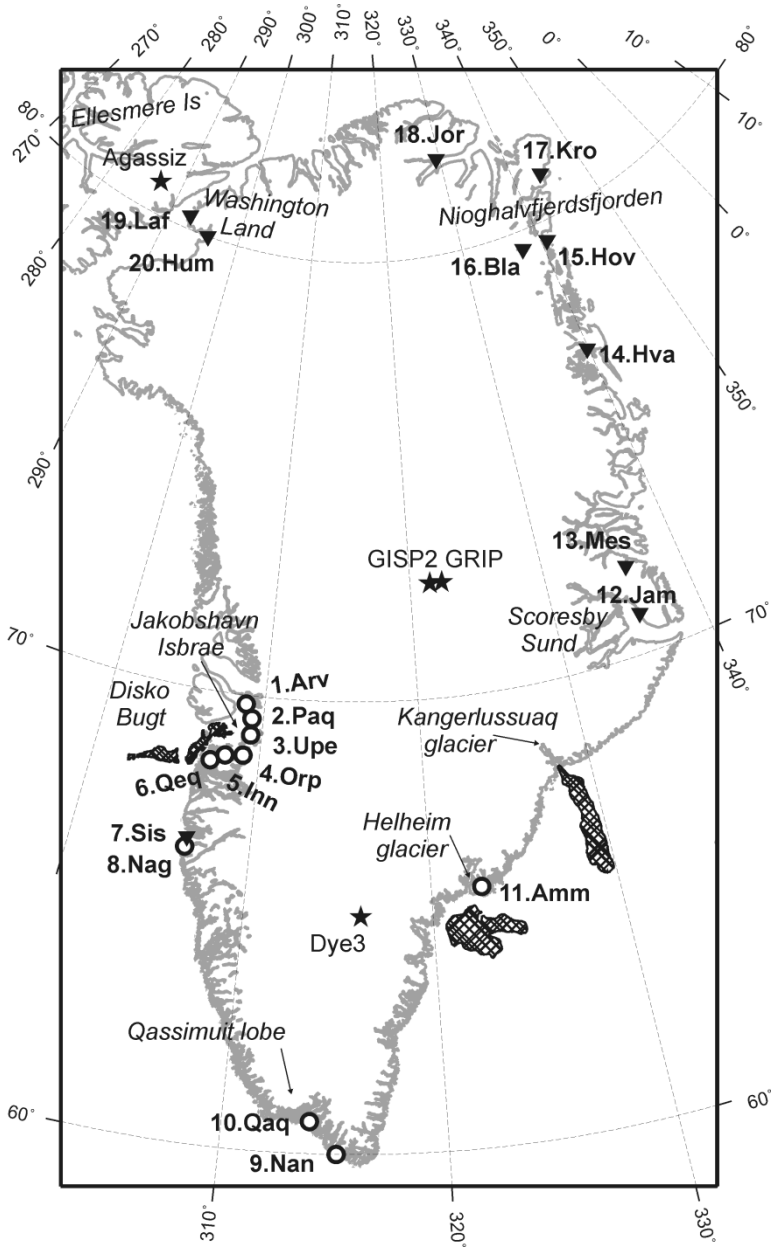

Fig. 3. Map showing the locations of the RSL observations used in this study as well as place names referred to in the text. Circles and inverted triangles mark, respectively, the locations of index point data and limiting data used in this analysis. Stars mark locations of ice core sites mentioned in the text. The crosshatched areas mark cross-shelf troughs associated with the named outlet glaciers. Table 1 lists RSL observations used and source literature.

However, for a number of shell dates plotted on a time-height diagram the upper height envelope of these observations can often tentatively be interpreted as past mean sea level. Fig. 4 shows a comparison of limiting dates (Rasch and Jensen, 1997) with index point data from an isolation basin study from Innaarsuit (Inn, Fig.1) in southern Disko Bugt. We select limiting dates that are close to the isolation basins to keep spatial differences in RSL small. Using only the isolation basin data as a guide we reconstruct past sea level on the time-height diagram (dashed line, Fig. 4) and on top of which the limiting dates are also plotted. Mostly we find the upper height envelope of the shell dates corresponds (within age error) to the past sea-level reconstruction. With more and better time-height coverage of the data we can have increasing confidence that the upper height envelope of the shell dates can be interpreted as past sea level.

Region	Site	Site name	Source Publication
West	1	Arveprinsen (Arv)	Long et al., 1999
	2	Paqitsoq (Paq)	Long et al., 2006
	3	Upernivik (Upe)	Long et al., 2006
	4	Orpissooq (Orp)	Long and Roberts, 2002
	5	Innaarsuit (Inn)	Long et al., 2003
	6	Qeqertarsvatsiaq (Qeq)	Long and Roberts, 2003
Southwest	7	Sisimiut (Sis)	Kelly, 1979; Weidick, 1972
	8	Nagtoralinguaq (Nag)	Long et al., 2009
South	9	Qaqortoq (Qaq)	Sparrenbom et al., 2006b
	10	Nanortalik (Nan)	Bennike et al., 2002; Sparrenbom et al., 2006a
Southeast	11	Ammassalik (Amm)	Long et al., 2008
East	12	Jameson Land (Jam)	Funder and Hansen, 1996
	13	Mesters Vig (Mes)	Washburn and Stuiver, 1962; Trautman and Willis, 1963
Northeast	14	Hvalrosodden (Hva)	Landvik, 1994
	15	South Hovgaard Ø and north-eastern Lambert Land (Hov)	Bennike and Weidick, 2001
	16	Blåsø (Bla)	Bennike and Weidick, 2001
	17	Kronprins Eijland (Kro)	Hjort, 1997
North	18	Jorgen Brunlund Fjord (Jor)	Funder and Abrahamsen, 1988
Northwest	19	Lafayette Bugt (Laf)	Bennike, 2002
	20	Humboldt Gletscher (Hum)	Bennike, 2002

Table 1. RSL observations used in this study to constrain our GIA model. The locations are marked in Fig. 3.

All of the limiting dates presented in the following analyses are assigned a height error that relates to the elevation sampling error and, importantly, not to their indicative meaning. Unless otherwise stated in the source literature we follow previous authors by ascribing a sampling elevation height error of ±5 m for marine shells and ±2 m for archaeological or freshwater organic material (Rasch and Jensen, 1997). Given the uncertainties inherent in the limiting dates we quantify data-model fits in two ways; (i) that limiting dates only provide a height limit and (ii) on the assumption the upper height envelope of the shell dates lies close to past mean sea level. For most of the analyses we consider limiting dates as only a height limit. In this case an RSL prediction would give fit to a shell date if it plotted either within the elevation error or above the date. For the analysis in Sub-Section 2.4.2.3 we assume that, for a given locality, the upper height envelope of the shell dates lies close to past mean sea level and a fit is achieved only if the prediction plots within the elevation error of these specific dates.

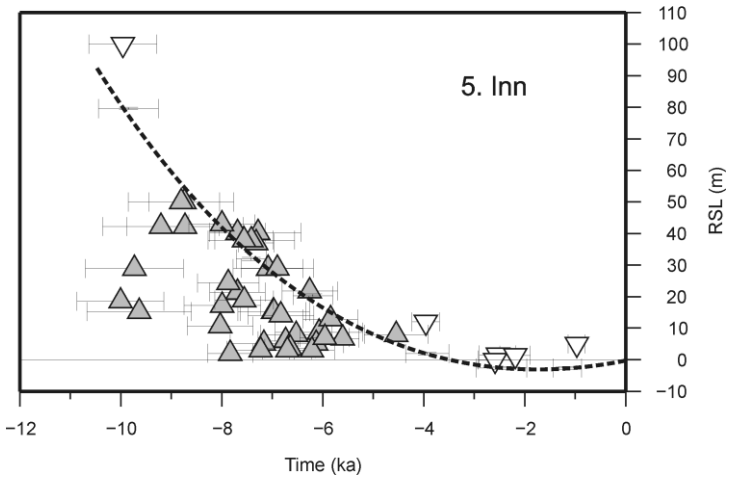

Fig. 4. A comparison of isolation basin data (index points) and marine shell and archaeological data (lower and upper limiting dates) from southern Disko Bugt. Lower limiting dates are shown as grey triangles. Upper limiting dates are shown as inverted white triangles. Sea-level index points are represented by both time and height error bars. The black dashed line represents the sea-level reconstruction based on the isolation basin data. An overall fall in RSL indicates that the solid Earth has rebounded and thus the ice sheet has undergone a local mass loss.

All radiocarbon dates used in this study have been calibrated using the programme CALIB Rev5.0.1 (Stuiver and Reimer, 1993) with the Intcal04 curve (Reimer et al., 2004) and are cited with a two-sigma age range. All dates given are in calibrated years. As adopted by Bennike and Björck (2002) a reservoir correction of 400 years is applied to marine samples from the west coast and a correction of 550 years to samples from the north and east coasts.

An additional RSL constraint that we use is the height of the Holocene Marine Limit (HML). The HML is traditionally thought to have formed immediately after deglaciation and is often marked by the lowest limit presence of perched boulders. The HML represents the highest point of past sea level for an ice-free region. In Greenland traceable contours of the HML define uplift domes that run parallel to the coast and characterise the emergence of the solid Earth from the sea surface (Funder and Hansen, 1996; Weidick and Bennike, 2007). It is possible to date the HML but organic material is often sparse and so, in many localities, it is necessary to extrapolate dates of material found at lower altitudes. Alternatively, lakes above the HML can be dated to determine the onset of organic accumulation and thus establish when an area became ice-free (Long et al., 2008).

As indicated above, we also consider field evidence pertaining to the past lateral extent of the GrIS. Geological and geomorphological features show how the ice sheet retreated from its maximum extent on the continental shelf (e.g. Evans et al., 2002) and radiocarbon dates can provide the minimum age of deglaciation for presently ice-free areas (e.g. Bennike and Björck, 2002).

2.3. Modelling results

2.3.1. Sea-level predictions based on the Huy1 model

Here we present sea-level predictions generated from our GIA model using the ice history Huy1 (see Sub-Section 1.4.1). The aims of this section are to: (i) examine sensitivity of the predictions to changes in Earth viscosity structure; (ii) determine a best-fit Earth model to partner Huy1 and (iii) assess whether acceptable data-model fits can be obtained using the Huy1 ice model and a spherically symmetric Earth model.

2.3.1.1. Sensitivity of predictions to Earth viscosity structure

Making changes to Earth parameters alters the isostatic response to a given surface load. We start by focussing on one site - Arveprinsen in west Greenland (Arv, Fig. 3) - to provide a general example and explain how the envelopes of predictions shown in subsequent analyses are generated.

Fig. 5 shows RSL predictions at Arveprinsen for our reference model (dashed-dotted black line) and six other models which are the same as the reference model except for one parameter value. The solid lines show predictions for a model Earth in which the lithospheric thickness has been increased to 120 km (grey) or decreased to 71 km (black). Comparing these curves shows that this range of lithospheric thickness has a significant influence on the magnitude of the RSL prediction but little impact on the shape of the curve. In contrast, changing the value of viscosity in the upper or lower mantle affects both the magnitude and the shape of the curve. The dashed lines show the sensitivity of the predictions to changing the viscosity in the upper mantle from a value of 3×10^{20} Pa s (black) to 10^{21} Pa s (grey). The dotted lines show the influence of varying lower mantle viscosity from 10^{21} Pa s (black) to 5×10^{22} Pa s (grey). In general, lower viscosity values permit a more rapid isostatic

response to a given loading event (e.g. note the more rapid sea-level fall of the black dashed line compared to the grey dashed line following local ice unloading at c. 15 ka BP). One important point to note from this sensitivity study is that the timing of the initial RSL fall is not affected by these Earth model changes and so is controlled by changes in ice load.

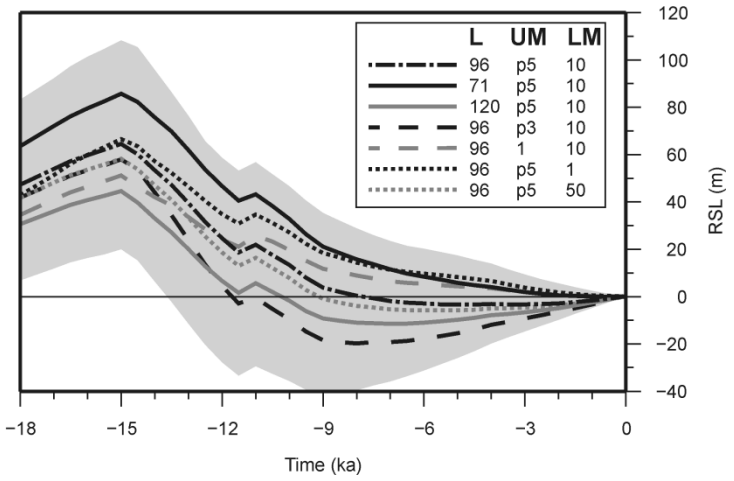

Fig. 5. Sensitivity of sea-level predictions at Arveprinsen to changes in Earth viscosity structure. All changes are relative to our reference Earth structure which has a 96 km thick lithosphere, upper mantle viscosity of 0.5×10^{21} Pa s and lower mantle viscosity of 10^{22} Pa s. Predictions for this model are shown by the dashed-dotted black line. Shown are predictions for lithospheric thicknesses of 71 km (solid black) and 120 km (solid grey), upper mantle viscosities of 0.3×10^{21} Pa s (dashed black) and 10^{21} Pa s (dashed grey) and lower mantle viscosities of 10^{21} Pa s (dotted black) and 50×10^{21} Pa s (dotted grey). The grey shaded region denotes the variation in RSL for 108 model runs that sample the viscosity parameter ranges defined above.

We generated predictions at Arveprinsen for a suite of 108 different Earth viscosity models that sample the range of values specified above. The grey shaded region in Fig. 5 bounds the suite of predictions generated from these model runs and so illustrates the sensitivity of the predictions at this site to a large range of plausible Earth viscosity models. Note that the bounds of these envelopes may well be defined by more than one prediction. The envelopes can be considered as a measure of the uncertainty in the predictions associated with limited knowledge of mantle viscosity

structure. We show these envelopes for all the data sites in Section 2.3.1.3 to examine whether the Huy1 model is consistent with the data to within this uncertainty.

2.3.1.2. Determining an optimal viscosity model

We compute RSL at all 20 data sites considered for each of the 108 Earth models introduced above and quantify the goodness of fit for each Earth model using the χ^2 criterion:

$$\chi^2 = 1/n \sum_{i=1}^{n} \left(\frac{y_i^{pr} - y_i^{obs}}{\sigma_i} \right)^2 . \qquad \text{(Eqn. 1)}$$

The χ^2 value indicates the difference between predicted (y^{pr}) and observed sea level (y^{obs}) for a specified observational error (σ) and given RSL data point (i). A value of one or less indicates a fit to the data (within error) whilst a misfit can produce a very large value due to the squared term. In this first analysis limiting dates are considered only as height limits and therefore can still give fit even when there are large differences between the model results and the elevation height error. If predicted sea level passes above a shell date, for example, then a fit is still achieved due to the associated uncertainty of lower limiting data and its relationship to contemporaneous sea level. In this situation the χ^2 value is assigned a value of one. Fig. 6 shows how the goodness of fit varies with upper and lower mantle viscosity for lithospheric thicknesses of 71, 96 and 120 km. We see a general pattern of increasing data-model misfit for smaller upper mantle and larger lower mantle viscosities. The misfit also increases as the lithosphere is thickened. The 71 km pane shows a zone of relatively good fit for middling values of upper and lower mantle viscosities; this area represents the best-fit Earth model for Huy1. Specifically, a model characterised by a 71 km lithosphere, an upper mantle viscosity of 5×10^{20} Pa s and a lower mantle viscosity of 5×10^{21} Pa s provides the optimum fit. It is worth noting that the χ^2 test and best-fit model will have a bias toward fitting the west Greenland dataset as: (1) there are numerous data from this region and (2) the data here are mostly from

isolation basins which have good height precision and so the χ^2 values will increase quickly with an increasing misfit.

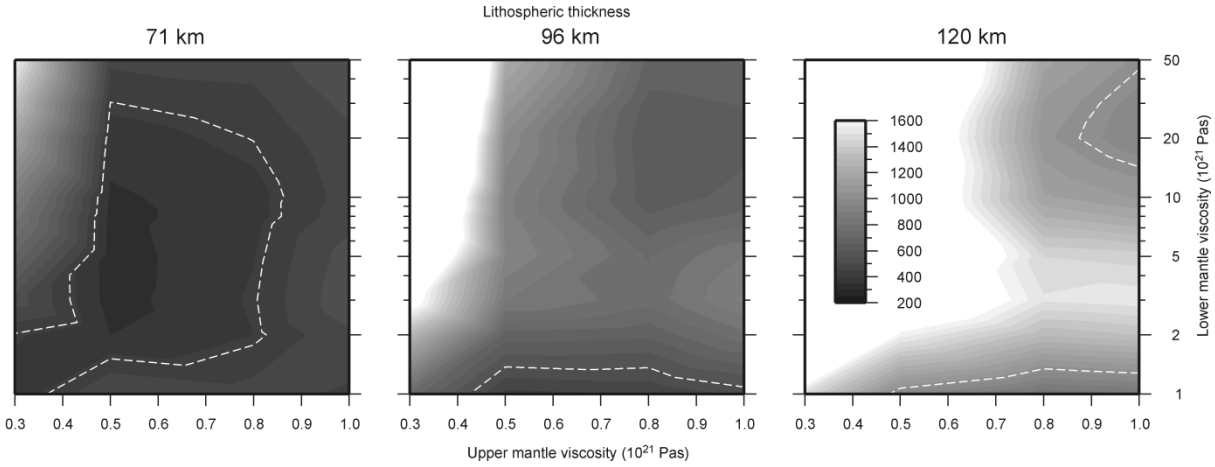

Fig. 6. The Chi-squared results for the Huy1 ice model and 108 different Earth viscosity models (see text for details). Each frame is based on a fixed value for lithospheric thickness (as indicated). The scale bar for the Chi-squared results is shown in the right-hand frame. The 95% confidence level is marked by the white dashed line.

2.3.1.3. Comparison of Huy1 model to RSL observations

In the near-field of Greenland we can expect that a primary control on past sea-level change is the isostatic adjustment of the solid Earth due to changes in the load distribution of the GrIS. This is reflected in the field observations which, at most localities, show an overall fall in RSL from Lateglacial time to the present-day (Fig. 7), indicating that the solid Earth has rebounded and thus the ice sheet has undergone a mass loss. Clearly, patterns of past sea-level change vary across Greenland – a more detailed discussion of regional sea-level variation follows in this sub-section. These inter-regional differences in RSL change can be used to infer the pattern of ice sheet evolution at various levels of sophistication: from the direct interpretation of maps of the HML to identify regions that have experienced greatest ice load loss (Funder and Hansen, 1996; Weidick and Bennike, 2007) to the more involved geophysical modelling studies that constrain 3-D models of GrIS history (Tarasov and Peltier, 2002; Fleming and Lambeck, 2004).

Isolation basin studies (e.g. Long et al.,1999; Bennike et al., 2002; Sparrenbom et al., 2006a) have shown that in some areas Holocene RSL fall continued to a height below present-day sea level (e.g. Fig. 5a, site 1). When RSL does fall below present-day sea level it is followed by a small rise which gives the curve a characteristic 'J-shape'. This shows that sea level in some areas of Greenland underwent a late Holocene transgression; a change also evident from archaeological studies of paleo-Eskimo sites which are now partly submerged (e.g. Hjort, 1997; Rasch and Jensen, 1997; Mikkelsen et al., 2008). Eustatic sea-level change is thought to have decelerated during the mid-Holocene from a rate of c. 1 to 0 m/ka by 2 ka BP (e.g. Lambeck and Purcell, 2005) and so the RSL switch likely represents a change from rebound to subsidence of the solid Earth surface. Past sea-level investigations have attributed the RSL switch to a downward deflection of the solid Earth as the result of both/either (i) the collapse of a forebulge and/or (ii) the neoglacial ice loading in Greenland (Kelly, 1980; Weidick, 1993; Long et al., 1999).

Beginning in west Greenland and working anti-clockwise we briefly review the RSL history of each region and compare predictions to the observations (Fig. 7). In grouping the data into single RSL curves we used the model to check that spatial differences in RSL predictions were small. In general, for a given site, the data are clustered within an area of dimension less than a few 100s km^2.

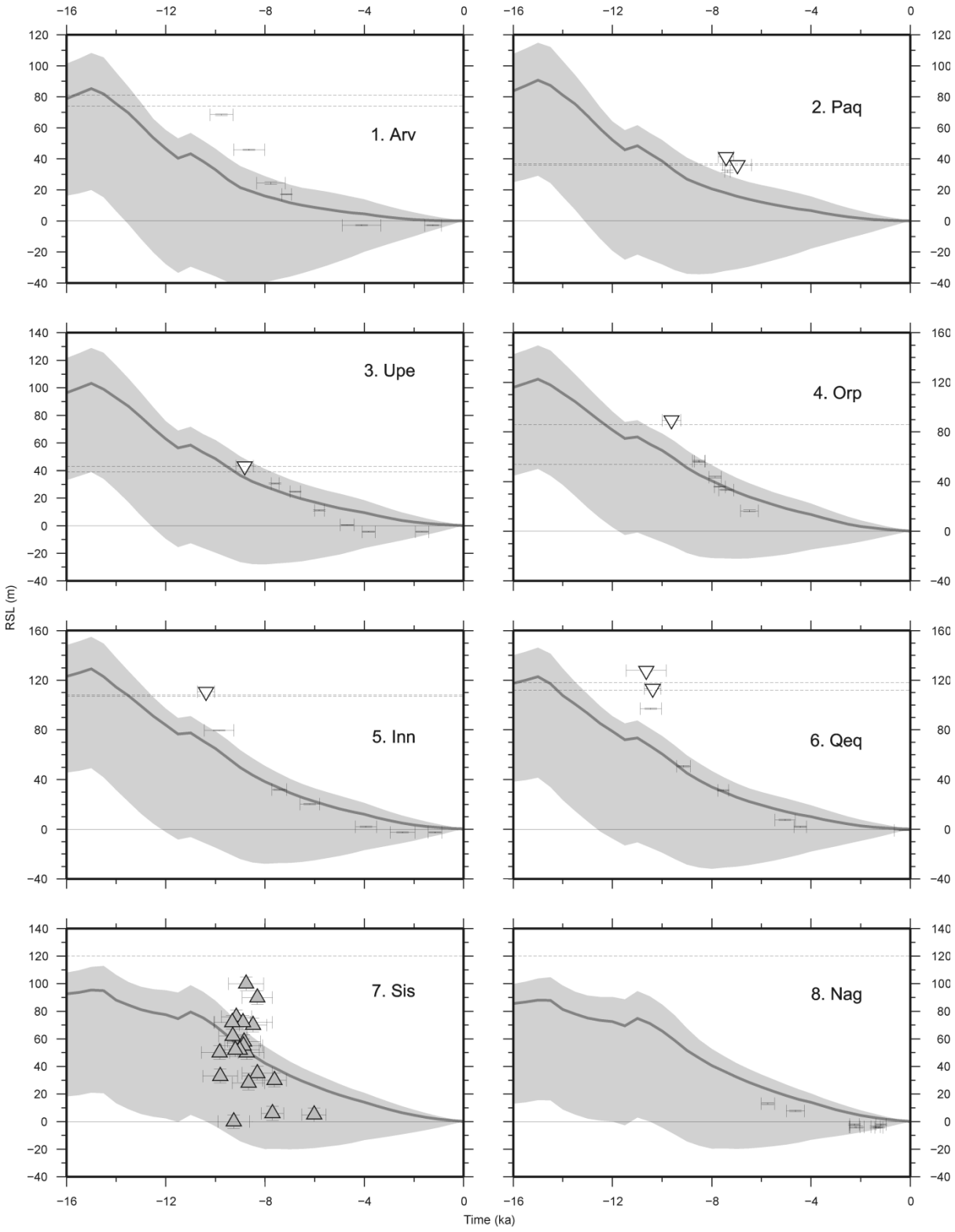

Fig. 7a. RSL predictions and observations at the 20 sites considered in this analysis. Predictions, based on the Huy1 ice model and 108 Earth models, fall within the light grey shaded area (see Sub-Section 2.3.1.1). The dark grey line denotes the RSL prediction for the best-fit Earth model of Huy1; characterised by a 71 km thick lithosphere, upper mantle viscosity of 5×10^{20} Pa s and lower mantle viscosity of 5×10^{21} Pa s (see Sub-Section 2.3.1.2). Lower limiting dates are shown as grey triangles.

Upper limiting dates are shown as inverted white triangles. Sea-level index points are represented by both time and height error bars. The HML at each site is indicated by a horizontal dashed line; if two lines are shown their vertical displacement represents the uncertainty in this value.

Situated on the central west Greenland coast, the marine embayment of Disko Bugt has become a classic area for sea-level investigations. Studies on Disko Island (Ingolfsson et al., 1990) and in Disko Bugt (Rasch, 2000) show a clear decline of the HML from c. 120 m in southeast Disko Bugt to c. 60 m in northwest Disko. It is well established that Disko Bugt sits upon the northern flank of a high uplift dome that runs parallel to much of the ice-free southwest coast (first mapped by Weidick (1976)). Numerous RSL isolation basin investigations (Long et al., 1999, 2003, 2006) have shown conclusively that after a rapid early Holocene fall, RSL fell below present-day sea level c. 5-4 ka BP to reach a lowstand c. 2 ka BP before rising 1-5 m to present. Comparing the predictions to the data in this area (sites 1-6, Fig. 7a) indicates that the fall from the HML occurs too early and at too low a rate. In addition, at all of these sites the best-fit sea-level prediction fails to provide fit to the oldest index point.

In southwest Greenland (sites 7 and 8, Fig. 7a) best-fit predicted sea level reaches a height of c. 100 m, this is around 20 m below the HML (Funder and Hansen, 1996). It should be noted that for Sisimiut (site 7) we have omitted the partially published dates of Petersen and a dated whale cranium which is presumed to be contaminated (Kelly, 1979). The lower limiting dates from Sisimiut suggest a rapid fall in RSL from c. 100 m at 10 ka BP to close to present-day sea level by 6 ka BP. Further south at Nagtoralinguaq (site 8) new sea-level index points have revealed that RSL dipped c. 4 m below present-day sea level at around 2 ka BP (Long et al., 2009). For southwest Greenland, modelled RSL fall is too early and too slow, while the magnitude of the signal is under predicted (in contrast to sites in the central west).

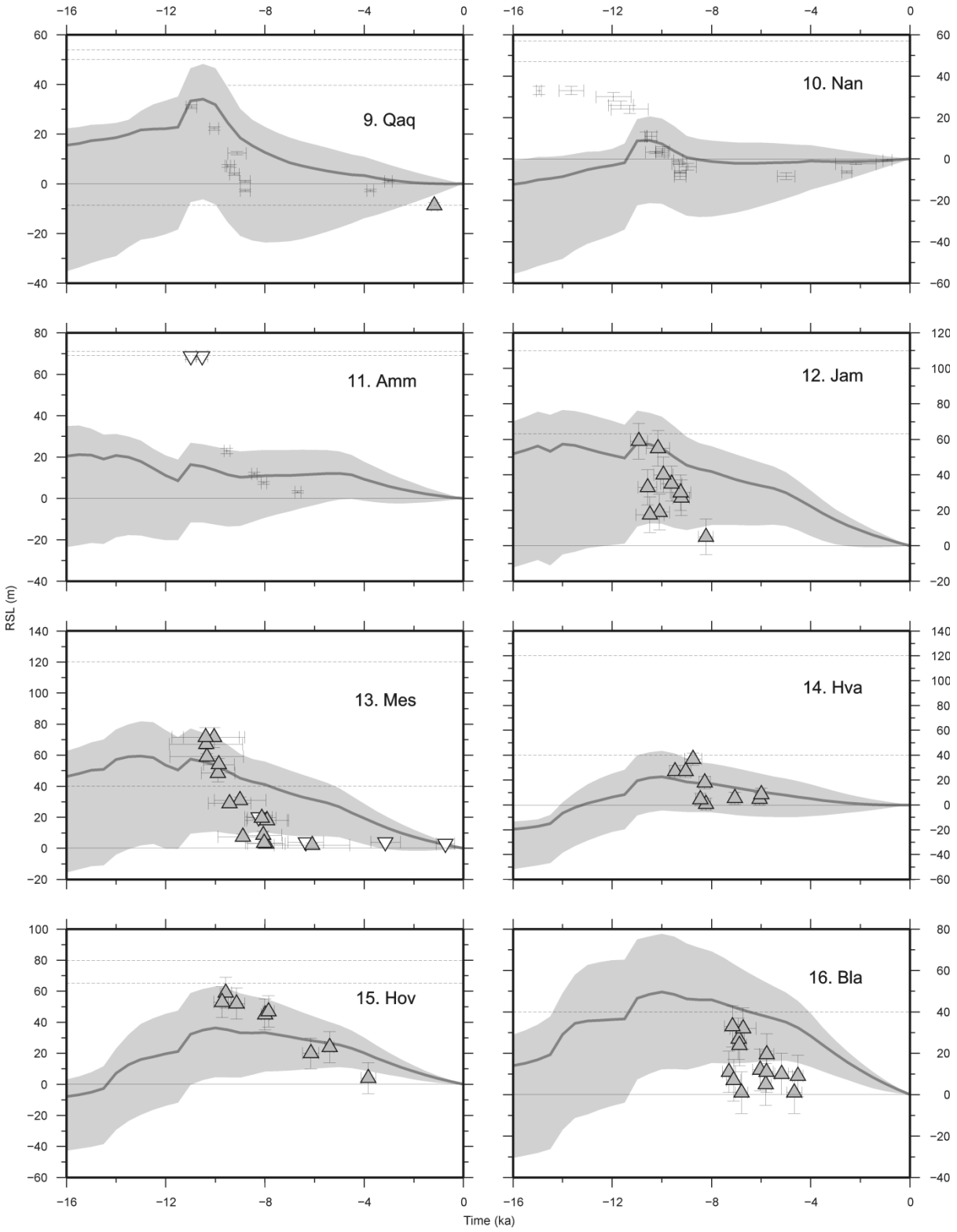

Fig. 7b. *(Continued)*. Qaqortoq (site 9) includes additional observational constraints, indicated by two extra horizontal dashed lines. The line at -8.7 m marks a marine basin that shows no evidence of freshwater incursion and defines a lower bound on RSL change. The line at 39.7 m and traced from 9.5 ka BP to present-day marks the minimum age of deglaciation for a basin and defines an upper bound on RSL change.

A map of the HML in south Greenland (Fig. 5 in Weidick et al., 2004) shows a drop from c. 60 m near the Qassimiut lobe to c. 20 m at the southern tip of Greenland. At Qaqortoq and Nanortalik (sites 9 and 10, Fig. 7b), RSL falls below present-day sea level at c. 10-9 ka BP, earlier than recorded anywhere else in Greenland. At Qaqortoq the prediction shows some agreement with the index point data but does not reach the HML. Other evidence from a drowned isolation basin at this site indicates that RSL fell 6-8 m below present-day sea level (Sparrenbom et al., 2006b) - this is not captured in the model predictions. RSL at Nanortalik is predicted to be largely negative and the best-fit prediction is 30-40 m below the HML. The two earliest index points from Nanortalik come from a lake situated offshore which is c. 15 km from the cluster of other lakes cored and so including these on the same RSL plot is not strictly appropriate (Sparrenbom et al., 2006a).

Ammassalik (site 11, Fig. 7b) represents the only RSL data from the southeast of Greenland. Two cored lakes show that ice-free conditions were established here c. 11 ka BP, which is also interpreted to be the time RSL fell from the HML (c. 70 m) (Long et al., 2008). There is a c. 50 m misfit between the HML and best-fit predicted sea level at this time. The lowest lying lake is at c.1 m and shows no marine incursion from 6.7 ka BP to present-day. During this period RSL must have been below the height of the lake. These results indicate that Huy1 significantly underestimates the magnitude of ice unloading in this area.

In east Greenland, RSL predictions for Jameson Land (site 12, Fig. 7b) are not consistent with the earliest lower limiting dates and do not capture the rapid fall suggested by the data. A similar mismatch exists at Mesters Vig (site 13, Fig. 7b). In addition, at this site, a number of late Holocene upper limiting dates suggest RSL was close to present-day sea level at c. 6 ka BP and best-fit predicted sea level at 6 ka BP reaches no lower than 30 m.

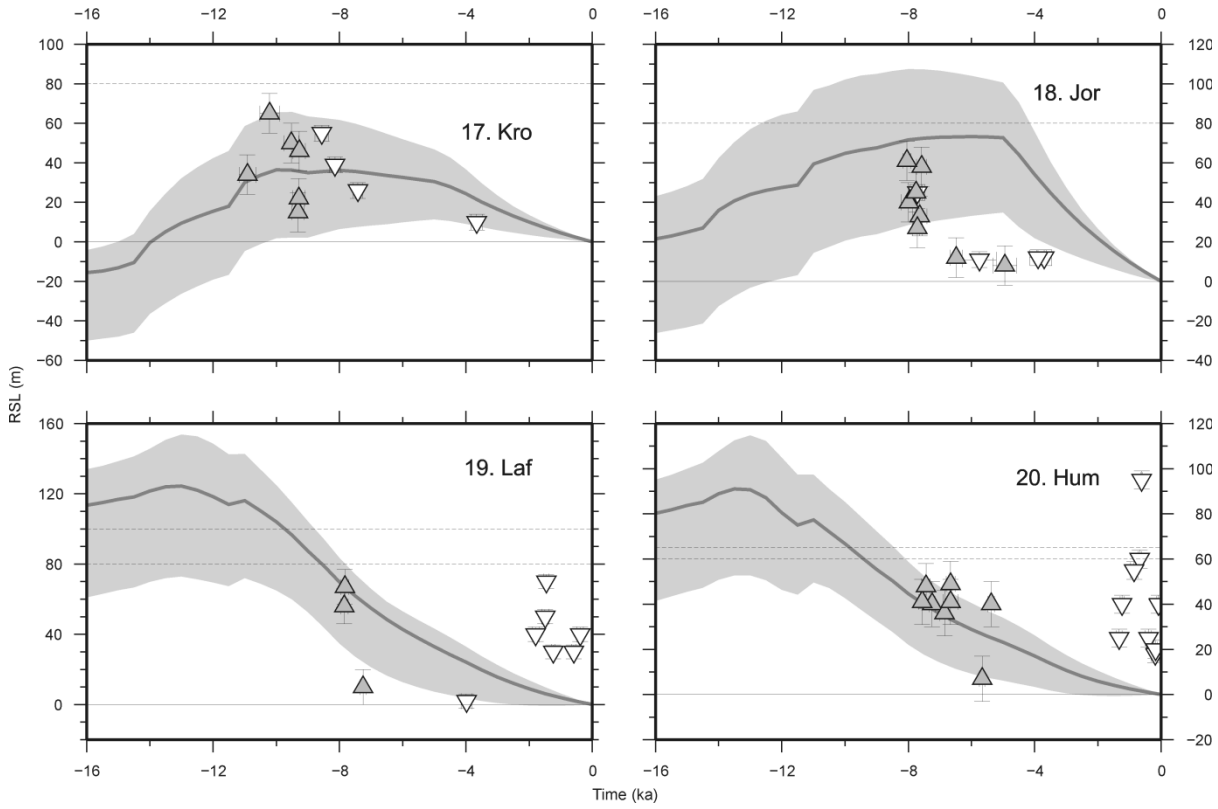

Fig. 7c. *(Continued)*.

Largely, the data from the northeast consist of lower limiting dates so we cannot be sure of their contemporaneous relationship to RSL. At Hvalrosodden and Hovgaard (sites 14 and 15, Fig. 7b) predicted RSL fails to reach above the HML and also fails to plot above some of the early lower limiting dates. The prediction at Blåsø (site 16, Fig. 7b) is broadly consistent with the data but does not produce the expected rate of sea-level fall. The RSL observations are insufficient to show a fall below present-day sea level but c. 100 km northward of this site, archaeological findings suggest a minor late transgression may have happened at Kronprins Eijland (site 17, Fig. 7c) (Hjort, 1997). Here also the prediction does not reach the HML or produce the observed rate of Holocene RSL fall; which is well constrained by upper and lower limiting dates. The data at this site were collected along a broad stretch of coastline (across which there may have been differential isostatic response) and so should be treated with caution.

In the north of Greenland RSL observations from Jurgen Bronlund Fjord (site 18, Fig. 7c) suggest a very rapid fall in sea level at c. 8 ka BP. The prediction for Huy1 shows a very late switch to RSL fall when compared to the early data from this site. As a consequence, the best-fit prediction grossly misfits the upper limiting dates that lie close to present-day sea level and are dated to the mid-Holocene.

Across Washington Land in the northwest of Greenland, investigations have shown that the HML declines from c. 100 m in the north to c. 60 m in the southwest (Bennike, 2002). The RSL data are grouped into Lafayette Bugt (site 19, Fig. 7c) and Humboldt Gletscher and Cass Fjord (site 20, Fig. 7c). The sparse time-height coverage of the data in this region means that past RSL change is not well defined. At our final site, the best-fit prediction is inconsistent with some of the older minimum limiting dates (i.e. RSL is too low too early).

We summarise the above discussion with the following conclusions. At seven sites, predicted RSL does not reach the HML (even considering the spread associated with mantle viscosity sensitivity). In west, south (at Nanortalik) and southeast Greenland sea level does not reach high enough to fit the earliest index point data. At the majority of sites the timing of the predicted RSL fall is too early and rate of the fall too slow when compared with the observations. The exception to this is north Greenland where predicted sea-level fall is too late. Observations across Greenland indicate RSL was very close to or even below present-day levels for some part of the Holocene; predicted sea level either does not produce this result or incorrectly produces the timing and magnitude of this fall.

Inspection of the results in Fig. 7 indicates that a significant portion of the data-model misfit cannot be accounted for by varying Earth viscosity parameters within the ranges considered. An important result of our Earth model sensitivity analysis is that the timing of RSL fall at most localities is insensitive to changes in viscosity structure and so must be driven by the ice model. We conclude that the Huy1 model is not capable of providing acceptable fits to the RSL observations for a broad suite of Earth viscosity models. We therefore proceed, in the next section, to address some of these ice model-related misfits by altering key ice model parameters.

2.3.2. Calibrating the ice model

In the following Sub-Sections (2.3.2.1-2.3.2.3) we outline the changes made to the Huy1 model to try and address the data-model misfits discussed above. It is important to note that each change introduced to the Huy1 model is retained and implemented in all following Sub-Sections. We begin with the LGM extent of the GrIS and then go on to examine two aspects of the ice model forcing: sea level and temperature. We justify and constrain each of these forcings using a combination of both independent evidence and RSL data-model misfits. We demonstrate the sensitivity of the ice model output as well as the RSL response to plausible parameter variations where appropriate.

2.3.2.1. LGM extent

The maximum extent of the Huy1 model is limited by a mask which acts to confine the growth of the ice sheet across the continental shelf. The mask is based upon sparse evidence of the LGM extent taken from Funder (1989), Funder et al. (1998) and Solheim et al. (1998). The Huy1 mask allows the LGM ice model to reach (approximately) the mid-shelf in the west, the outer shelf in the south and southeast and only the fjord mouths and inner shelf in the east and northeast (Fig. 8). More recent

studies, however, are elucidating a pattern of LGM extent that is somewhat larger than these previous findings suggest.

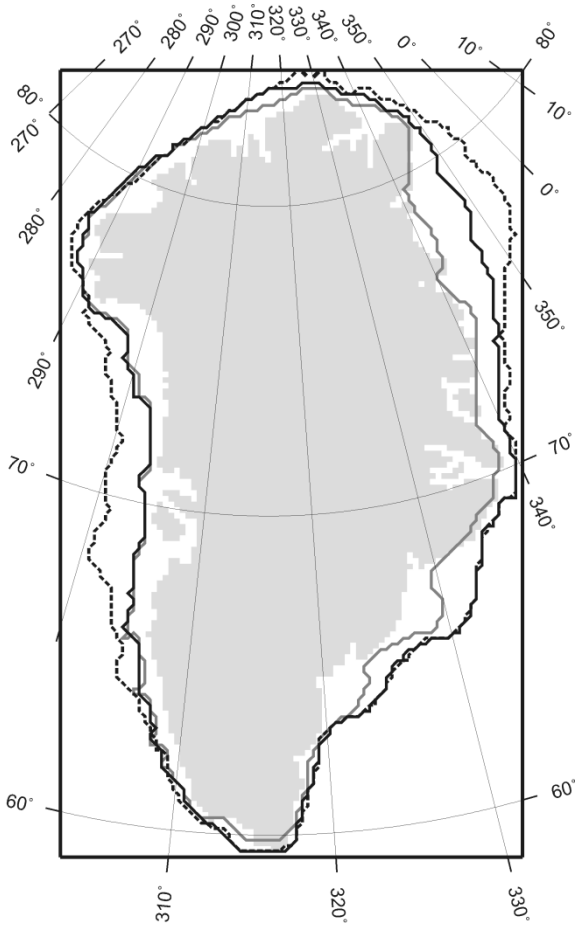

Fig. 8. The three LGM ice mask extents considered in this analysis: the original mask of Huy1 (solid grey); the shelf break mask (black dashed; which roughly coincides with a 400 m bathymetric depth) and our chosen (hybrid) mask (solid black). See main text for more information. Modelled present-day coastline is shaded light grey.

Marine observations from northeast Greenland have produced perhaps the most compelling new evidence. Geophysical surveys and gravity cores taken from the continental margin in this region (the area approximately 72-75^{o}N) indicate that LGM ice extended to the mid-shelf (Wilken and Mienert, 2006) or even to the outer shelf and may have reached the shelf break (O'Cofaigh et al., 2004). Geophysical data have shown a moraine on the mid-shelf, which may define maximum LGM ice extent (Evans et al., 2002), or it is a recessional feature and so marks a post-LGM margin position.

Further north, at Nioghalvfjerdsfjorden, Bennike and Björck (2002) suggest that LGM ice may have reached the shelf edge. Whilst at Scoresby Sund, where LGM ice is thought to have reached no further than the fjord mouth (Dowdeswell et al., 1994), recent cosmogenic dates suggest that in east Greenland LGM ice may have also reached to the outermost shelf (Håkansson et al., 2007). These recent findings are in contrast to the coastal position of LGM ice extent defined by the mask of Huy1 for northeast and east Greenland. The continental shelf is wide and shallow in the northeast and so the changes suggested by these new observations are significant (e.g. compare grey and black dashed lines in Fig. 8). If the ice margin was positioned on the outer shelf rather than the coast we would expect a marked difference in LGM ice load over this region.

In southeast Greenland radiocarbon dates from the shelf adjacent to the Kangerlussuaq outlet glacier (Jennings et al., 2006) imply LGM ice terminated near the shelf break (also see a review of the evidence by Andrews (2008)). Farther south and close to the Helheim outlet glacier, new cosmogenic exposure ages (Roberts et al., 2008) and other radiocarbon dates from the shelf similarly indicate that the ice margin was at or close to the shelf break (Kuijpers et al., 2003). Moreover, a GIA modelling study constrained by new RSL data from Ammassalik has shown that the LGM position of the Huy1 model is insufficiently extended onto the shelf in southeast Greenland (Long et al., 2008). Similar modelling studies in south Greenland have found that the LGM ice margin reached the shelf break (Bennike et al., 2002; Sparrenbom, Ph.D. thesis). Across west and southwest Greenland there are no new observations to challenge or validate the traditional model of LGM extent as reflected in the Huy1 mask. Two distinct moraine systems have been identified on the inner and outer shelf in this region (Brett and Zarudzki, 1979). Kelly (1985) uses the height of a nunatak moraine system in southwest Greenland to infer that the ice margin terminated on the inner shelf. Other moraine systems from south Disko (Ingolfsson et al., 1990) are interpreted as LGM extent, although it cannot be ruled out that these mark a readvance or are recessional features (Weidick and Bennike, 2007).

The current evidence is insufficient to precisely define the LGM position of the ice margin across Greenland. Given this uncertainty, it is appropriate to examine the sensitivity of RSL predictions to a small suite of plausible LGM ice margin configurations to see if some of the misfits discussed above can be reconciled through this aspect of the ice model. We introduce two alternative masks that delimit the LGM ice extent. The first allows the ice sheet to expand, if in positive mass balance, to the shelf break (dashed black line – Fig. 8). The second mask is a hybrid scenario that most closely reflects the new geomorphological and modelling evidence outlined above (solid black line – Fig. 8). This allows the ice sheet to expand to the mid-to-outer shelf in the northeast, the shelf edge from east to south Greenland and follows the original Huy1 mask elsewhere. Even though there remains considerable uncertainty in the LGM extent of the ice sheet, we consider this hybrid scenario as the most accurate at this time. We note that in each case the ice model grows to completely cover the area defined by the mask.

We show, in Fig. 9, the modelled ice volume and spatial extent for the past 80 ka BP based on the three LGM masks introduced above. These results indicate that there are large differences in LGM volume and spatial extent for the different scenarios considered. For example, the Huy1 model predicts 2.7 m excess ice-equivalent sea level at the LGM, compared to 5.2 m for the maximum (shelf break) extent model and 4.1 m for our preferred hybrid model.

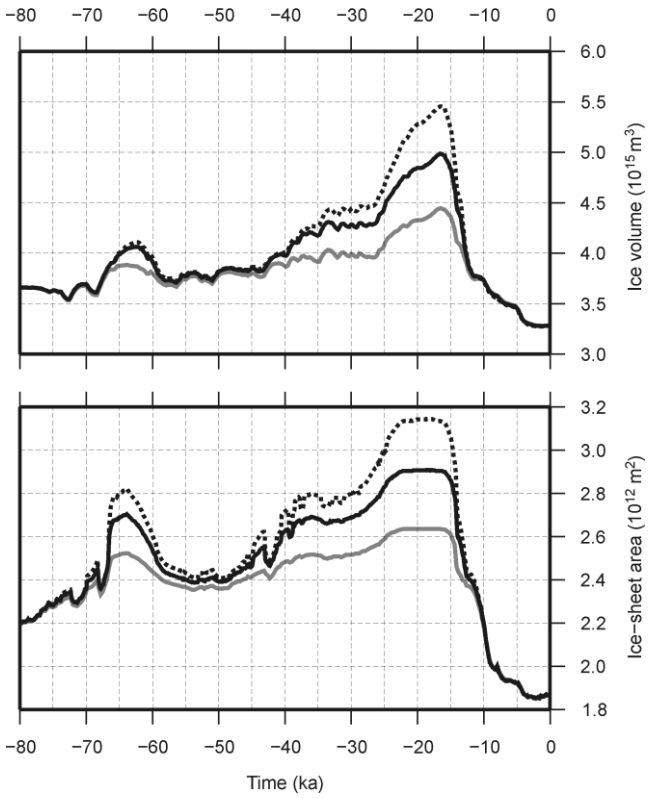

Fig. 9. Ice sheet volume and extent changes for the three different LGM extent scenarios shown in Fig. 7: Shelf break (black dashed), our chosen (hybrid) LGM extent (solid black) and Huy1 mask (solid grey).

The sea-level predictions generated from the three LGM extent scenarios considered are illustrated for eight representative RSL sites in Fig. 10 (note that the colour and style of the lines shown correspond to those in Figs. 8 and 9 for a given LGM mask). In general (and unsurprisingly) we find the largest differences in the RSL response where the distances between the masks are largest. For northeast Greenland where the shelf is at its widest and the original Huy1 mask hugs the coastline, there is a c. 100 m difference between RSL predictions at 10 ka BP for Hovgaard (site 15, Fig. 10). The comparison was made at 10 ka BP because this is when the largest discrepancy occurs during the period that observational constraints exist at this site. Using this same approach in south Greenland, the RSL response at 15.5 ka BP for Nanortalik (site 10, Fig. 10) varies by c. 20 m. Here the shelf is narrow c. 30-60 km and so the differences between the masks are relatively small.

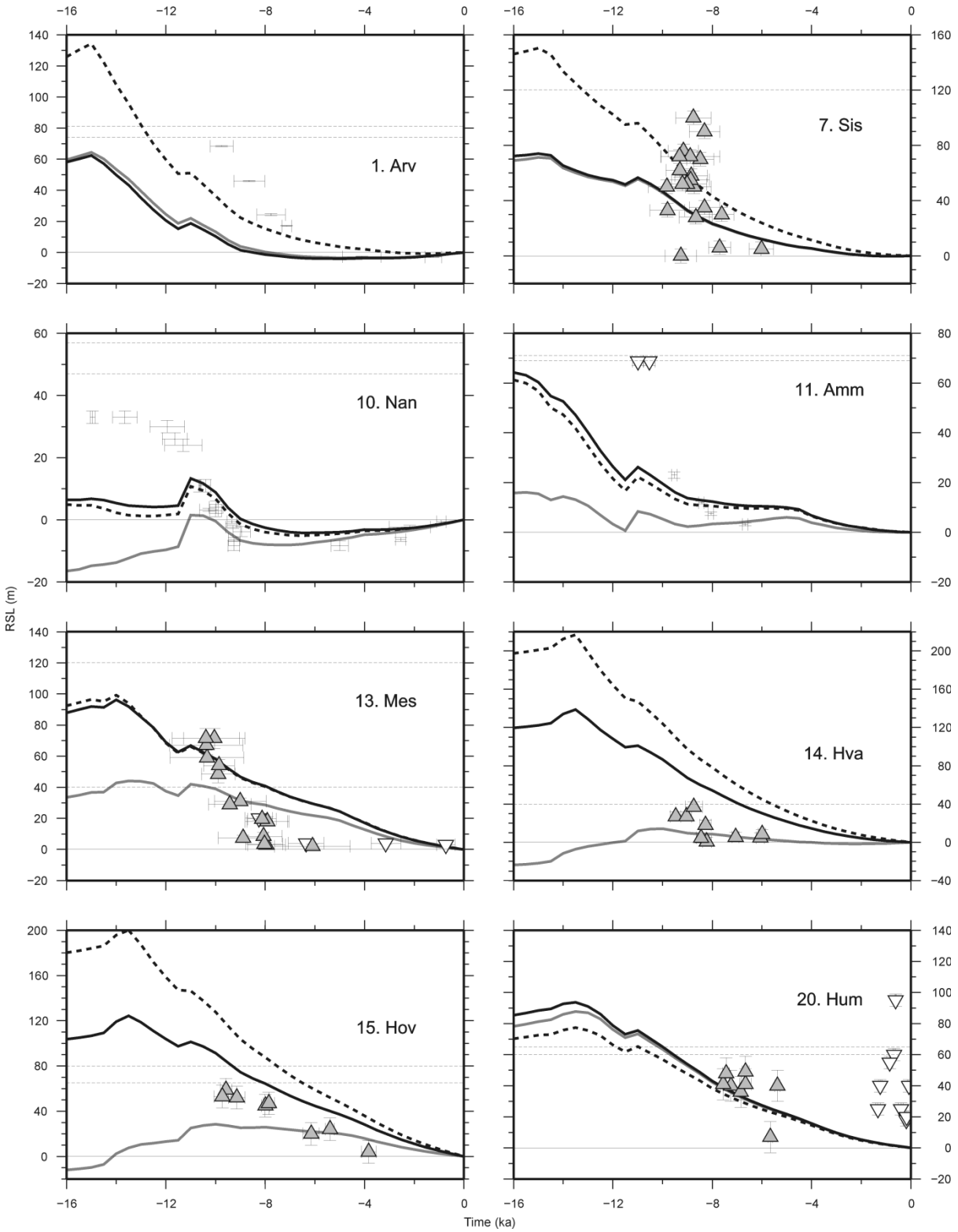

Fig. 10. The influence of LGM extent on the sea-level predictions for our reference Earth model. The shelf break (black dashed), our chosen mask (solid black) and original Huy1 mask (solid grey). Lower limiting dates are grey triangles. Upper limiting dates are inverted white triangles. Sea-level index points are represented by both time and height error bars. The HML at each site is indicated by a horizontal dashed line; if two lines are shown their vertical displacement represents the uncertainty in this value.

Changes to the LGM mask do not influence the timing of predicted RSL fall; a similar finding as from our Earth model sensitivity analysis. Our preferred LGM hybrid mask is most different to the original Huy1 mask in southeast, east and northeast Greenland. Here our preferred hybrid mask generally predicts higher RSL and a more rapid RSL fall. The revision of the mask improves the data-model fit for northeast Greenland where lower limiting observations now show fit to predicted RSL for our reference Earth model. For southeast Greenland predicted sea level now reaches to the HML. But in both the southeast and east, however, the observations still indicate that RSL fall is mistimed and/or the rate of RSL fall is too low. For areas where the mask is little changed or its position not revised the data-model misfits described in Section 2.3.1.3 remain.

2.3.2.2. Sea-level forcing

At present there is no reliable way to simulate the grounding-line (Vieli and Payne, 2005) or the position of the calving front if there is no ice shelf. The application of simple marine parameterisations has been shown to successfully reproduce first-order ice margin changes in areas below sea level (Zweck and Huybrechts, 2003, 2005). The sea-level forcing of Huy1 uses an empirical formulation that parameterises the maximum grounding depth of the ice sheet (H_c) as a function of eustatic sea-level change (ΔH_{sl}):

$$H_c = -0.25 \times (\Delta H_{sl} + 80)^2 + 2\Delta H_{sl} \text{ for } \Delta H_{sl} < -80,$$

$$H_c = 2\Delta H_{sl} \text{ for } \Delta H_{sl} > -80. \qquad \text{(Eqn. 2)}$$

This assumes that water depth is the sole control on the extent of the marine margin and that beyond the maximum grounding depth all ice is calved. It should be noted that the eustatic sea-level record (ΔH_{sl}) used in Huy1 is derived from the SPECMAP stack of marine oxygen-isotope values (Imbrie et al., 1984). The empirical relationship, given in Eq. (2), is hybridised to reproduce the

advancement of the ice sheet over the continental shelf. During times of low eustatic sea level this relationship allows the ice sheet to expand onto the continental shelf and reach the maximum margin extent (as defined by the mask). Conversely, rising eustatic sea level will force the ice margin landward.

Observational evidence on the timing of ice margin retreat across the continental shelf is generally limited. In northeast Greenland retreat commenced after c. 18 ka BP and had abandoned the inner shelf by c. 14.6 ka BP (Evans et al., 2002). The beginning of deglaciation is dated to c. 18.6 ka BP in east Greenland (Nam et al., 1995). In southeast Greenland dates from the cross-shelf Kangerlussuaq trough suggest the GrIS remained near to the shelf edge until 17 ka BP (Mienert et al., 1992). Other dates from the trough indicate the mid-shelf became ice-free c. 16-15 ka BP (Smith and Licht, 2000; Jennings et al., 2002, 2006). Just south of Ammassalik (site 11) another marine core study shows ice margin retreat in this area occurred shortly before c. 15 ka BP (Kuijpers et al., 2003). The timing of marine retreat in other areas of Greenland is less well known; in west Greenland the deglaciation of the main part of Disko Bugt was dated to a minimum of 10.2 ka BP (Long et al., 2003; Lloyd et al., 2005) but less is known about the shelf west of Disko Island.

Given the remaining uncertainty in margin retreat across the shelf in many areas, we follow the procedure adopted in the previous sub-section and construct a small number of plausible but contrasting retreat scenarios. We make changes to the marine extent parameterisation knowing that (1) the ice model must be allowed to reach its newly defined maximum extent at LGM and (2) the ice sheet had essentially retreated from the continental shelf by c. 10 ka BP (Bennike and Björck, 2002). We apply three different parameterisations of Eq. (2) to consider three different shelf retreat

scenarios. The first is a simple linear relationship between maximum grounding depth and eustatic sea-level change:

$\Delta H_c = 10.27 \times (H_{sl} + 52)$ for $\Delta H_{sl} \leq -52$,

$\Delta H_c = 0$ for $\Delta H_{sl} > -52$. (Eqn. 3)

The second produces an early retreat leaving large parts of the shelf ice-free by 14 ka BP - this forcing creates a similar pattern of recession as the original sea-level forcing of the Huy1 model:

$H_c = -0.185 \times (\Delta H_{sl} + 80)^2 + 5.14 \times (\Delta H_{sl} + 52)$ for $\Delta H_{sl} \leq -80$,

$H_c = 5.14 \times (\Delta H_{sl} + 52)$ for $-80 < \Delta H_{sl} < -52$,

$H_c = 0$ for $\Delta H_{sl} \geq -52$. (Eqn. 4)

The third sea-level forcing produces a relatively late (c. 12 ka BP) and very rapid retreat of the ice margin:

$H_c = 6\Delta H_{sl}$ for $\Delta H_{sl} \leq -80$,

$H_c = 0.398 \times (\Delta H_{sl} + 80)^2 + 6\Delta H_{sl}$ for $-80 < \Delta H_{sl} < -52$,

$H_c = 0$ for $\Delta H_{sl} \geq -52$. (Eqn. 5)

In each case the marine retreat does not begin until after 16 ka BP. Further, in all experiments we Prescribe the hybrid mask as detailed in the previous sub-section. The resulting GrIS extent changes for each scenario are shown in Fig. 11.

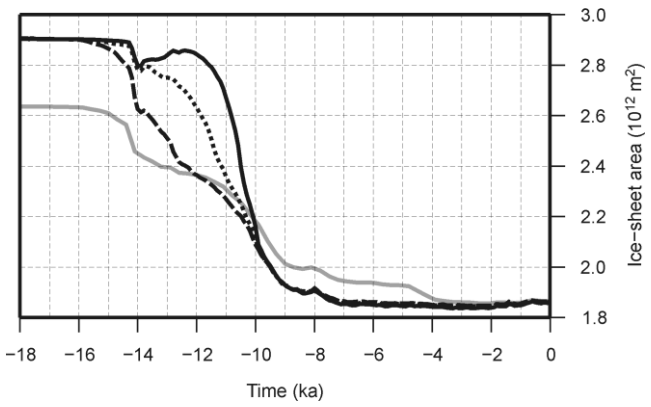

Fig. 11. Ice sheet extent changes for four different sea-level forcing scenarios: original Huy1 model (solid grey), linear retreat from shelf (dotted black), early retreat (dashed black), and late retreat (solid black). Note that the predictions shown in black include the optimum LGM extent discussed in Section 2.3.2.1.

On inspection of Fig. 12, it is clear that the changes made to the sea-level forcing exert a strong control on the predicted timing of the initial RSL fall (note that the colour and style of the lines shown correspond to those in Fig. 11 for a given sea-level forcing). The difference in this timing is most pronounced in areas where the continental shelf is flat and wide and/or there is the presence of cross-shelf troughs. In these areas a small change in the allowed maximum grounding depth of the ice sheet (H_c) can result in a very large migration of the modelled ice margin. In southeast Greenland at Ammassalik (site 11, Fig.12) the timing of initial predicted RSL fall shows a c. 5 ka difference depending on the sea-level parameterisation implemented. Ammassalik sits close to the entrance of the Helheim outlet glacier and its associated cross-shelf trough. The trough is deeper than the surrounding continental shelf and therefore rapidly calves ice once the ice margin reaches its edge. Whereas in south Greenland at Nanortalik (site 10, Fig. 12), where the shelf is narrow, the timing of initial RSL fall shows little sensitivity to changes of the sea-level parameterisation.

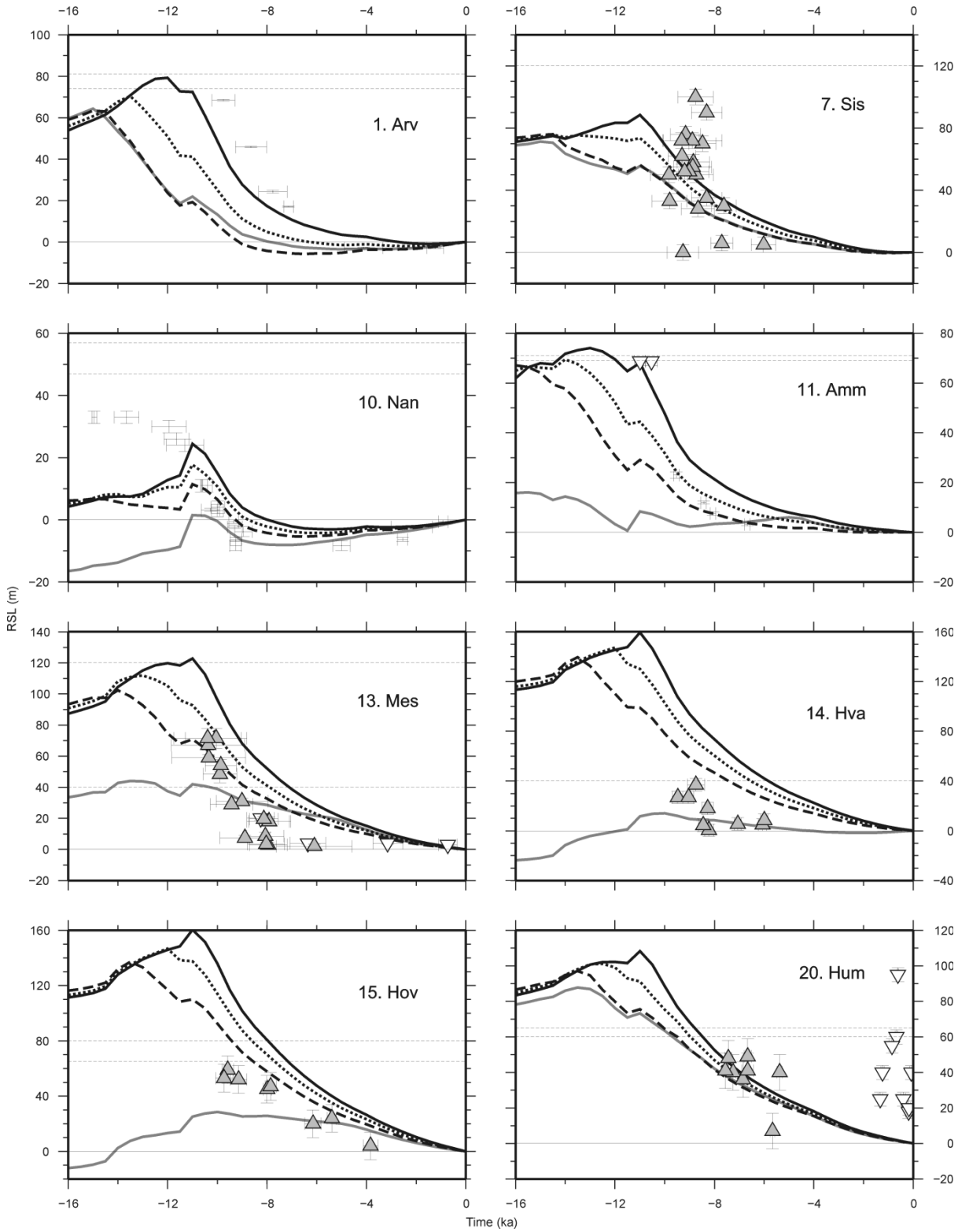

Fig. 12. The influence of different sea-level forcing parameterisations on the sea-level predictions for our reference Earth model. The linear parameterisation (dotted black), the relatively early marine retreat (dashed black), relatively late retreat (solid black) and Huy1 model (solid grey). Upper limiting dates are inverted white triangles. Sea-level index points are represented by both time and height error bars. The HML at each site is indicated by a horizontal dashed line; if two lines are shown their vertical displacement represents the uncertainty in this value.

Across west (site 1), southwest (site 7) and arguably southeast Greenland (site 11) the RSL data favour a relatively late and rapid retreat from the shelf (Fig. 12). The timing of predicted RSL fall from the HML is in better agreement with the sea-level data from these regions. If LGM ice terminated on the inner shelf in west Greenland then we suggest retreat initiated c. 12 ka BP. Elsewhere in Greenland the picture is less clear: with poorer quality limiting dates it is difficult to discriminate between the different parameterisations as in some cases they all provide an adequate fit (e.g. Hovgaard, site 15). If the limiting dates do correspond closely to past mean sea level, then RSL data from the east and northeast could be interpreted as favouring the earlier retreat scenario. Care must be taken when using RSL observations alone to discriminate between the different forcing scenarios due to the sensitivity of the predictions to other poorly known input parameters (e.g. Earth viscosity structure). However, the independent observational evidence discussed above suggests a relatively early deglaciation down the entire east coast of Greenland. As different retreat scenarios are favoured in different regions of Greenland then it indicates the pattern of retreat is not well produced by the model. It is also possible that these differences reflect changes in lateral Earth structure and rheology (see Sub-Section 2.4.3.3). Further, we note that the sea-level parameterisation considers the maximum grounding depth to be a function of the eustatic signal and the expected pattern of sea-level change across Greenland would likely depart significantly from this. Changes to the sea-level parameterisation will only alter the timing of the marine retreat; the spatial pattern of retreat from the continental shelf will remain fairly uniform. Given this, we opt for the relatively late deglaciation scenario as this gives best-fit to the highest quality RSL data from west, southwest, south and southeast Greenland.

Across southwest, south and southeast Greenland we find that the retreat from the shelf is not continuous; the ice model undergoes a marine retreat and subsequent readvance from 14 to 12 ka BP (Fig. 13). This change indicates that, over this period, the migration of the modelled ice margin is

being driven by mass balance changes rather than sea-level rise (this is also evident from the departure of the dark blue from the red line in Fig. 15). The initial retreat of the ice margin can be correlated to Bolling–Allerod (c. 14 ka BP) warming whilst the subsequent readvance marks the transition to the Younger Dryas (YD, c. 11.5 ka BP) cold period. This suggests that any sign of an YD readvance of the ice sheet margin would have been recorded on the continental shelf in the southern sectors of Greenland. Evidence for this can be found in south Greenland where Weidick et al. (2004) argue that the Neria stade records an ice sheet readvance on the inner shelf that occurred shortly before 11 ka BP. Weidick et al. (2004) note that past interpretation of the Neria stade is of LGM age (Kelly, 1985) and that LGM ice extent in west Greenland was similarly interpreted and therefore the chronology there requires similar revision. Indeed, very recent and preliminary findings from a cosmogenic study in west Greenland suggest that a moraine 40 km offshore may be tentatively correlated to the YD (Rinterknecht et al., 2009).

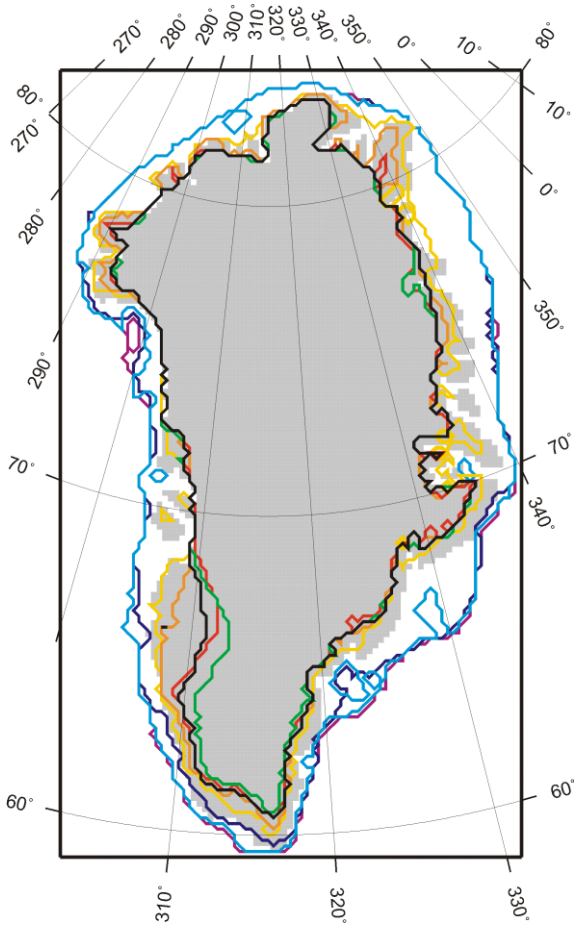

Fig. 13. Modelled ice margin chronology for the new Huy2 model; pink - 16 ka BP, dark blue - 14 ka BP, light blue - 12 ka BP, yellow - 10 ka BP, orange - 9 ka BP, red - 6 ka BP, green - 4 ka BP (minimum extent) and black - present-day. Modelled present-day coastline is shaded dark grey.

2.3.2.3. Temperature forcing

The Huy1 ice model is forced using temperature changes inferred from the GRIP $\delta^{18}O$ ice core record (Dansgaard et al., 1993). The transformation from $\delta^{18}O$ to a temperature record (ΔT) (Eq. (6)) is dependent on a conversion factor (d) and is corrected for elevation changes that occur at the ice core site (ΔT_E):

$$\Delta T\ (t) = d(\partial^{18}O(t) + 34.83) - \Delta T_E(t)\,. \qquad \text{(Eqn. 6)}$$

The conversion factor (d) is equal to the inverse of the climatic isotopic sensitivity (as described in Cuffey (2000)) and taken as a constant. The transformation does not take into account the influence of elevation changes on the climatic isotopic sensitivity. Such changes may well be important over periods of small temperature change (Huybrechts, 2002). This may explain why the temperature forcing of Huy1 shows little evidence of warming over the Holocene period (Fig. 14).

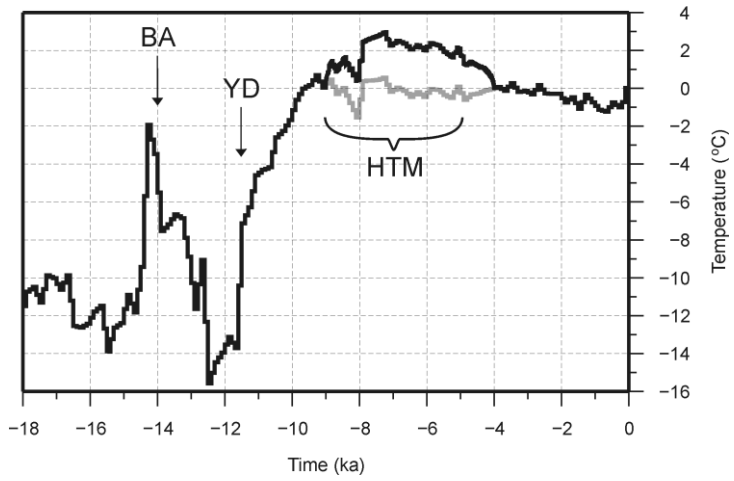

Fig. 14. The Huy1 temperature record (grey) and our revised temperature forcing with imposed Holocene thermal maximum (black) at the GRIP site. Spatial changes made to the temperature forcing over the Holocene thermal maximum are outlined in the text. Annotations show the climatic events of the Bolling-Allerod (BA, c. 14 ka BP), Younger Dryas (YD, c. 11.5 ka BP) and Holocene Thermal Maximum (HTM, c. 9-5 ka BP).

Temperature profiles obtained from ice borehole studies are able to resolve Holocene surface air temperature change at the GRIP and Dye3 sites (Dahl Jensen et al., 1998) and they indicate that the HTM at summit (GRIP) had an amplitude of 2.5 ^{o}C (all temperatures are relative to present-day) and that it was 1.5 times warmer to the southwest (Dye3). Another ice core study from summit Greenland (GISP2) indicates a smaller amplitude HTM (Cuffey et al., 1995). To the north of Greenland the amplitude of the HTM is observed to be 2 ^{o}C at the Agassiz Ice Cap on Ellesmere Island in the Canadian Arctic (Koerner and Fisher, 1990). Given the clear and widespread evidence

for the HTM, we superimpose a parabolic warming to the original temperature forcing of Huy1 so that the above data constraints are broadly reproduced. At GRIP the imposed amplitude of warming is 2.5 ^{o}C and increases linearly with decreasing latitude to reach a value 1.5 times larger at the Dye3 site (the forcing remains fixed south of this). North of GRIP the forcing is decreased linearly with latitude to the site of the Agassiz Ice Cap where it has a value of 2 ^{o}C. We also consider results from Kaufman et al. (2004) (see their Fig. 9) to constrain the spatial and temporal pattern of the HTM in Greenland. Much of the evidence described comes again from borehole studies (Dahl Jensen et al., 1998) that indicate that the HTM peaked during the period 8-5 ka BP at GRIP and between 6 and 3 ka BP at Dye3. Other palaeoenvironmental evidence from lake cores and terrestrial archives supports the finding that warming is generally thought to have occurred later in south Greenland (e.g. Kaplan et al., 2002). In northwest Greenland, warming at the Camp Century site is thought to have occurred between 8 and 4 ka BP (Dansgaard et al., 1971) with similar timing (at least when considering millennial-scale changes) found in the northeast (Bennike and Weidick, 2001). The duration of the imposed HTM changes linearly between 8 and 4 ka BP in the north, 8 and 5 ka BP at summit to 6 and 3 ka BP in the south. Fig. 14 illustrates the temperature record at summit Greenland (GRIP) as implemented for Huy1 (grey line) and for our revised record that includes an imposed HTM (black line).

The Huy1 model is tuned to fit the adapted (P. Huybrechts, personal communication) observations of present-day ice sheet elevation and thickness of Bamber et al. (2001). Given our new imposed HTM warming, the modelled present-day ice sheet elevation and thickness now differs from both the Huy1 model and the present-day observations. As part of the ice model's melt- and runoff treatment (Braithwaite, 1995; Janssens and Huybrechts, 2000); degree day factors (DDFs) are used to calculate the amount of meltwater, eventually leading to runoff after saturation of the snowpack. The DDFs are applied uniformly and for snow and ice melting are 3 and 8 mm/day/^{o}C (water

equivalent), respectively. We therefore make gradual changes to the DDFs over the Holocene period to ensure the present-day ice sheet is produced as closely as possible (Fig.15). The DDFs are reset to their original values over the last few thousand years so that the model evolves to its present-day reference state and therefore matches the modelled present-day volume and extent of Huy1 (which is tuned to fit the observed ice sheet). We find that a reduction of the DDFs by 30% over the mid-Holocene gives the best-fit to the present-day observations. This change to the DDFs is within the typical uncertainty on these model parameters as inferred from direct ablation measurements (Braithwaite, 1995).

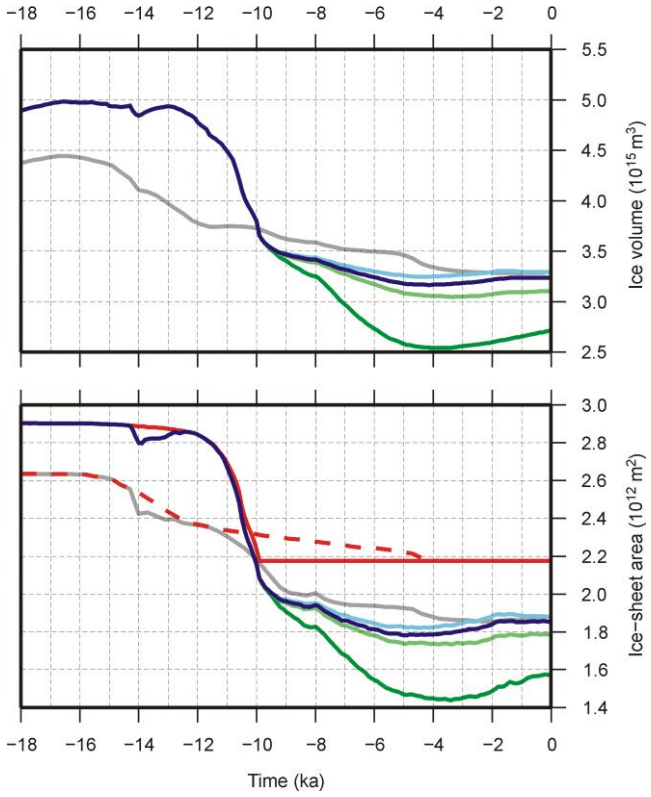

Fig. 15. Predictions of ice sheet volume and extent for the revised temperature forcing. Changes are made to the degree day factors to obtain agreement with the observed present-day GrIS. Changes to the degree day factors are 0% (dark green), -25% (light green), -30% (dark blue - which represents the best-fit) and -35% (light blue). Note that the predictions shown include the optimum LGM extent mask and sea-level forcing discussed, respectively, in Sections 2.3.2.1 and 2.3.2.2. The evolution of the Huy1 model is shown as grey. The maximum allowed ice extent as defined by the LGM mask and sea-level forcing is shown for Huy1 (dashed red) and the new ice model (red).

The influence of the imposed HTM on the sea-level predictions is shown in Fig.16 (compare dotted and solid black lines). It should be noted that for this experiment we prescribe the relatively late deglaciation (c. 12 ka BP) and hybrid mask as detailed in the previous sub-sections. In regions where the ice margin has a larger response to the increased HTM warming we find the RSL curve is lowered over the mid-late Holocene. RSL data from west, southwest and south Greenland are well constrained over this time period. As a result of the imposed warming, predicted mid-Holocene RSL (using our reference Earth model) in west Greenland falls below present-day levels and is in better agreement with the data. The data-model fit is also improved for both southwest and south Greenland; bringing the curve lower and nearer the index point data situated below present-day sea level. We note that RSL predictions are shown relative to present-day sea level, which is why the RSL curve intercepts the y-axis at zero height. This means that imposing a HTM that changes both Holocene and present-day predicted sea level will also impact predictions at earlier times (note differences in the dotted and solid black lines prior to 9 ka BP).

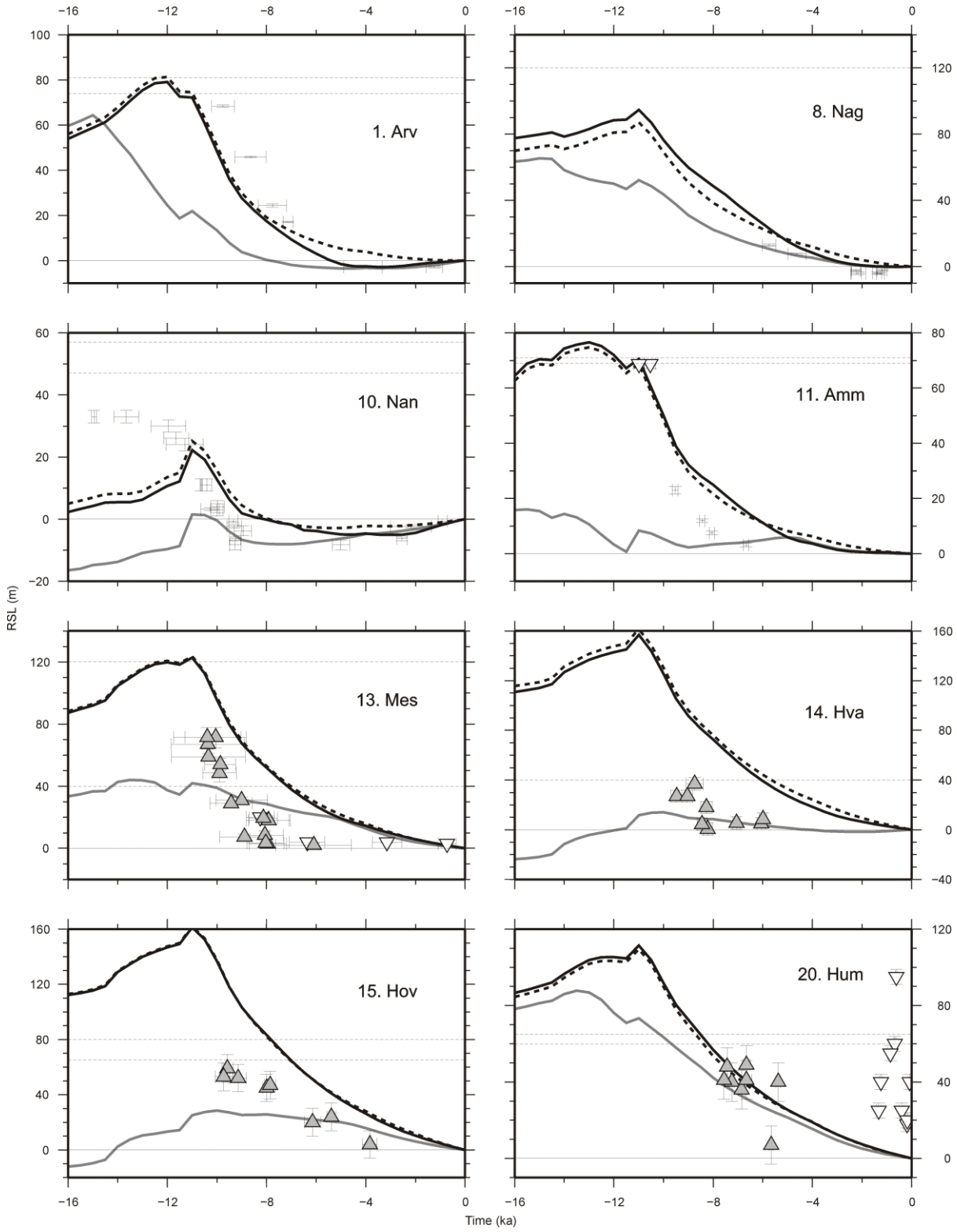

Fig. 16. RSL predictions at selected sites based on our standard Earth model and three different ice models: one that includes a HTM (solid black; see main text for details), one that does not (dotted black) and the original Huy1 model (solid grey). Note that the predictions indicated by the solid black and dashed black lines include the optimum LGM extent mask and sea-level forcing discussed, respectively, in Sub-Sections 2.3.2.1 and 2.3.2.2. Upper limiting dates are inverted white triangles.

Sea-level index points are represented by both time and height error bars. The HML at each site is indicated by a horizontal dashed line; if two lines are shown their vertical displacement represents the uncertainty in this value.

2.3.3. Sea-level predictions based on the Huy2 model

In this section, we adopt the new ice model resulting from the revisions described in Section 2.3.2 (hereafter referred to as Huy2) and compare the RSL data to predictions at all of the data sites.

2.3.3.1. Determining an optimal viscosity model

We computed model predictions for the Huy2 model using the suite of Earth viscosity models described in Sub-Section 2.3.1.1. Comparing these predictions to the data gives the χ^2 values shown in Fig. 17. Comparison of these results to those of Huy1 (shown in Fig. 6), demonstrates that the Huy2 model gives an improved data-model fit. Additionally, it indicates that the class of viscosity models providing good fits with the Huy2 ice model is distinct from those identified for the Huy1 model. For example, Earth models with a 71 km thick lithosphere no longer produce the best-fits; the minimum χ^2 values are obtained by models with a 96 or 120 km thick lithosphere. For the 96 km lithosphere model there is a large zone that indicates fit to the data. This is an unsurprising result given that we have been largely focussing on and trying to reduce misfits between RSL observations and sea-level predictions generated using our reference Earth model. The 120 km lithosphere panel shows that the observations favour small values for the lower mantle viscosity and are generally insensitive to upper mantle viscosities. For Huy2 the best-fit model is a 120 km lithosphere with an upper mantle viscosity of 5×10^{20} Pa s and a lower mantle viscosity of 10^{21} Pa s. We note that a model with a 96 km lithosphere, upper mantle viscosity of 5×10^{20} Pa s and a lower mantle viscosity 5×10^{21} Pa s (close to our reference model) gives almost the same fit so we cannot discriminate between these two Earth models.

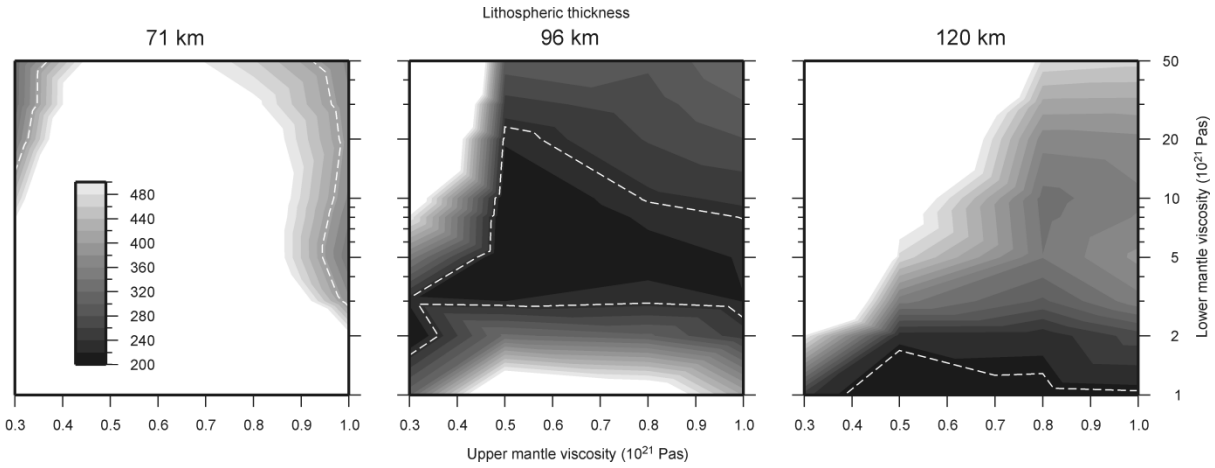

Fig. 17. The Chi-squared results for the Huy2 ice model. The scale bar for the Chi-squared results is shown how in the left-hand frame. The 95% confidence level is marked by the white dashed line.

2.3.3.2. Comparison of Huy2 model to RSL observations

In Fig. 18 we compare predictions for the Huy2 model to data at all sites considered in this analysis. We show the envelope of predictions for the suite of Earth models discussed above (indicated by dashed black lines) and isolate the prediction based on the best-fit 120 km lithosphere model established in the previous subsection (solid black line). For comparison, we also show the equivalent predictions for the Huy1 model (as shown in Fig. 7). A visual inspection of the envelope generated using the Huy2 model shows that across Greenland the data-model misfit has been reduced and, in general, sea-level data lie inside and give fit to the envelope. In the following, we address regional data-model fits of the Huy2 model, with focus on the best-fit result and implications for regional ice histories. Given that constraining a GIA model with RSL data is a non-unique inversion problem, we discuss crucial parameter trade-offs and further examine the independent observational evidence that can help reduce this inherent ambiguity. Further, we compare our results with other modelling work (here on a regional scale and with overall results in Section 2.4).

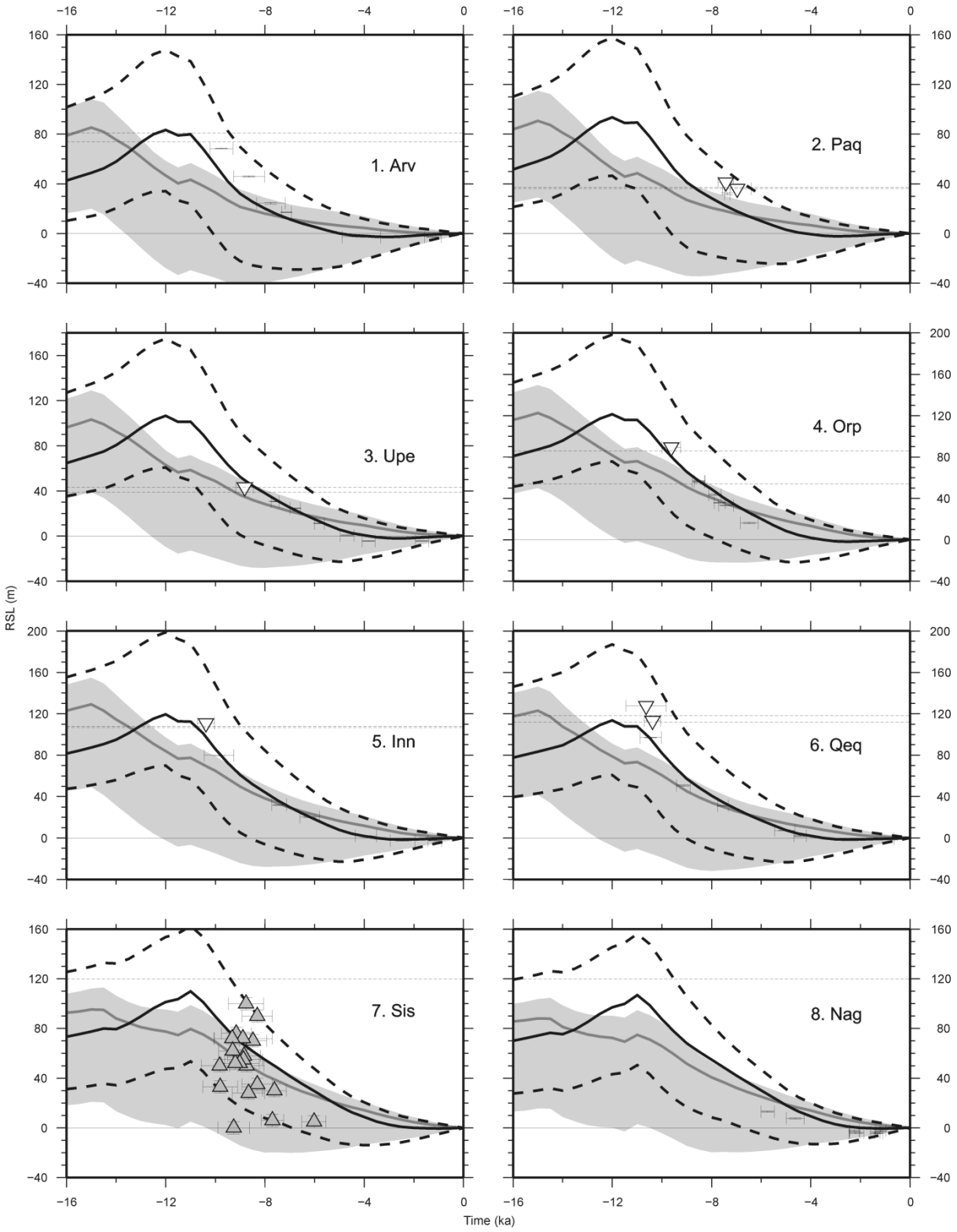

Figure. 18a. RSL predictions for the Huy1 (light grey shaded area) and Huy2 (area enclosed by black dashed lines) ice models based on a suite of 108 Earth viscosity profiles. The solid dark grey line denotes the RSL prediction for the best-fit Earth model of Huy1; characterised by a 71 km thick lithosphere, upper mantle viscosity of 5×10^{20} Pa s and lower mantle viscosity of 5×10^{21} Pa s (see Sub-Section 2.3.1.2). The solid black line denotes the RSL prediction for the best-fit Earth model of

Huy2; characterised by a 120 km thick lithosphere, upper mantle viscosity of 5×10^{20} Pa s and lower mantle viscosity of 10^{21} Pa s (see Sub-Section 2.3.3.1). Lower limiting dates are grey triangles. Upper limiting dates are inverted white triangles. Sea-level index points are represented by both time and height error bars.

Across west Greenland (sites 1-6, Fig. 18a), we find that the Huy2 best-fit prediction gives excellent fit to the majority of index point data; although, as discussed above, the χ^2 results are biased toward this part of the dataset and so this is not a surprising result. The central west coast of Greenland is the location of the Jakobshavn Isbrae ice stream that drains c. 7% of the GrIS (Bindschadler, 1984) into Disko Bugt. It is well accepted that Disko Bugt was covered by ice at the LGM (Kelly, 1985; Funder, 1989; Funder and Hansen, 1996; Weidick and Bennike, 2007) and likely housed a predecessor of the Isbrae. There are also suggestions of a late ice shelf west of Disko prior to the last deglaciation (Bennike et al., 1994). Our modelling results imply that if the LGM ice margin did terminate on the inner shelf then the onset of deglaciation appears to be relatively late, starting c. 12 ka BP, followed by a very rapid retreat leaving the embayment ice-free by c. 10 ka BP (Fig. 13). In a previous interpretation of the sea-level data, Long and Roberts (2003) hypothesised that the Isbrae was able to survive the high rates of eustatic sea-level rise and remain on the shelf west of Disko Bugt because of its high rate of ice discharge and the shallow water depths. The subsequent rapid retreat may well be a consequence of the large bedrock trough that runs out of the entrance of Disko Bugt. Models of tidewater glaciers, supported by observations, have shown that changes in the bedrock topography are the dominant control on such episodes of rapid retreat (e.g. Vieli et al., 2001; Schoof, 2007).

The Sisimiut data (site 7, Fig. 18a) capture the broad sea-level changes over the early Holocene in southwest Greenland. The best-fit prediction does not reproduce these RSL changes well; the predicted sea-level fall is too gradual and the early-Holocene predicted RSL values are generally too

low. However, the upper bound of the predicted envelope indicates that the majority of lower limiting data could be fitted. Nearby at Nagtoralinguaq (site 8, Fig. 18a) the best-fit prediction does not produce the expected late Holocene fall below present-day sea level. The ice margin is known to respond to even moderate warming due to the low accumulation and low altitudes that characterise this region (Letréguilly et al., 1991). Presently the southwest contains the largest area of ice-free land in Greenland across which observational evidence of the Holocene retreat is well recognised. Previous ice modelling studies compared with dated recessional moraine systems show there was a fairly continuous Holocene retreat (Van Tatenhove et al., 1995) and the ice margin was behind the present-day margin after c. 6 ka BP (Van Tatenhove et al., 1996). This is in reasonable agreement with ice history of the Huy1 and Huy2 models; Huy2 retreats behind the present-day margin in southwest Greenland between 7 and 6 ka BP (Fig. 13 shows the 6 ka BP ice margin). The GrB Greenland model of Tarasov and Peltier (2002) shows a good fit to the Inner and Outer Søndre Strømfjord RSL data (Ten Brink and Weidick, 1974) from southwest Greenland but differs from Huy1 and Huy2 in its Holocene evolution; at 10 ka BP the modelled ice margin is at the coastline and by 8 ka BP has retreated well inland of its present-day position to reach its minimum state. After this time, GrB undergoes a readvance in southwest Greenland; comparison of predictions from the ICE-5G model to recent geodetic measurements suggests that this readvance is too large or mistimed (Khan et al., 2008).

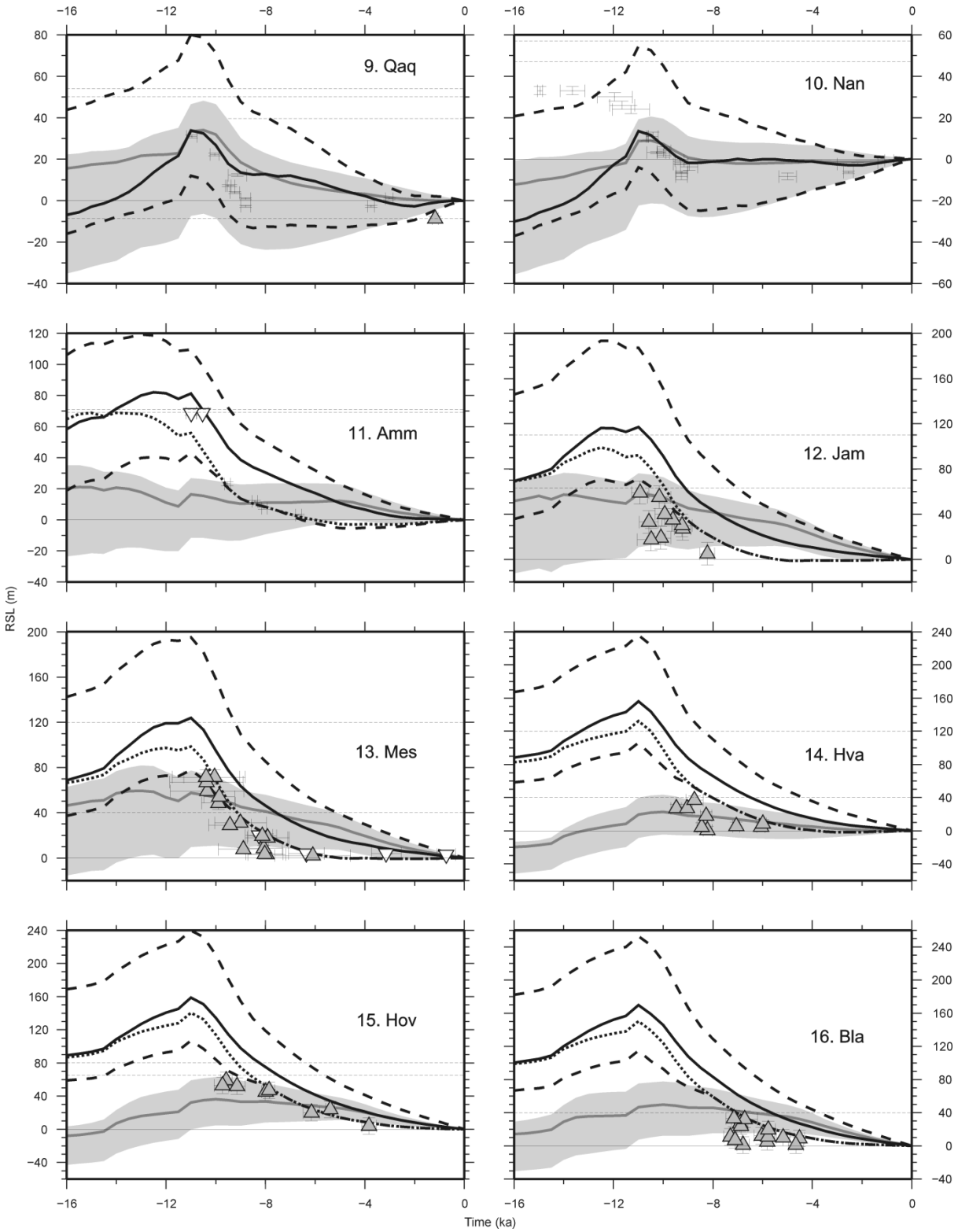

Fig. 18b. *(Continued)*. The dotted black line shown for sites 11-17 indicates the Huy2 best-fit Earth model for regions across east Greenland; characterised by a 120 km thick lithosphere, upper mantle viscosity of 3×10^{20} Pa s and lower mantle viscosity of 5×10^{22} Pa s (see Sub-Section 2.4.2.3). Qaqortoq (site 9) includes additional observational constraints, indicated by two extra horizontal dashed lines. The line at -8.7 m marks a marine basin that shows no evidence of freshwater incursion and defines a lower bound on RSL change. The line at 39.7 m and traced from 9.5 ka BP to present-day marks the minimum age of deglaciation for a basin and defines an upper bound on RSL change.

In south Greenland the Huy2 best-fit model shows little improvement on the Huy1 results. For Nanortalik (site 10, Fig. 18b), the Huy2 envelope does not encompass the earliest two index points; although, as mentioned previously, these data are from an area some distance from the other lakes cored and so should perhaps be plotted on a separate graph (across the Nanortalik lake locations there is a c. 7 m spread in predicted RSL at 14 ka BP). Similar to the GREEN1 Greenland model of Fleming and Lambeck (2004), sea-level predictions for Huy2 suggest insufficient LGM ice load for southern Greenland. Huy2 has LGM (21 ka BP) ice thicknesses of c. 1100 m at Qaqortoq (site 9, Fig. 18b) and c. 900 m at Nanortalik (site 10). A synthesis of the available data by Weidick et al. (2004) suggests that the ice margin in south Greenland was behind its present-day position from c. 9 ka BP. The retreat of Huy2 is not continuous but roughly commences after 16 ka BP and, with good agreement to the observations, reaches the present-day modelled margin at c. 9 ka BP. Another GIA modelling study, in which the best-fit prediction shows good agreement with the RSL data, indicates the ice sheet started an earlier retreat from its LGM position at 22 ka BP and was inland of the present-day coast by 12 ka BP (Sparrenbom, Ph.D. thesis).

The preliminary findings of Long et al. (2008) indicate that the LGM ice load in southeast Greenland as represented in the Huy1 and GrB models is insufficient. The analyses here show that if we allow the GrIS to extend to the shelf edge with retreat off the shelf occurring c. 12 ka BP, the best-fit prediction for Ammassalik (site 11, Fig. 18b) reaches the HML, but does not give fit to the index point data. However, the rate of sea-level fall is reasonably well reproduced by Huy2 and the lower bound of the envelope indicates a fit to the observations may be achieved.

In a similar manner, the lower bound of the predicted RSL envelope tracks the data quite well for both Jameson Land (site 12, Fig. 18b) and Mesters Vig (site 13, Fig. 18b) in the east. Huy2 shows the

fjord ice-free with ice having retreated to the present-day ice margin by 9 ka BP. A date of deglaciation c. 8-7.5 ka BP (Funder, 1987) close to the ice margin suggests a slightly later retreat.

In northeast Greenland, results from Kronprins Eijland (site 17, Fig. 18c), where upper limiting dates can further constrain the predictions, indicate a similar pattern of data-model misfit as seen from southeast and east Greenland. This suggests there may be a common reason why a fit cannot be achieved to RSL observations across the entire east coastline. Huy2 shows a retreat behind the present-day ice margin close to Hvalrosodden (site 14, Fig. 18b) and the lower bound of the envelope indicates that predictions could produce a fall below present-day sea-level.

In north Greenland the best-fit prediction of Huy2 does not fit the data at Jorgen Bronlund (site 18, Fig. 18c). Given that the timing of initial predicted sea-level fall is largely insensitive to Earth structure the trend of observations at Jorgen Bronlund suggests the data-model misfit cannot be resolved using the Huy2 ice history.

Washington Land is close to the Nares Strait which separates Greenland from the neighbouring Ellesmere Island ice sheet. It is well established that these two ice sheets were coalesced at LGM (England, 1999); the final deglaciation of the strait is dated to c. 10 ka BP (Zreda et al., 1999). This is fairly consistent with the timing of ice retreat in Huy2. A synthesis of dates indicates that deglaciation started at the entrances of the strait with the central parts becoming ice-free later (England, 1999). The ice margin of Huy2 is made to terminate at the axis of the straits, it does not coalesce with Innuitian ice and we do not see the pattern of retreat inferred from the HML data. The Huy2 best-fit model shows a relatively good fit to lower limiting data that define a sea-level fall,

although the temporal coverage of these data is poor. The Huy2 model does not show a fall below present-day sea level for northwest Greenland. The nearby Humboldt Gletscher outlet glacier is thought to have readvanced (Bennike, 2002) so we might expect a late transgression.

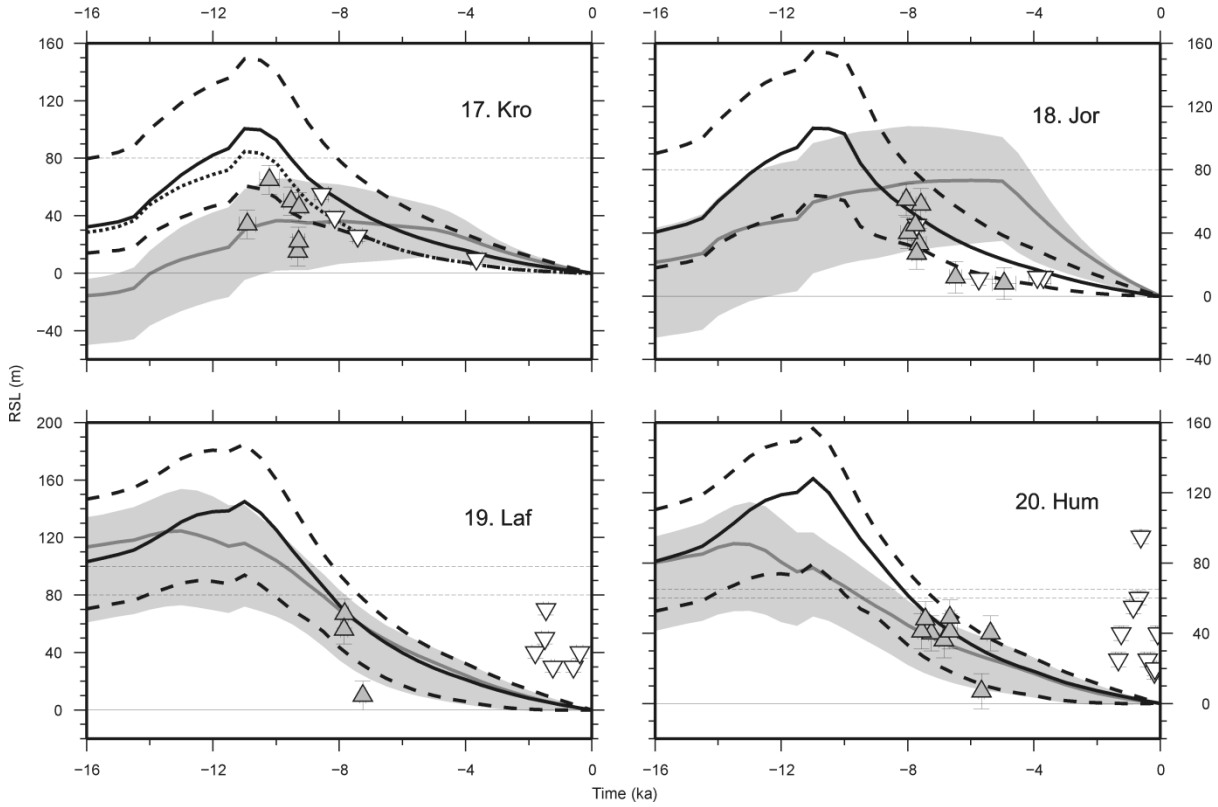

Fig. 18c. *(Continued)*.

When compared to RSL predictions based on Huy1, those generated from theHuy2 best-fit model generally show an improved data-model fit. The Huy2 model improves the fit to the earliest RSL data and in the majority of cases ascertains the HML (except in southwest and south Greenland). For Huy2, the timing of predicted initial RSL fall is later and therefore more rapid than Huy1 and shows better agreement with the data. In west Greenland where RSL observations record a fall below present-day sea level, the Huy2 prediction is able to reproduce this result well.

2.4. Discussion

The Huy2 model was calibrated using RSL data and observations of ice extent. In performing this calibration, we targeted ice model parameters that: (i) were effective in addressing large data-model misfits and (ii) required revision from the previous Huy1 model based on recent observational constraints (LGM margin position, Holocene temperature forcing). Clearly, there are many other parameters that can be varied in our adopted ice model and so the solution (Huy2) is non-unique. However, a more complete sensitivity test goes beyond our aims in this study and so we refer the reader to past analyses of the GrIS for more detail in this regard (e.g. Calov and Hutter, 1996; Greve, 1997; Huybrechts, 1994, 1996, 2002; Ritz et al., 1997; Van de Wal, 1999). In addition, we note Zweck and Huybrechts (2005) performed a comprehensive sensitivity study of northern hemisphere ice sheet evolution in which 11 important parameters were varied. They found that climate parameters are the most important control on ice sheet evolution and extent, suggesting it is uncertainties in the climate forcing, rather than in the ice-dynamic model, that will introduce the largest errors. Changes to the parameters affecting ice flow have the largest influence on ice thickness and the profile of the ice sheet (see also Ritz et al., 1997). Parameter variations in the treatment of isostasy, marine calving and basal processes impacted ice evolution to a lesser degree. Making changes to some of these parameters, therefore, could lead to an alternative solution that provides an improved fit to the data.

It is also plausible that some of the data-model misfits are due to limitations in our adopted ice and Earth models. With regard to the Earth model, the assumption of a laterally homogeneous Earth is likely one of the more significant (see Sub-Section 2.4.2.3). As outlined in the description of the ice model (see Sub-Sections 2.2.2 and 2.3.2), physical processes such as calving and ice stream dynamics are either poorly represented or absent, partly because some of these processes are not fully understood. The Huybrechts (2002) model is built upon the shallow ice approximation, as are the

majority of current ice sheet models. Numerous studies have applied this approximation to successfully simulate the long-term behaviour of continental ice sheets like the GrIS (e.g. Greve, 1997; Huybrechts, 1996, 2002; Letréguilly et al., 1991; Ritz et al., 1997; Van de Wal, 1999). Although this approach can satisfactorily simulate large-scale dynamics, the approximation is inaccurate at the ice margin (Baral et al., 2001) and so could significantly impact our RSL predictions as these are sensitive to relatively small changes in margin position (see also Sub-Section 2.4.2.2). This issue is therefore an important target for future research. We note that there are a few three-dimensional ice sheet models which include higher-order stress gradients (e.g. Pattyn, 2003; Saito et al., 2003) but these are computationally intensive and so cannot be used effectively in the type of analysis presented here (which requires the generation of multiple simulations over 100 ka time intervals).

2.4.1. GrIS ice history and palaeoclimate: Huy2 model

2.4.1.1. Large-scale changes since the LGM

Broadly speaking the Huy2 model indicates a larger LGM extent and volume, a more rapid retreat from the continental shelf and larger retreat in response to the HTM when compared to the Huy1 model (Fig. 15). Ice thickness evolution for the times 18, 10 and 4 ka BP illustrates the major changes of the Huy2 model (Fig. 19). Accompanying plots of RSL evolution show that the 10 ka BP time-slice gives a close match to maps of the HML (Funder and Hansen, 1996; Weidick and Bennike, 2007). Huy2 has an LGM (21 ka BP) volume of 4.1 m (Huy1 has 2.7 m) excess ice-equivalent sea level; larger than the estimates of between 2 and 3 m from Clark and Mix (2002). Huybrechts (2002) finds, by altering crucial ice model parameters, LGM ice-equivalent sea level for Huy1 varied between 1.9 and 3.5 m (that is ±30% of his best estimate of 2.7 m).We would expect a similar ±30% variation in LGM ice-equivalent sea level for Huy2 if these sensitivity experiments were performed again. As with Huy1, the Huy2 model reaches its maximum volume at 16.5 ka BP, when it contains 4.6 m excess ice-

equivalent sea level (Huy1 has 3.1 m). The volume is predicted to be a maximum at this time as increased accumulation rates in Greenland (Cuffey and Clow, 1997) still outweigh the larger ablation from increased temperatures. The sea-level forcing of Huy2 means the marine retreat does not begin in earnest until after 12 ka BP; changes to the ice sheet before this time are therefore driven, mainly, by temperature and accumulation changes. For comparison, the GrB model maintains its full glacial extent until 12 ka BP and reaches its maximum volume just prior to the Holocene, while GREEN1 favours a deglaciation starting at 14 ^{14}C (c. 16.3 ka BP). The subsequent marine retreat of Huy2 is very rapid and largely a consequence of the sea-level forcing. However, there is a difference between the maximum extent allowed by the marine parameterisation and the output from the model (Fig. 15), indicating that some aspects of the retreat were caused by increased temperatures. Warming that took place after the YD was abrupt and temperatures may have increased by 10 ± 4 ^{o}C in central Greenland (Grachev and Severinghaus, 2005).

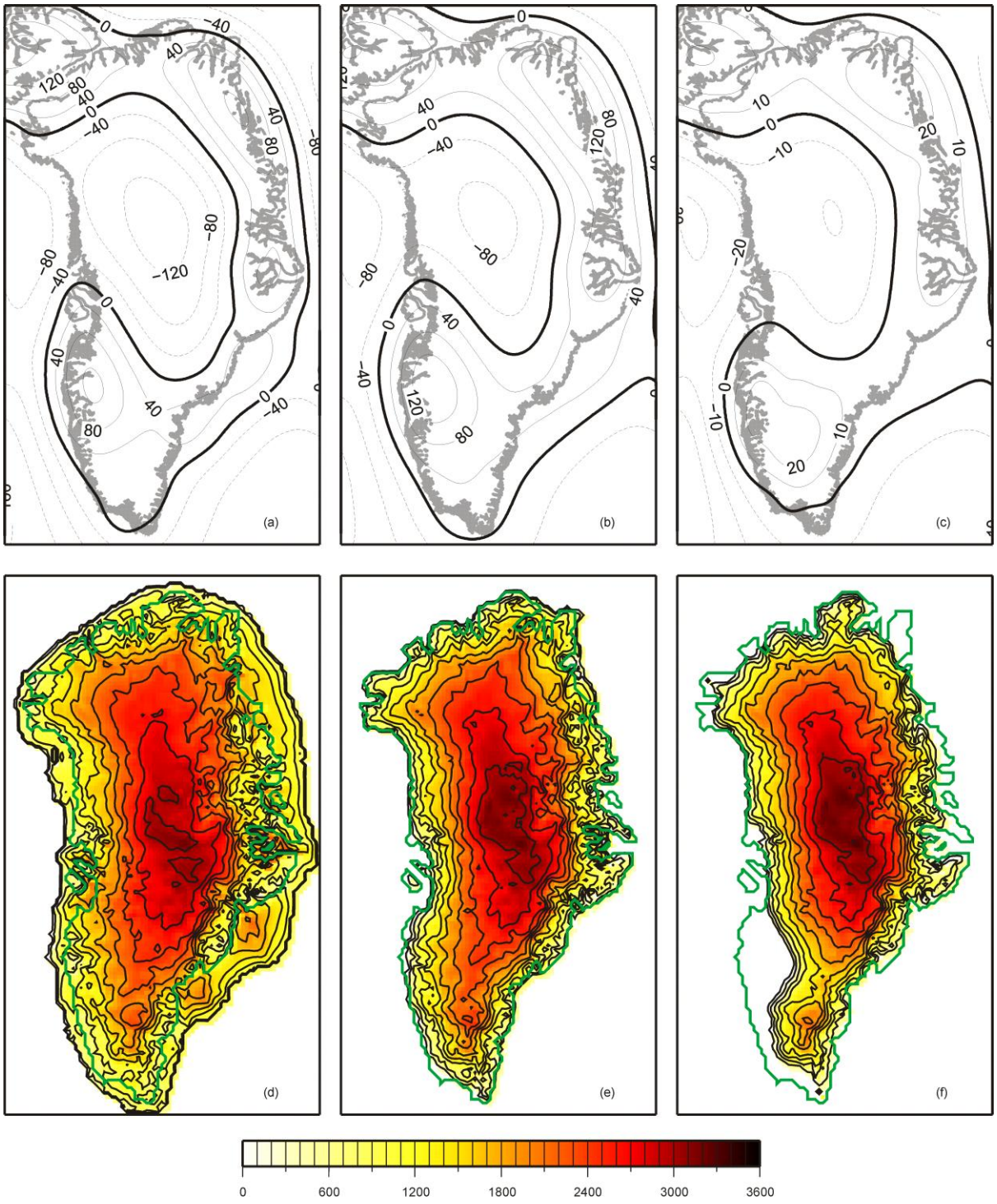

Fig. 19. Top frames show spatial plots of RSL (metres) generated from Huy2 with our reference Earth model for the times (a) 18, (b) 10 and (c) 4 ka BP. Actual coastline is outlined by the grey line. Bottom frames show Huy2 ice thickness evolution (in metres) for the times (d) 18, (e) 10 and (f) 4 ka BP. Modelled present-day coastline is outlined by the green line.

2.4.1.2. The retreat behind present-day ice margin and neoglacial regrowth

For Huy2, the timing of retreat behind the present-day modelled margin is between 8 and 6 ka BP in west and southwest Greenland and around 9 ka BP in the south (Fig. 13). This is in good agreement with both the regional observations described above and a synthesis of deglaciation dates taken from close to the present-day ice margin (Bennike, 2008). Huy2 reaches a minimum state at 4-5 ka BP with a retreat of up to 80 km in the southwest, 20 km in the south and 80 km near Hvalrosodden (site 14) in the northeast of Greenland. We note that the horizontal resolution of the model (20 km) limits the accuracy and reliability of margin prediction over these relatively short distances. The response to the HTM corresponds to a deficit volume of 0.17 m ice-equivalent sea level (relative to present-day); illustrating that changes in the ice margin position, of the order of 10s km, correspond to small changes in eustatic sea-level. In comparison, Huy1 predicts a minimum state at 3 ka BP with a 50 km retreat in southwest Greenland but with very little change in ice volume. Some observational evidence at the ice front has enabled the reconstruction of past glacial transport routes that suggest the ice margin in west Greenland was 15-20 km inland of its current position (Weidick et al., 1990). Previous ice modelling studies that compared model output with dated recessional moraine systems (Van Tatenhove et al.,1995,1996) place the retreat up to 50 km behind the present-day modelled margin in southwest Greenland. Fleming and Lambeck (2004) introduce a neoglacial component to GREEN1 which suggests a retreat of c. 40 km behind the observed present-day margin in west Greenland. Tarasov and Peltier (2002) show ice volume and margin changes for GrB that indicate the ice model reached a minimum state around 8 ka BP (the magnitude of margin retreat was not specified). These latter two studies concluded that a neoglacial regrowth of the GrIS is required to fit RSL data from west Greenland. We note that Sparrenbom (Ph.D. thesis) reached the same conclusion for the south of Greenland.

2.4.2. Data-model misfits

The results shown in Fig. 18 show that the Huy2 ice model cannot account for all data-model misfits evident from Huy1 in Fig. 7 (for a wide range of plausible 1-D viscosity models). Here we briefly consider the influence of non-Greenland ice load, the mismatch between present-day observed and modelled ice surface elevation and lateral changes in Earth structure.

2.4.2.1. Role of non-Greenland ice load

The total global ice load, as outlined previously, is the amalgamation of Greenland ice (Huy1 or Huy2) and non-Greenland ice (ICE-5G). Given the close proximity of some ice sheets to Greenland, most prominently the Laurentide ice sheet, it is not surprising that they have an effect on the sea-level history of Greenland (this issue is the focus of Chapter 4). Fleming and Lambeck (2004) demonstrated that together the North American and European ice sheets made a contribution to sea-level change around Greenland on the order of 10s of metres. It should be noted that in the ICE-5G reconstruction, North American ice load has an LGM volume of 74 m ice-equivalent sea level and is characterised by a multidomal structure (see Peltier (2002) for the model description). The influence of the ICE-5G loading history, minus the Greenland component, on RSL predictions is shown in Fig. 18. For Arveprinsen (site 1), Nanortalik (site 10) and Mesters Vig (site 13), we find that non-Greenland ice mass loss and the associated direct effect dominate the predictions at early times and this results in RSL fall. After 8 ka BP, North American ice has largely melted and so the dominant effect is vertical land motion associated with subsidence of the peripheral bulge leading to a net RSL rise. This pattern of RSL change is broadly similar to the results of Fleming and Lambeck (2004); although we note that there are significant differences in northwest Greenland. At Humboldt Gletscher (site 20, Fig. 20), for example, we find predictions show a continuous fall from c. 150 m at

20 ka BP. Lafayette Bugt is in such close proximity to Ellesmere ice that the solid surface undergoes postglacial rebound rather than forebulge collapse.

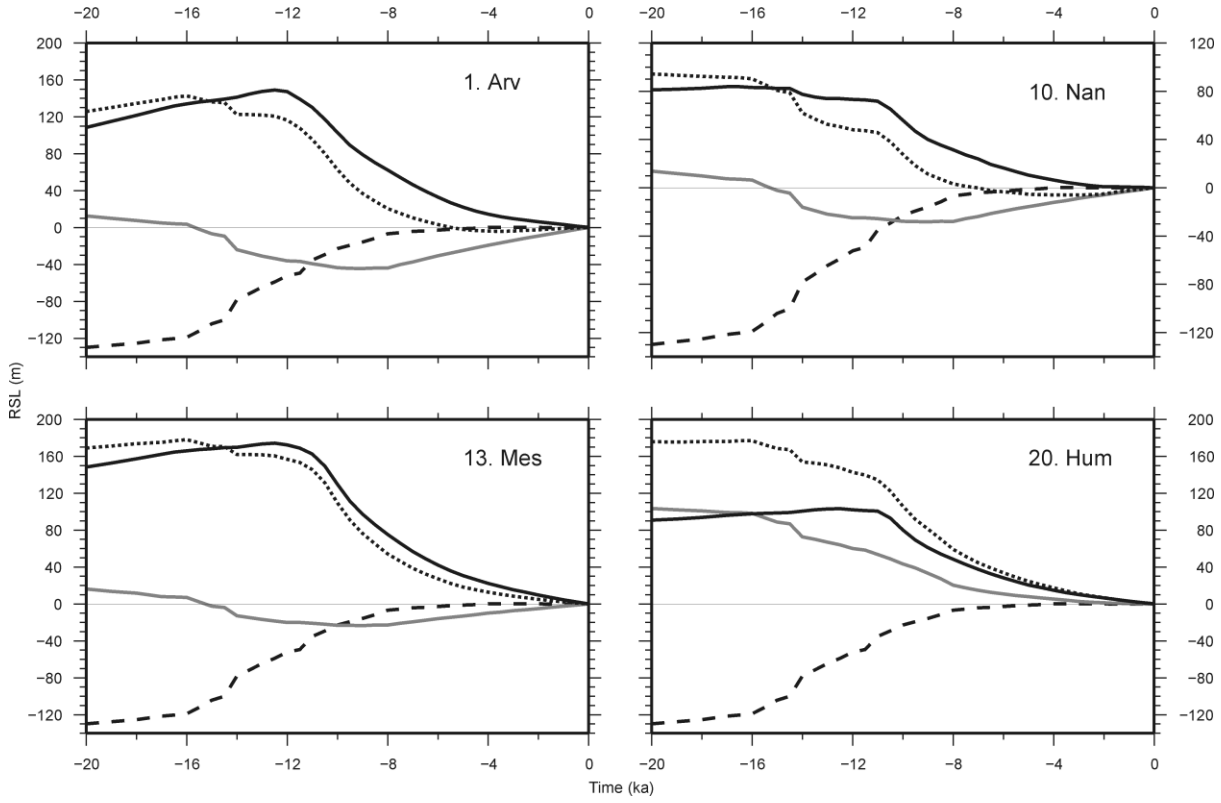

Fig. 20. The influence of Greenland ice load (Huy2; solid black), non-Greenland ice load (ICE-5G; grey line) and their sum (black dotted) on sea-level predictions at four sites around Greenland for our reference Earth model. The black dashed line represents eustatic sea level for the total (Greenland plus non-Greenland) ice model.

Over the Holocene period we find that RSL change driven by non-Greenland ice load changes can sometimes be equal and opposite to that driven by Greenland ice load changes. This effect is particularly marked for sites in the west and south. At Nanortalik (site 10, Fig. 20), for example, at 8 ka BP the predictions for non-Greenland and Greenland ice load are -30 and 30 m, respectively. Two spatial plots show the influence of vertical land motion on RSL from Greenland and non-Greenland ice at 10 ka BP (Fig. 21).

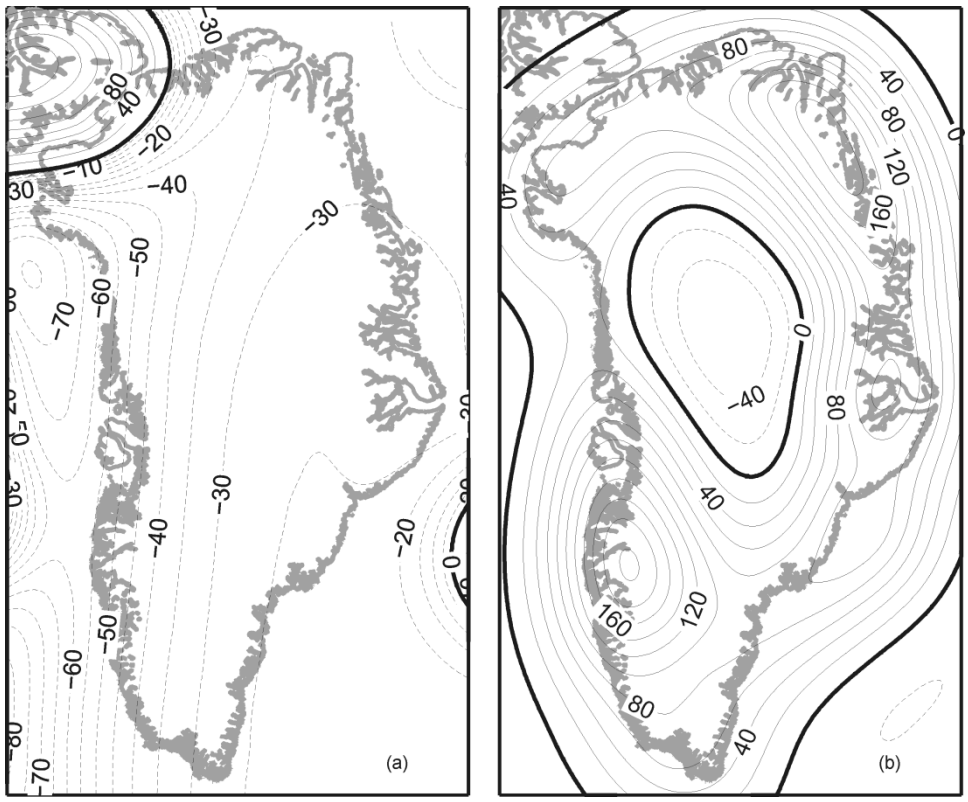

Fig. 21. Spatial plots of RSL predictions (in metres) generated using our reference Earth model and showing the vertical land motion component at 10 ka BP; for (a) non-Greenland ice (ICE-5G) and (b) Greenland ice (Huy2).

2.4.2.2. Comparison to present-day ice sheet

Huy2 gives a root mean square fit to the observed surface elevation and ice thickness of 292.1 and 239.3 m, respectively (the Huy1 model gives very similar values of 293 and 238.7 m). Observations of present-day ice sheet elevation and thickness have been adapted (P. Huybrechts, personal communication) from Bamber et al. (2001). The difference between observed and modelled (Huy2) ice surface elevation (Fig. 22) is small over the central parts of the ice sheet and large at the ice margin. The model clearly over-predicts present-day ice elevation (and thickness although not shown) along the margin. This misfit appears largely due to differences between the location of the modelled and observed ice margin. The gradient at the margin is steep and a misfit between observed and modelled ice margin location will result in large differences between the

corresponding observed and modelled ice elevation. This will have repercussions for the predicted RSL histories since they are very sensitive to changes in the ice margin position. The misfits between observations and model are a combination of the simplifications made in the climatic forcing, the physics of ice flow (see start of Section 2.4), and shortcomings in the observational data used as input. It is difficult to ascertain exactly which factors are dominant and therefore explain certain features in Fig. 22a. Another likely reason for the misfit is the ice model grid spacing, which is too large to resolve or account for small-scale processes at the margin. The 20 km ice model discretisation, which is standard in many glacial cycle simulations, is now regarded as too coarse. Moreover, conventional numerical schemes are known to introduce systematic errors at the ice margin (Huybrechts et al., 1996; Van den Berg et al., 2006).

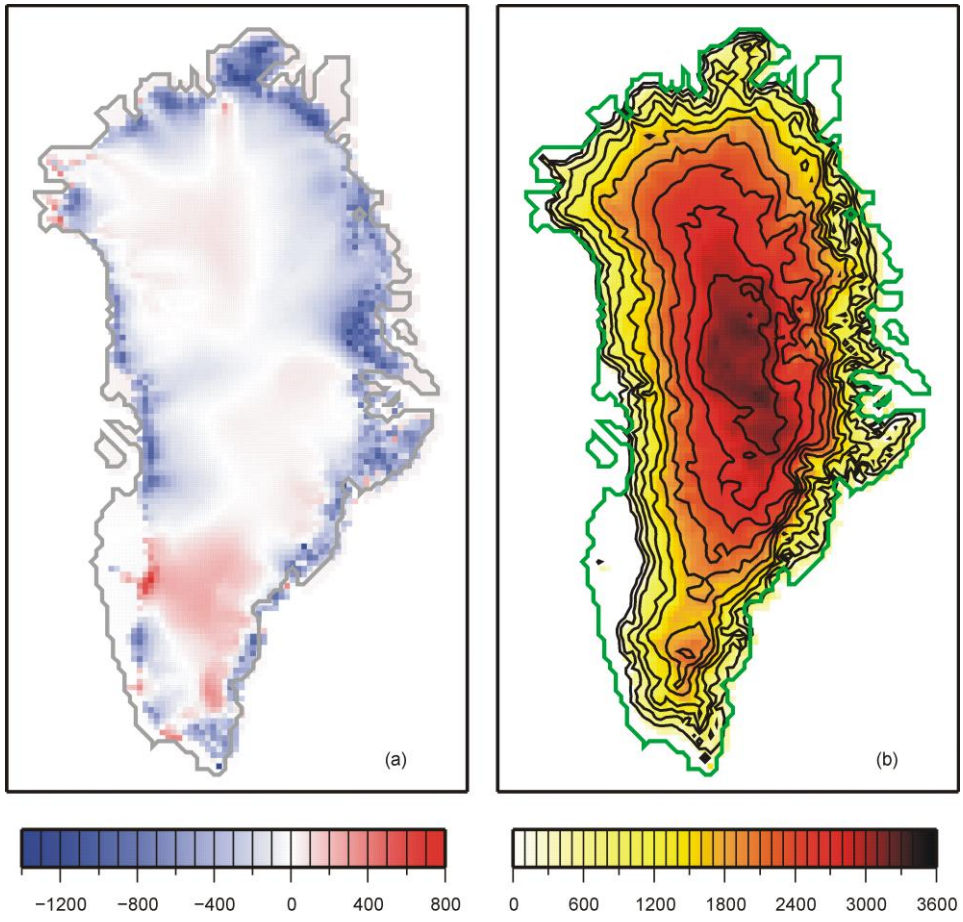

Fig. 22. (a) Observed minus modelled (Huy2) ice surface elevation (metres). Modelled present-day coastline is outlined in dark grey. (b) Huy2 modelled present-day ice thickness (metres). Modelled present-day coastline is outlined in green.

2.4.2.3. Lateral changes in Earth structure

The Earth models used in this and the majority of GIA studies are 1-D only and so do not account for lateral variations in Earth structure. This model limitation may offer another explanation as to why data-model misfits cannot be reconciled. The geology of Greenland is largely Precambrian in age with flood basalts present on the central west and east coastline that define the past track of the Iceland plume beneath the continent (Henriksen et al., 2000; Storey et al., 2004). The trace of the plume track may indicate why there is a general trend of decreasing seismological lithospheric thickness as you move from west to east (Kumar et al., 2005). Farther east in Iceland, rapid rates of

postglacial rebound indicate a very thin mechanical thickness (Sigmundsson, 1991). Darbyshire et al. (2004) find a similar pattern of decreasing seismological lithospheric thickness; they also find that the lithosphere exhibits higher shear wave velocities than the seismic model PREM (on which our Earth model is based) (Dziewonski and Anderson, 1981).

In order to make a preliminary assessment of the magnitude of lateral structure required to address some of the remaining data-model misfits, we divide the RSL data between west Greenland (sites 1-8) and regions across east Greenland (sites 11-17). Data outside these regions are omitted. For these separate datasets the χ^2 test is repeated and, in this case, the observational error of the limiting dates is taken into account. For the case of a 120 km thick lithosphere, the east Greenland data very clearly favour a reduced upper mantle viscosity when compared to west Greenland (Fig. 23). A plot of the east Greenland best-fit model (Fig. 18, dotted black line) illustrates the excellent fit that can be achieved when fitting these data independently. This result certainly suggests that lateral variation in Earth properties can accommodate at least some of the data-model misfit shown in Fig. 18.

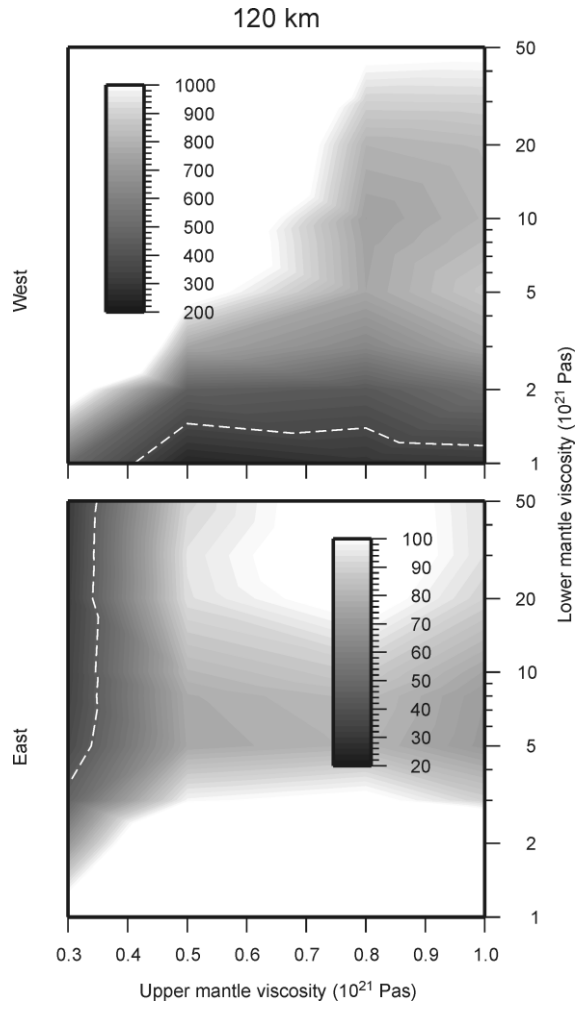

Fig. 23. The Chi-squared test based on the Huy2 ice model and assuming a 120 km thick lithosphere. The two frames are based on data from either west (top) or east (bottom) Greenland. A scale bar for the Chi-squared results is shown how in each frame (note the difference in magnitude between frames. The 95% confidence level is marked by the white dashed line.

2.5. Conclusions

1. The new Huy2 ice history for Greenland shows good agreement to the sea-level data and is also well constrained by independent observations of ice extent.

2. The Huy2 model contains 4.1 m excess ice-equivalent sea level at the LGM (21 ka BP); this is larger than previously found, mainly because the ice sheet now grounds further out on the continental

shelf in the east. The ice sheet did not reach its maximum volume of 4.6 m excess ice-equivalent sea level until 16.5 ka BP.

3. Our results suggest that the ice margin retreat from the continental shelf may not have been continuous and a readvance may have occurred over the Younger Dryas period. Final retreat from the continental shelf began late (c. 12 ka BP) and retreat was rapid such that the GrIS was inland of the present-day coastline by 10 ka BP.

4. The reaction of the ice sheet to the Holocene Thermal Maximum may have produced a margin retreat of up to 80 km across the southwest sector of the ice sheet. This corresponds to a deficit volume of 0.17 m ice-equivalent sea level. This relatively large response of the GrIS to the imposed HTM improves the RSL data-model fit but we cannot be sure that it is a robust constraint given uncertainties in other model parameters.

5. The role of non-Greenland ice is significant. Especially over the last 8 ka BP across the southwest sector where Greenland and non-Greenland contributions to RSL are equal and opposite.

6. The fit of Huy2 (and Huy1) to present-day observations indicates that the model does not accurately reproduce the present ice terminus position and over-predicts ice load at the margin. This will likely have a significant impact on the RSL predictions.

7. A significant improvement to the RSL data-model fit was obtained when modelling data from the east and west independently. This suggests an east-west change in Earth structure. On the other hand, it is also plausible that these differences reflect inaccuracies in the modelled pattern of ice margin retreat (see Sub-Section 2.3.2.2).

Chapter 3:

Present-day vertical land motion in Greenland.

3.1. Introduction

The ongoing response of the Earth, in regions of past and present glaciation, records a unique pattern of surface load change. The development of space-geodetic techniques over the last two decades has enabled us to image this pattern of deformation to a high degree of precision. GPS measurements are able to determine the rate of present-day Earth deformation to within a mm/yr. In North America and Eurasia, GPS observations show that the Earth is deforming in response to past ice mass loss that occurred from the LGM up until the eventual diminishment of these ice sheets in the early Holocene (e.g. Milne et al., 2001, Sella et al., 2007). In these areas, the present-day velocity field is governed, largely, by the deglaciation history and the Earth's viscosity structure. Generally speaking, the highest rates of uplift correspond to areas of thickest ice at the LGM. Whilst present-day deformation in these regions is dominated by the continuing viscous relaxation of the Earth's mantle in response to past ice mass changes, in areas currently glaciated, like Greenland, the rate of present-day deformation is complicated by the additional signal associated with the Earth's elastic response to contemporary ice mass changes. Recent GPS observations, for example, have revealed very high rates of elastic uplift caused by current ice mass loss from outlet glaciers in the southeast of Greenland (Khan et al., 2007). The present-day deformation field in Greenland, therefore, is the sum of the viscous signal associated with past ice changes and the instantaneous elastic signal due to mass changes during the monitoring period. As this pattern of Earth response is

complex and given the small number and limited coverage of GPS observations (see Section 3.2), Greenland GIA models have yet to be calibrated to GPS data.

The ongoing Greenland GPS Network project (GNET) aims to establish around 50 new continuous GPS stations around the periphery of the ice sheet (see www.polenet.org). The number and coverage of GPS observations, therefore, is set to dramatically increase in the coming years, resulting in a far more extensive dataset. The accurate interpretation of this data set requires the elastic and viscous components of the motion to be isolated. Khan et al. (2008) demonstrated one method for achieving this goal: Altimetry and interferometry satellite data (e.g. Rignot and Kanagaratnam, 2006; Stearns and Hamilton, 2007) can be used to estimate contemporary ice mass change and therefore the corresponding elastic term. If the elastic term is then removed from the observed rate of uplift, we can assume that the remaining signal is the viscous component, which can then be compared to GIA model predictions to place constraints on both past ice mass changes and Earth viscosity structure. An alternative approach to that adopted by Khan et al. (2008) involves the reverse procedure; the use of a well-calibrated GIA model to predict and remove the viscous component of the signal so that the residual can be employed to infer contemporary ice mass changes. Regardless of the approach taken, GIA models have a central role to play in arriving at a robust understanding of contemporary land motion in Greenland observed using GPS.

The primary aim of this Chapter (Section 3.3) is to use the Huy2 model to predict contributions to the present-day vertical land motion in Greenland associated with different aspects of the loading history (in both time and space). Deconstructing the signal in this manner will be useful when using the model in the above-described applications. The predictions generated using the Huy2 model are also compared to some published GPS data. Recent work has shown predicted present-day uplift

rates are potentially very sensitive to ice mass changes over the last two millennia (Ivins and James, 2005). As a secondary aim of this Chapter (Section 3.4), we explore this issue for Greenland but focus on the shorter timescale of a few centuries. RSL data used to calibrate Greenland GIA models (e.g. Long et al., 1999), are largely dated to the Holocene period and are unable to resolve changes over century-scales (or less). Thus, for models such as Huy2, there is little constraint on changes over the past millennia, particularly over century timescales. Recent analyses have considered changes of the GrIS over the last hundred years or so (e.g. Hanna et al., 2002, 2005; Huybrechts et al., 2004; Box et al., 2006; Rignot et al., 2008; Wake et al., 2009). Therefore, improved models of recent ice sheet behaviour are available to consider what role ice mass changes over the past few centuries play in determining the present-day Earth response. Of these new models, we use the surface mass balance (SMB) reconstruction of Wake et al. (2009), which covers the period 1866-2005. We show predicted present-day uplift rates generated using the Wake et al. (2009) model and compare these results to predictions of the Huy2 model for the last 100 years of loading change. In the final part of Section 3.4 we amalgamate the loading history of the Huy2 model with the reconstruction of Wake et al. (2009) and compare the resulting predictions to the GPS data.

3.2. GPS observations

There are only a small number of GPS stations in Greenland that have been operational for more than a few years and therefore yielded useful results (e.g. Wahr et al., 2001a; 2001b; Dietrich et al., 2005; Khan et al., 2007; 2008). Figure 24 shows the locations of the GPS stations considered in these past studies. Initial work was conducted by Wahr et al. (2001a); they analysed data from Kellyville and Kulusuk and determined uplift rates of -5.8 ± 1 mm/yr and -2.1 ± 1.5 mm/yr, respectively. The high rate of subsidence observed at Kellyville was attributed to a neoglacial regrowth of the southwest margin of the GrIS over the last 3-4 ka BP. A following study included GPS data from Thule, in northwest Greenland, which determined an uplift rate of -0.7 ± 0.9 mm/yr (Wahr et al.,

2001b). Dietrich et al. (2005) showed results from a GPS network of 10 sites, spread across the ice-free coast of southwest Greenland. Campaign-style (repeated) observations were made at these sites; the locations of which are shown by the circles in Figure 24. Data from the central site (Kangerlussuaq) - situated close by to Kellyville (see Fig. 1) - produced an absolute uplift rate of -3.1 ± 1.1 mm/yr. They also computed relative rates of uplift and established that the southwest region has an east-west gradient of present-day vertical Earth motion. Areas close to ice margin are subsiding but this changes to uplift as one moves west and towards the outer coast (see Fig. 8, Dietrich et al., 2005). This pattern of response was also ascribed to a readvance of the GrIS in southwest Greenland over the last 3-4 ka BP. The advantage of examining relative rates of uplift across a regional network is that issues surrounding the stability of the reference frame are minimised. The error term is estimated to be 1 mm/yr for all the relative rates presented by Dietrich et al. (2005). Most recently, Khan et al. (2008) extended the work of Wahr et al. (2001a,b) by reanalysing longer time series from Kellyville, Kulusuk and Thule. They also had access to data from GPS stations at Scoresby Sund in east Greenland, Qaqortoq in the south and also data from a tide gauge at Nuuk, which is on the southwest coast. We show the tide gauge and GPS locations (Fig. 24, stars) and corresponding secular uplift rates (Table. 2) determined by Khan et al. (2008). Note that the error terms reported in Table 2 are based on one-sigma formal errors but include other effects to provide a more realistic error estimate (see Khan et al., 2008).

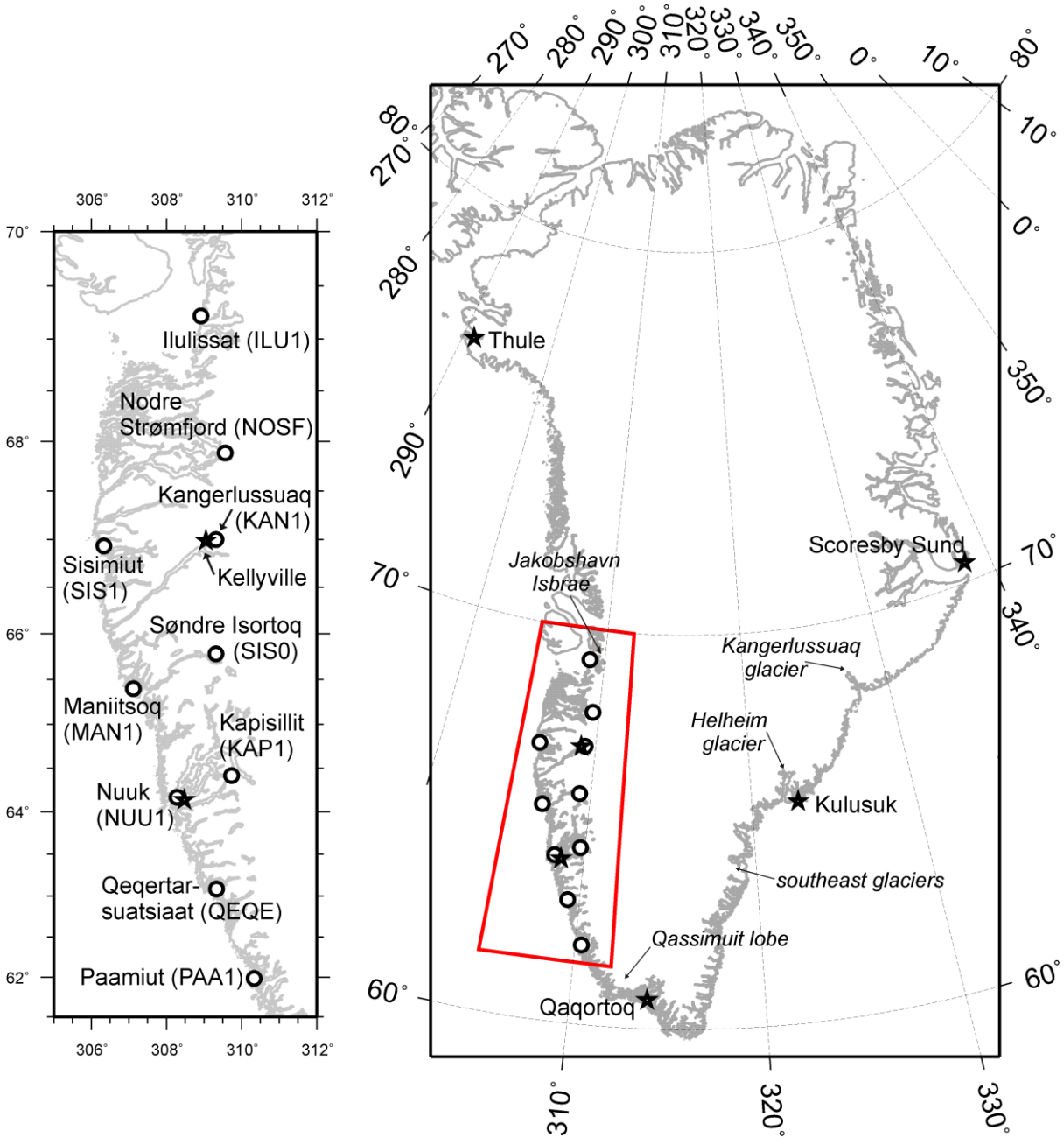

Fig. 24. Locations of GPS sites discussed in the text. The red box on the map to the right outlines the zoom box shown on the left. Observations made by Khan et al. (2008) and Dietrich et al. (2005) are marked by stars and circles respectively. In reality, the tide gauge and GPS campaign position at Nuuk lie in the same location, the star has been moved slightly to make sure both symbols are distinguishable.

The results from the GPS data reanalysis by Kahn et al. (2008) differ significantly from the earlier results of Wahr et al. (2001a, b); most notably for Kellyville. The rate determined for Kellyville is also

different to that obtained by Dietrich et al. (2005) for the nearby station (c. 20 km) at Kangerlussuaq. These differences can be attributed to the use of different reference frames for these separate analyses and/or also a consequence of the use of different processing techniques (Dietrich et al., 2005; Khan et al., 2008). Further, we note that Khan et al. (2008) corrected for elastic uplift arising from present-day ice mass change when calculating secular uplift rates. They account for the large contemporary ice mass loss occurring in southeast Greenland; principally at the major outlet glaciers of Helheim and Kangerlussuaq but also from the regions coastal glaciers (see also Khan et al., 2007). In their most recent analysis (Khan et al., 2008) they also correct for ice mass loss from Jakobshavn Isbrae in central west Greenland (Fig.24).

We analyse only vertical rates of uplift as observed horizontal rates are unpublished. Given that there is a large range in past solutions for absolute uplift rates in Greenland, we are cautious when comparing these data to model results. In terms of absolute rates, we focus on the results presented by Khan et al. (2008) as we consider these to be most accurate at this time (in addition, they are the only authors that correct for the contemporary elastic term). We also compare our results to the relative rates presented by Dietrich et al. (2005).

3.3. Modelling: Huy2

We refer the reader to Sub-Section 1.4.1 for a description of the GIA model components. The predictions of present-day uplift rates were calculated using an algorithm based on that detailed by Mitrovica et al. (1994).

3.3.1. Predicted present-day uplift rates

Figure 25 shows predicted present-day uplift rates generated using the complete Huy2 ice loading history (122 ka BP to present-day) with its corresponding best-fit Earth model; characterised by a 120 km thick lithosphere, an upper mantle viscosity of 5 x 10^{20} Pa s and a lower mantle viscosity of 10^{21} Pa s. This Earth model produced best fit to the sea-level data considered in Chapter 2 (see Sub-Sections 2.3.3.1 and 2.3.3.2). The predictions in Fig. 25 also take into account changes in non-Greenland ice (the ICE-5G model of Peltier (2004)) and the ocean load. Inspection of Fig. 25 shows the Earth is largely uplifting across the north and east of Greenland, with highest rates of uplift in the northeast that are in excess of 4 mm/yr. The central parts of Greenland are subsiding at around -0.5 mm/yr, the central west and southeast coasts exhibit a weak response that is less than ± 0.5 mm/yr. In contrast, the southwest is subsiding, with the lowest rates around -5 mm/yr. Generally, we find the Huy2 best-fit prediction exhibits a pattern of response broadly similar to that produced by the ICE-5G(VM2) global model of Peltier (2004) (see Fig. 9, Khan et al., 2008). As mentioned previously, it is the GrB model of Tarasov and Peltier (2002) which forms the Greenland component of the ICE-5G model. We note that the magnitude of our predictions are somewhat smaller than those generated using ICE-5G(VM2).

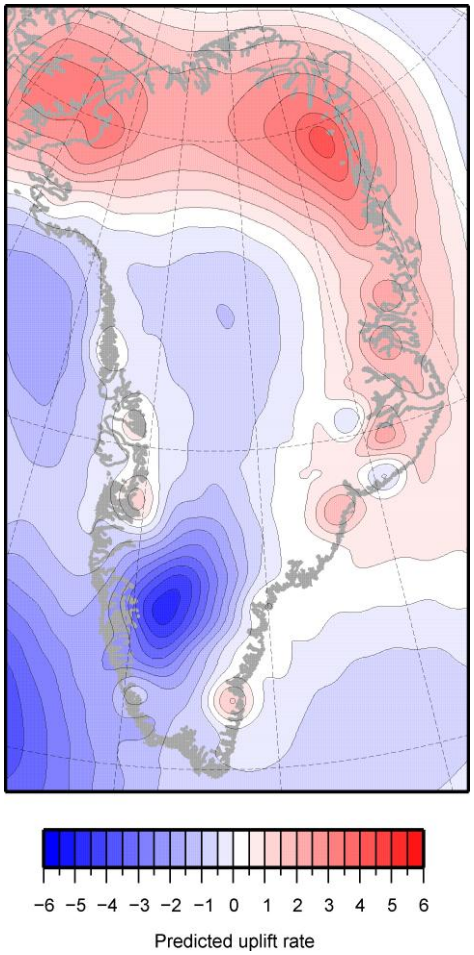

Fig. 25. Predicted present-day vertical crustal velocities (mm/yr) generated using the Huy2 ice history; including non-Greenland ice evolution (ICE-5G) and ocean load changes. The Earth model is characterised by a 120 km lithosphere, an upper mantle viscosity of 5 x 10^{20} Pa s and a lower mantle viscosity of 10^{21} Pa s (our best-fit model; see Sub-Section 2.3.3.1).

3.3.2. Sensitivity to changes in Earth viscosity structure

Figure 26 shows the sensitivity of the predicted present-day uplift rates to changes in Earth viscosity structure. In coastal and ice-free areas of Greenland (areas that have experienced most ice thickness change) the difference in predicted uplift rates is generally between 3-6 mm/yr; indicating that the predictions are strongly dependent on the adopted Earth model. The largest predicted differences are found in the southwest; in this region modelled ice thickness changes during the Holocene are larger than anywhere else in Greenland.

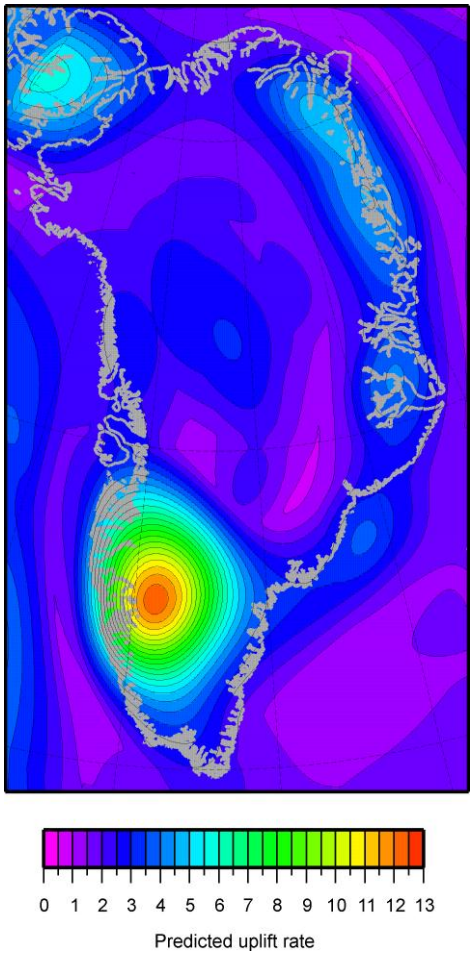

Fig. 26. The maximum difference in predicted present-day uplift rates (mm/yr) generated using Huy2 ice history and a suite of Earth models. All changes were made relative to our reference Earth model which has a 96 km thick lithosphere, upper mantle viscosity of 0.5 x 10^{21} Pa s and lower mantle viscosity of 10^{22} Pa s. Each Earth model parameter was varied independently; lithospheric thickness from 71 to 120 km, upper mantle viscosity from 0.3 x 10^{21} to 10^{21} Pa s and lower mantle viscosity from 10^{21} to 50 x 10^{21} Pa s.

The uplift predictions are very sensitive to changes in upper mantle viscosity; the differences shown in Fig. 26 are essentially due to variations in this Earth model parameter. Figure 27a shows the present-day viscous response for an Earth model with a relatively weak upper mantle. The pattern of uplift shows high rates of subsidence in southwest Greenland; this indicates the predictions are sensitive to ice thickness changes that have occurred over the late Holocene period. Figure 27b shows the present-day viscous response for an Earth model with a relatively stiff upper mantle. In this case, the predictions appear more sensitive to ice-ocean loading changes that occurred between

the LGM and the early Holocene. Over this period, the evolution of the Huy2 model is characterised by ice margin retreat from the continental shelf and thickening of the central dome (see Sub-Section 2.4.1.1).

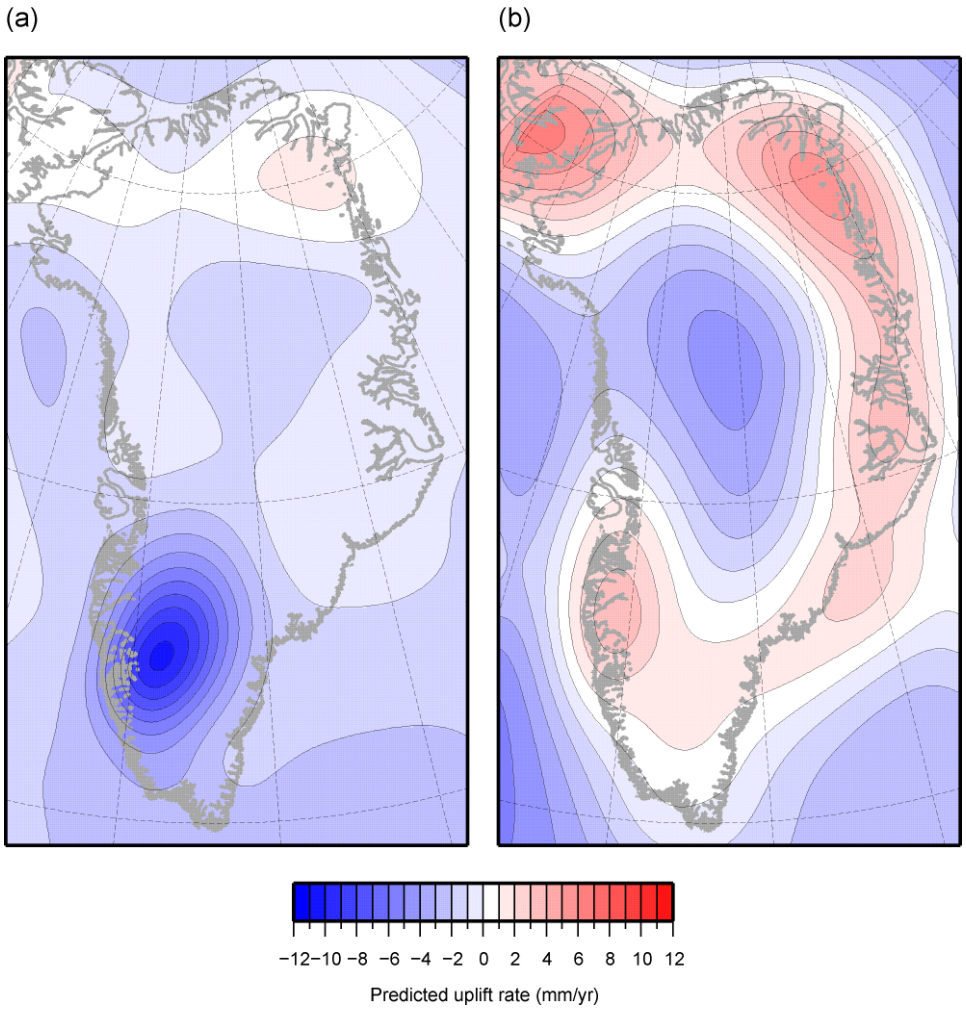

Fig. 27. Predicted present-day vertical crustal velocities generated using the Huy2 ice history; we show the viscous component of deformation only. Results are based on the reference viscosity model with the upper mantle viscosity reduced to 0.3 x 10^{21} Pa s (a) or increased to 10^{22} Pa s (b).

3.3.3. Non-Greenland ice load changes

In the previous Chapter we showed how non-Greenland ice load change significantly influenced land motion in Greenland over the last 10 ka (see Fig. 21). Figure 28 shows predicted present-day uplift

rates generated using only the non-Greenland ICE-5G ice history (Peltier, 2004); in general, the uplift rates in Greenland are generally less than ± 1 mm/yr. In west and ice-free southwest Greenland the Earth is subsiding, with rates here reaching as low as -1.5 mm/yr. This response is due to the collapse and migration of a forebulge developed during the evolution of the North American ice sheet. Present-day uplift rates associated with forebulge collapse are most sensitive to variations in mantle viscosity structure (e.g. Peltier, 1974). In the northwest of Greenland the solid surface is uplifting as a result of past ice mass loss on Ellesmere Island (see also Sub-Section 2.4.2.1).

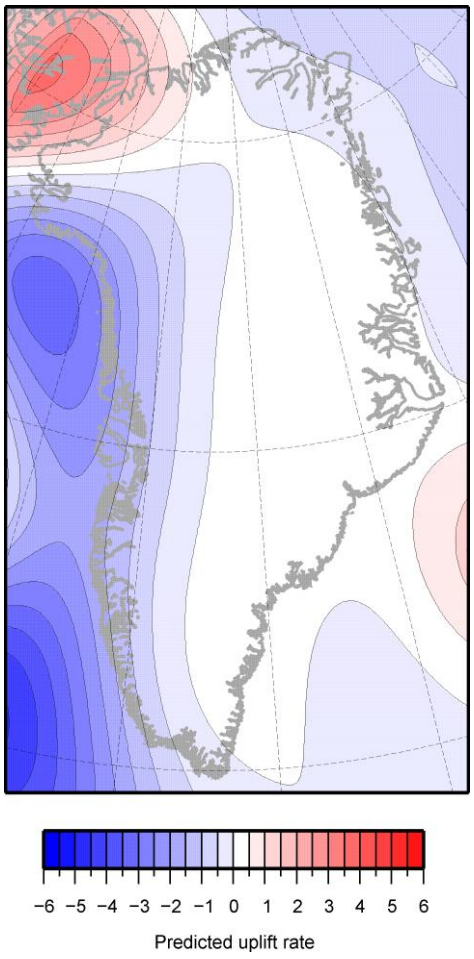

Fig. 28. Predicted present-day vertical crustal velocities (mm/yr) generated using the non-Greenland components of the ICE-5G model and corresponding ocean load changes. The Earth model is characterised by a 120 km lithosphere, an upper mantle viscosity of 5 x 10^{20} Pa s and a lower mantle viscosity of 10^{21} Pa s (our best-fit model; see Sub-Section 2.3.3.1).

3.3.4. Stages of post-LGM ice load change in Greenland

Figure 29 shows the influence of different periods in the post-LGM loading history of Huy2 on predictions of present-day vertical crustal velocities. Figure 29a shows a plot of the present-day viscous uplift rate generated using the complete ice load history of Huy2 Greenland model (123 ka BP to present-day). It shows a complicated pattern of uplift and subsidence. To understand how the Huy2 Greenland ice load history produced this result we examine how several different periods of the model's evolution contribute to the present-day rate of viscous deformation (Fig. 29b-e). The reader is also referred to Figure. 13 in the previous Chapter, which illustrates the ice margin chronology of Huy2 (see Sub-Section 2.3.2.2). During the period 21-10 ka BP, the ice sheet retreats from its LGM extent to become entirely land based. This retreat produces a belt of uplift around the coastline of Greenland (see Fig. 29b). Also over this time period, the dome of the GrIS thickened as accumulation rates increased (Cuffey and Clow, 1997) producing a central region of subsidence. The size of the present-day vertical velocities generated from the period 21 – 10 ka BP are not much larger than ± 1 mm/yr.

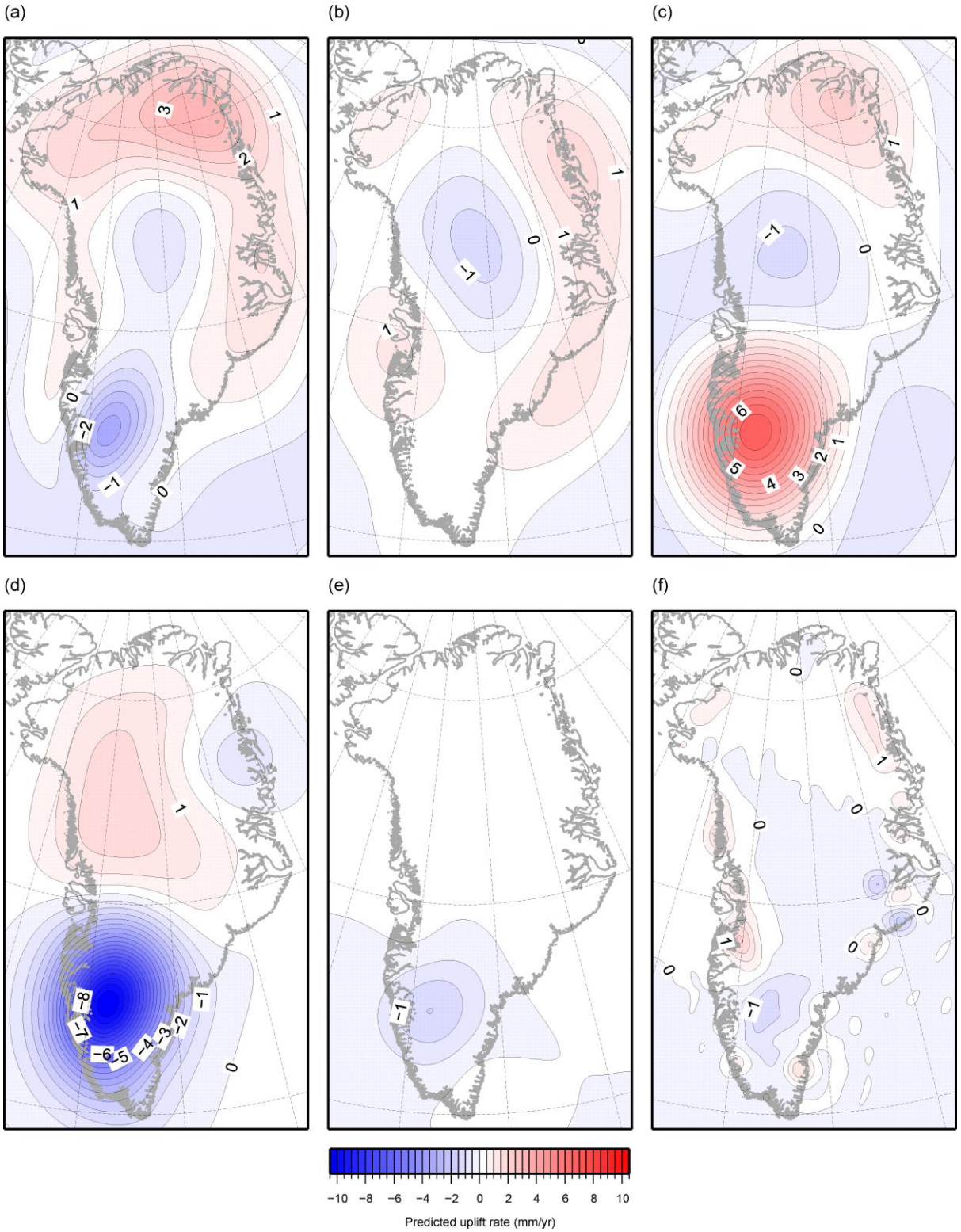

Fig. 29. Predicted present-day vertical crustal velocities generated using the Huy2 ice history only (no non-Greenland ice). The panels (a)-(e) illustrate how different periods of past loading contribute to the present-day viscous Earth response: (a) the full ice model history from 123 ka BP to present (b) 21 – 10 ka BP (c) 10 – 4 ka BP (d) 4 – 0.5 ka BP and (e) 0.5 ka BP to present. Panel (f) shows the elastic response to ice loading changes over the last 100 years. The Earth model is characterised by a

120 km lithosphere, an upper mantle viscosity of 5 x 10^{20} Pa s and a lower mantle viscosity of 10^{21} Pa s (our best-fit model; see Sub-Section 2.3.3.1).

Over the period 10 - 4 ka BP (Fig. 29c) the model is in continuous Holocene retreat. The most significant retreat is in southwest Greenland where the ice sheet retreats c. 80 km behind the present-day margin which produces a bull's-eye of uplift exceeding 6 mm/yr. The ice sheet also retreats from the outer coast at Kronprins Eijland (Fig. 13) during this time producing uplift of around 2 mm/yr in northeast Greenland. By 4 ka BP the GrIS has reached its minimum volume and extent (Fig. 15). The period 4 - 0.5 ka BP (Fig. 29d) marks the switch from retreat to neoglacial regrowth of the ice sheet as it advances back towards its present-day position. This causes subsidence in the southwest at a rate in excess of magnitude 10 mm/yr. The changes in the model over the most recent period 0.5 - 0 ka BP (Fig. 29e) are relatively minor as the ice sheet continues to evolve toward its present-day state. Continued regrowth in southwest Greenland over the last 500 yrs causes subsidence but this signal is relatively small (not much larger than 1 mm/yr in magnitude). The elastic response (Fig. 29f) to loading changes over the last 100 years is within ± 1 mm/yr (we discuss this result further in Sub-Section 3.4.1).

3.3.5. Comparison to the GPS data

Table 2 shows observed secular uplift rates from five GPS receivers analysed by Khan et al. (2008). For comparison, corresponding rates of uplift generated using the Huy2 model are also shown. Starting in southwest Greenland and working anti-clockwise we examine the observed and predicted absolute uplift rates. As mentioned in Chapter 2, Khan et al. (2008) compare GPS observations from across Greenland to predictions from the ICE-5G(VM2) model. They show that the ICE-5G(VM2) model overestimates subsidence in southwest Greenland. This leads them to suggest that the ICE-5G modelled readvance that occurs from c. 8 ka BP in southwest Greenland is too large or mistimed.

GPS locations	Observed uplift rates (mm/yr) Khan et al., 2008	Predicted uplift rates (mm/yr)	
		Huy2 best-fit	Huy2 best-fit east
Kellyville	-1.2 ± 1.1	-0.94	N/A
Nuuk	-2.2 ± 1.3	-2.06	N/A
Qaqortoq	-0.3 ± 1.1	-0.66	N/A
Scoresby Sund	0 ± 1.1	1.17	-1.14
Kulusuk	-0.4 ± 1.1	0.23	-1.72
Thule	3.6 ± 1.1	0.02	N/A

Table 2. Observed and predicted absolute rates of uplift at the GPS sites analysed by Khan et al. (2008). The best-fit Earth model of Huy2 is characterised by a 120 km thick lithosphere, upper mantle viscosity of 5×10^{20} Pa s and lower mantle viscosity of 10^{21} Pa s (see Sub-Section 2.3.3.1). The Huy2 best-fit Earth model for regions across east Greenland is characterised by a 120 km thick lithosphere, upper mantle viscosity of 3×10^{20} Pa s and lower mantle viscosity of 5×10^{22} Pa s.

At Kellyville and Nuuk, the Huy2 best-fit model predicts subsidence of -0.94 mm/yr and -2.06 mm/yr, respectively; these results are within error of the observations. This suggests that the Huy2 model of Holocene ice evolution in southwest Greenland, with a readvance of up to 80 km over the last 4 ka, is reasonably accurate. In the south of Greenland at Qaqortoq, the Huy2 best-fit model predicts subsidence of -0.66 mm/yr; this is also within error of the observations (-0.3 ± 1.1 mm/yr). Huy2 predicts subsidence in this area as the modelled ice margin undergoes a readvance of 20 km over the last c. 4 ka. Khan et al. (2008) indicate that a similar sized c. 33 km readvance of the Qassimuit lobe during the last c. 3 ka is required to reconcile data-model misfits between the ICE-5G(VM2) model and their GPS observations. In southeast Greenland at Kulusuk, the Huy2 best-fit model predicts uplift of 0.23 mm/yr; this is within error of the observations which indicate slight subsidence of -0.4 ± 1.1 mm/yr. It is in the southeast where the largest contemporary ice mass loss in Greenland has been observed (e.g. Rignot and Kanagaratnam, 2006). Khan et al. (2008) calculate that the elastic uplift resulting from this recent mass loss to be 5.6 mm/yr at Kulusuk. This elastic signal is removed from the GPS data to determine the observed secular uplift rate of -0.4 mm/yr. Errors in the estimated elastic correction could therefore influence the observed secular rate significantly.

As shown in Sub-Section 2.3.2.2 the RSL data from across the east Greenland coast favour a distinctly different Earth model to that determined for the Huy2 best-fit model. In Table 2 we also show predicted uplift rates using the east Greenland best-fit Earth model. For Kulusuk, the Huy2 east best-fit model predicts subsidence of -1.72 mm/yr; this result is slightly outside the error of the observations. At Scoresby Sund in east Greenland the Huy2 best-fit model predicts uplift of 1.17 mm/yr; a little too large when compared to the observed value of 0 ± 1.1 mm/yr. In comparison, the Huy2 east best-fit model predicts subsidence of -1.14 mm/yr; in this case the model slightly under predicts the observed uplift velocity. As neither result agrees with the GPS observations, this suggests that the timing of the Huy2 modelled retreat from the continental shelf is incorrect (see also Sub-Section 2.3.2.2). At Thule in northwest Greenland the Huy2 best-fit model under predicts uplift by c. 4 mm/yr. A similar result was found for the ICE-5G(VM2) model, which suggests that modelled ice thicknesses are insufficient in northwest Greenland at the LGM (Khan et al., 2008). In the Huy2 model, ice extends only to the axis of Nares Strait at the LGM, although observations have shown Greenland and Ellesmere Island ice coalesced at this time (England, 1999). It is also possible the GrIS extended farther onto the continental shelf west of Thule and this may explain the discrepancy between the GPS data and our predictions. It is also worth noting that the Huy2 model is not well constrained in the northwest as the temporal coverage and height precision of the RSL data in this region is poor (see Sub-Section 2.3.3.2).

On considering the observations of Dietrich et al. (2005) we find that the Huy2 best-fit model does not show agreement to most of the data. Figure 30 shows their observed and our predicted relative rates of uplift for the network of GPS sites in southwest Greenland. As an example, observations show that relative to Sisimiut (SIS1) on the outer coast the GPS site at Kangerlussuaq (KAN1) is subsiding by -4.1 mm/yr. For these same sites Huy2 predicts a far smaller relative subsidence rate of -0.39 mm/yr. This suggests the regional pattern of Holocene ice load change is not accurately captured by the Huy2 model. Although predicted relative rates of uplift for specific GPS sites are not in agreement with the observations, our predictions (Fig. 25) exhibit a similar east-west pattern as shown by Dietrich et al. (2005) (see their Fig. 8). We note that, whilst the Huy2 uplift predictions show poor agreement to the observations of Dietrich et al. (2005), they do show fit to the observations of Khan et al. (2008) from southwest Greenland. This difference could be due to the discrepancy between absolute uplift rates determined for these two data sets (as discussed above). Additional new data from the GNET project will help resolve such observational discrepancies. As the observations of Dietrich et al. (2005) have not been corrected for contemporary ice mass change (i.e. the elastic term); this may also explain some of the data-model misfit.

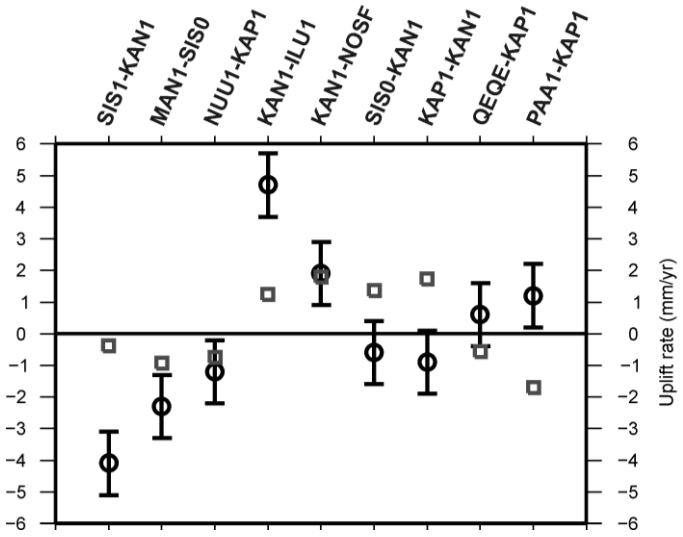

Fig. 30. Relative rates of uplift across southwest Greenland. The observations of Dietrich et al. (2005) are marked by open circles and have vertical error bars (which denote the rms error value). The predictions of the Huy2 best-fit Earth model (see Sub-Section 2.3.3.1) are marked by dark grey squares.

3.3.6. Summary and discussion; the Huy2 model

We have presented predictions of present-day uplift generated using the Huy2 ice history coupled with our best-fit Earth model (sea-level predictions made using this Earth model show best-fit to the RSL data; see Sub-Section 2.3.3.2). Our Earth model sensitivity study showed the predicted present-day rates are strongly dependent on the adopted Earth viscosity structure; the predictions are most sensitive to changes in upper mantle viscosity. Results from Chapter 2 (see Fig. 23), show that the current RSL data set is not able to place a useful bound on upper mantle viscosity, this suggests that: (1) the accuracy of uplift predictions made using GIA models constrained by RSL data will be limited in accuracy and (2) the extended GPS data should provide an additional means of arriving at better constraints on this parameter. Predictions made using a relative stiff upper mantle generate a pattern of present-day uplift that reflects ice thickness changes between the LGM and early Holocene period. On the other hand, predictions made using a relatively weak upper mantle generate very high rates of uplift and correspond to ice loading changes that have occurred in

southwest Greenland over the last few thousand years. Ivins and James (2005) found similar Earth model sensitivities in a study of the Antarctic ice sheet. These findings have important implications with regard to the loading period that dominates the present-day response in a given region and the potential importance of very recent ice sheet changes (which are poorly resolved in millennial-scale models like Huy2). This latter issue is considered more fully in Section 3.4.

In response to past non-Greenland ice load change, the ongoing collapse and migration of a forebulge developed over west Greenland causes subsidence. These non-Greenland present-day uplift rates are no larger than ± 1 mm/yr. However, we did not show how this signal is sensitive to changes in Earth model parameters; past studies have shown that the dynamics of a forebulge are strongly controlled by mantle viscosity structure (e.g. Peltier, 1974). Analysis of post-LGM Greenland loading change shows how different periods of loading change dominate in particular regions of Greenland. The present-day viscous Earth response in the North of Greenland is most sensitive to the early-mid Holocene evolution of Huy2 while the east is most sensitive to changes from the LGM to beginning of Holocene period. The present-day viscous signal in southwest Greenland is highly sensitive to the predicted ice thickness changes over the Holocene period. These results are illustrated in Fig. 29; which will be a useful resource when interpreting existing and future observations of vertical land motion in Greenland.

In comparison to the secular uplift rates presented by Khan et al. (2008), the uplift predictions show good agreement to some sites. Although, it is difficult to draw firm conclusions about the performance of the model as there are so few data. One noticeable data-model misfit was found at the Thule GPS station; this result strongly suggests that the modelled LGM ice thicknesses are insufficient in northwest Greenland. At Kellyville and Nuuk in southwest Greenland and Qaqortoq in

south Greenland the Huy2 model predicts rates of ongoing subsidence which agree with the observed values (Khan et al., 2008). Note that it is in west and south Greenland where the Huy2 model is best constrained by numerous and high quality RSL data (see Chapter 2). In contrast, comparison to the relative rates observed across a network in southwest Greenland (Dietrich et al., 2005), reveals relatively poor data-model agreement. However, we note our predictions show a similar east-west pattern as described by Dietrich et al. (2005). These results suggest that although the Huy2 model is able to reproduce the broad features of the ice sheet's Holocene evolution in southwest Greenland, the exact nature of the neoglacial readvance may not be accurately captured. Of course, as discussed above, uplift predictions in this region of Greenland are highly sensitive to changes in the adopted Earth model. Furthermore, the observations of Dietrich et al. (2005) have not been corrected for contemporary ice mass change (i.e. the elastic term); which may also explain some of the data-model misfit (see Section 3.4).

3.4. Modelling: The influence of the last c. 100 years of ice load change

As mentioned, a recent study of Antarctic GIA showed that predicted present-day uplift rates are potentially very sensitive to ice mass changes over the last two millennia (Ivins and James, 2005). This indicates that to generate accurate uplift predictions, we require a sound understanding of the relatively recent history of the Antarctic ice sheets. In this Section and as the secondary aim of the analysis, we address this issue for Greenland. However, we focus on the ice sheet's more recent history; the last century (or so). We begin by examining the Huy2 model (as detailed in Chapter 2). As mentioned previously, the 100 year BP ice-ocean loading increment marks the last timestep prior to present-day for this GIA model. For comparison with Huy2, we also show uplift predictions for the Wake et al. (2009) surface mass balance reconstruction, which covers the period 1866-2005 and is forced by more accurate climate data.

3.4.1. The Huy2 model

As with other millennial-scale ice sheet models the temperature record used to force Huy2 is derived from ice core δO^{18} isotope data (see Sub-Section 2.3.2.3). The time resolution of the GRIP δO^{18} data (Dansgaard et al., 1993) as input to the Huy2 ice model is 100 years and so Huy2 does not capture sub-century scale variability. Unsurprisingly, closer inspection of the Huy2 model output (every 20 years) reveals almost no change in the surface mass balance over the last century. For Huy2 we find the average rate of ice volume change over this period is -16 km^3/yr; indicating that the ice sheet is in negative mass balance. Modelled ice thickness changes over the last 100 years are mostly less than ± 20 m; the spatial pattern is characterised by accumulation of < 10 m in the interior with ice mass loss around the majority of the margin (figure not shown). In some marginal areas this ice thickness loss is as large as 80-100 m; the most extensive and largest negative changes are in central west Greenland. The largest mass gain is in southwest Greenland, ice thickness increases here are between 20-40 m. Previous studies that have used millennial-scale ice sheet models to predict the most recent evolution of the GrIS have shown similar patterns of ice thickness change (Huybrechts, 1994; Le Meur and Huybrechts, 1998; Huybrechts and Le Meur, 1999; Huybrechts et al., 2004). The Huy2 model exhibits essentially the same pattern of ice thickness change as shown in Fig. 8a of Huybrechts et al. (2004). This is not surprising as the Huy2 model is adapted from the ice model presented by Huybrechts (2002) and the ice sheet's evolution over the last 100 years should not differ significantly from these earlier results.

The ice thickness changes over the past c. 100 years are thought to largely reflect the response of the GrIS to increased temperatures following Little Ice Age cooling (Huybrechts, 1994). It should be noted that predicted ice thickness changes over the last 100 years, to some extent, will also reflect longer term changes to the GrIS. It is well accepted that the ice sheet is still reacting to past (c. 10 ka BP) climate change (e.g. Abe-Ouchi et al., 1994; Huybrechts, 1994; Huybrechts and Le Meur, 1999). It

has been suggested that the thickening that occurs in southwest Greenland may represent a long-term ice-dynamic trend arising after the last deglacial transition (Huybrects, 1994). For the Huy2 model, it is possible that some part of this thickening may also be due to the continued recovery of the GrIS following the Holocene Thermal Maximum (HTM) (see Chapter 2). However, we note that Huybrechts (1994) demonstrated that the ice sheet's evolution over the last 100 years appears insensitive to the HTM.

Figure 31 shows both the elastic and viscous components of uplift generated using the last 100 years of ice load change in the Huy2 model. The pattern of Earth response broadly reflects the ice thickness changes as detailed above. The viscous response is around ± 0.2 mm/yr; although this signal is small it indicates that even relatively recent ice mass variability plays a role in determining the long-term viscous signal accurately. The elastic response (± 2 mm/yr) is an order of magnitude larger than the viscous response, which is what we would expect over this relatively short period.

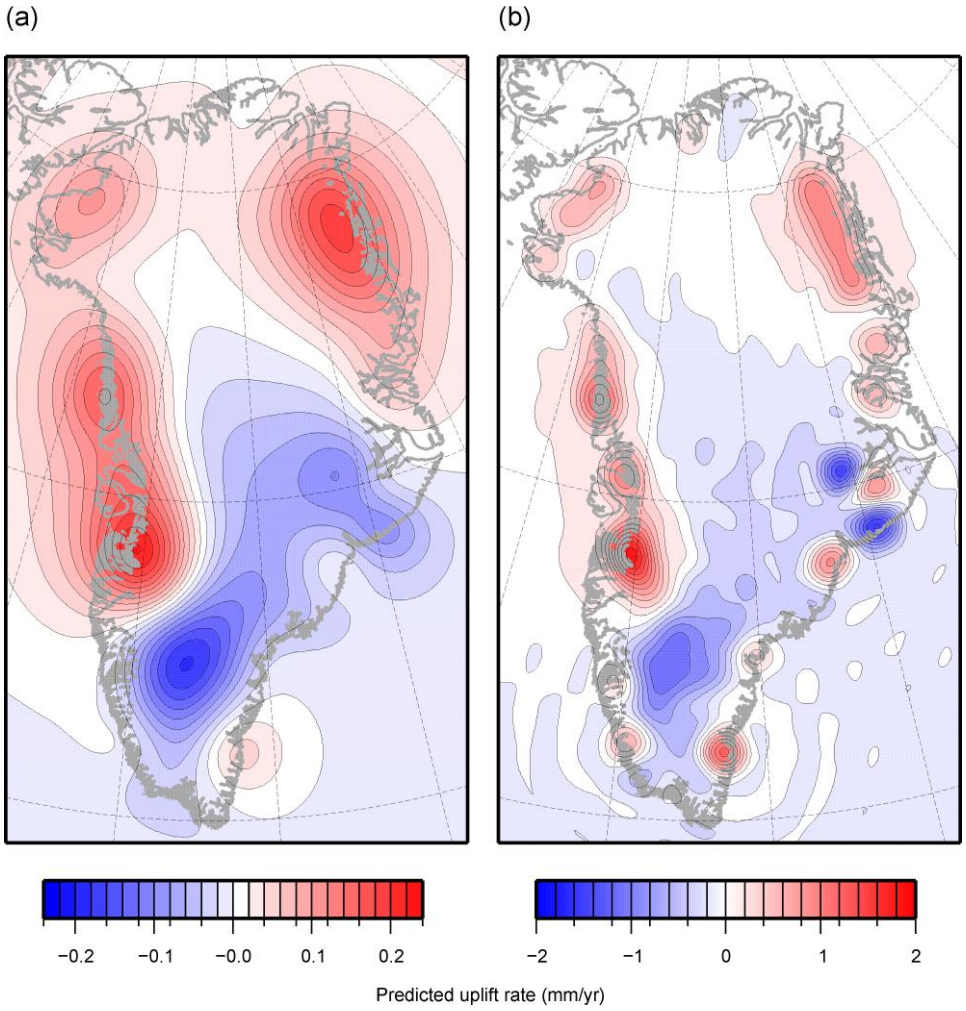

Fig. 31. Predicted present-day vertical crustal velocities showing the viscous (a) and elastic (b) response generated from the Huy2 model for the last 100 yrs of ice load change only. The Earth model is characterised by a 120 km lithosphere, an upper mantle viscosity of 5 x 10^{20} Pa s and a lower mantle viscosity of 10^{21} Pa s (our best-fit model; see Sub-Section 2.3.3.1).

3.4.2. The Wake et al. (2009) model

The Wake et al. (2009) model is a surface mass balance reconstruction of the GrIS over the period 1866-2005. To calculate mass balance they use the runoff model of Janssens and Huybrechts (2000), which is based upon the positive degree day method (Braithwaite, 1995). The model was forced using monthly temperature and annual precipitation data. From 1866 to 1957 they input climatic data from Box et al. (2006, 2008) and from 1958 to 2005 they input data from Hanna et al. (2008). The horizontal grid resolution is 5 km, which corresponds to 329 X 561 horizontal grid cells for

Greenland. Ice dynamics were considered in a relatively crude sense by including a steady-state ice-dynamic field (e.g. see Paterson, 1994).

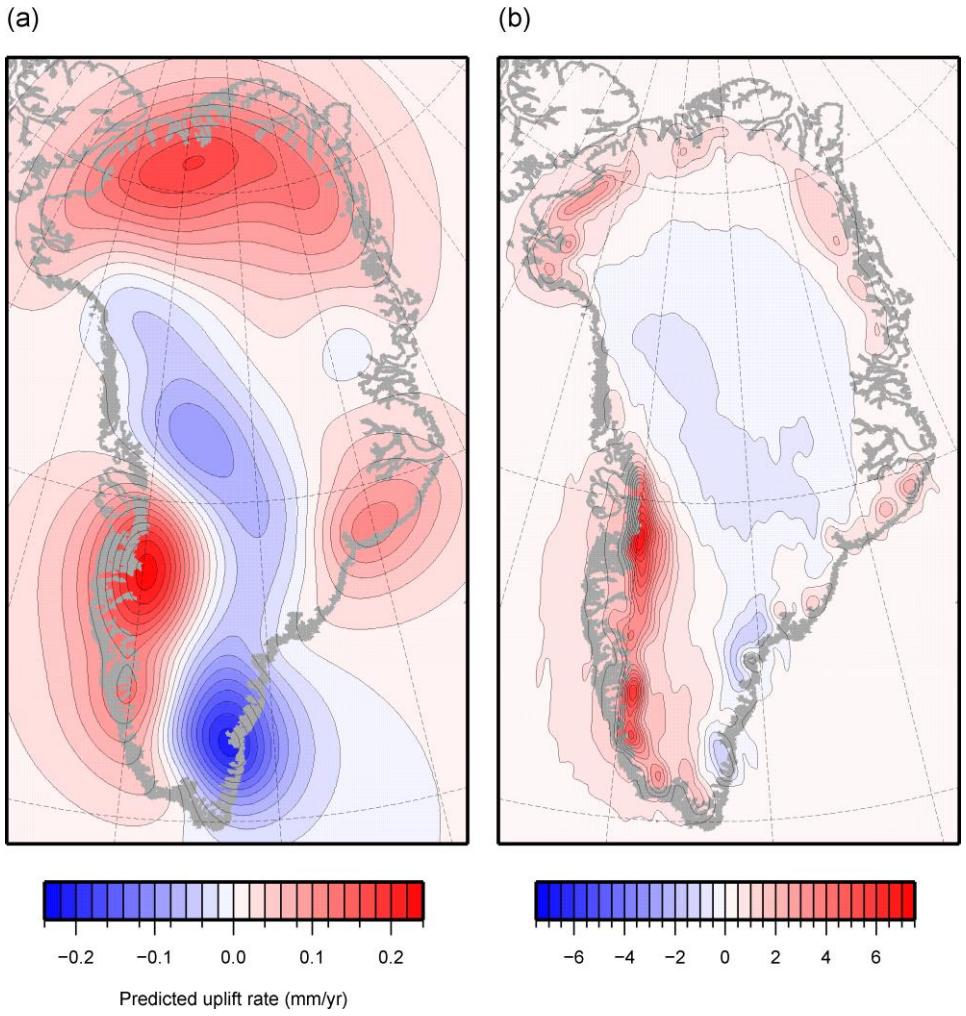

Fig. 32. Predicted present-day vertical crustal velocities generated using the surface mass balance reconstruction of Wake et al. (2009) with a steady state ice-dynamic field. We show (a) the viscous response to ice loading changes from 1866-2005 and (b) the elastic response to ice loading changes from 1995-2005. The Earth model is characterised by a 120 km lithosphere, an upper mantle viscosity of 5 x 10^{20} Pa s and a lower mantle viscosity of 10^{21} Pa s (the Huy2 best-fit model; see Sub-Section 2.3.3.1).

The SMB record presented by Wake et al. (2009) shows that over the c. 140 year study period the GrIS has been losing ice volume at a rate of -0.89 ± 0.15 km^3/yr (they calculate this figure using a

linear regression of the time series). Although the ice sheet has generally been in a state of slight negative mass balance, we note the SMB record shows considerable temporal variability; between 1866 and 1922 the ice sheet is mainly in a state of positive SMB, the authors calculate the average rate of mass gain over this time to be 37 ± 11 km^3/yr. From 1922 to 2005 this changes to a state of largely negative mass balance, although several years in this latter period show the ice sheet having a high amplitude mass gain (see Fig. 3 of Wake et al. (2009) for the SMB time series). The Wake et al. (2009) SMB model also exhibits a considerable degree of spatial variability. In general, most ice thickness is lost at the margins in the more southerly areas of Greenland; up to 100-200 m over the study period (see Fig. 4 of Wake et al. (2009) for the cumulated SMB changes over the period 1866-2005). In contrast, in the far southeast of Greenland, ice thicknesses have increased by 100-200 m due to the high accumulation rates that characterise this region.

Figure 32a shows the viscous response to ice loading changes over the period 1866-2005. The spatial pattern is characterised by subsidence of around -0.2 mm/yr in southeast Greenland and highest rates of uplift from 0.1 to 0.2 mm/yr in the central west and north. Unsurprisingly, the viscous term appears to largely reflect the general trend of ice mass change the Wake et al. (2009) model predicts to occur over the 140 yr period (as described above). We note that this pattern of uplift shows similarities to the prediction generated using the Huy2 model (see Fig. 31a). The size of the signal is also similar to that predicted using Huy2; both predictions show that uplift rates do not far exceed ± 0.2 mm/yr. This suggests that the last 140 years of ice mass change plays only a small role in determining present-day viscous response.

Figure 32b shows the elastic response which was calculated using ice load changes over the period 1995-2005, which is approximately the same timeframe over which the GPS data were recorded

(Dietrich et al., 2005; Khan et al., 2008). The spatial pattern is characterised by large rates of uplift (over 6 mm/yr) in some areas close to the margin of the ice sheet, most notably in west and southwest Greenland. These are driven by rates of peripheral thinning high as 5-10 m/yr (see Fig. 5 of Wake et al. (2009)); which dominate the SMB signal and result in an average rate of -69 km^3/yr for this 10 year period. As mentioned, the Wake et al. (2009) model does not account for non-steady-state ice-dynamic features. Therefore, for areas of the GrIS where observations show that outlet glaciers are losing mass (e.g. Joughin et al., 2004; Howat et al., 2005; Rignot and Karagaratnam, 2006; Stearns and Hamilton, 2007), our predictions will underestimate elastic uplift (see also Sub-Section 3.4.4). Whilst the Wake et al. (2009) model has this limitation, it does show that surface mass balance changes are generating a large elastic response. The highest rates of elastic uplift are around 3 times larger than those generated using the Huy2 ice history (Fig. 31b), which highlights the limitation of using a millennial-scale scale to determine sub-century variability.

3.4.3. A new hybrid model

In this section we attempt to reconstruct a more accurate loading history for Greenland by amalgamating the long-term evolution of the Huy2 model (up until 140 yr BP) with the 1866-2005 SMB reconstruction of Wake et al. (2009). Hereafter, we refer to this resultant combined loading history as the Huy2-Wake model. Figure 33 shows the predicted pattern of present-day uplift generated using the Huy2-Wake ice history.

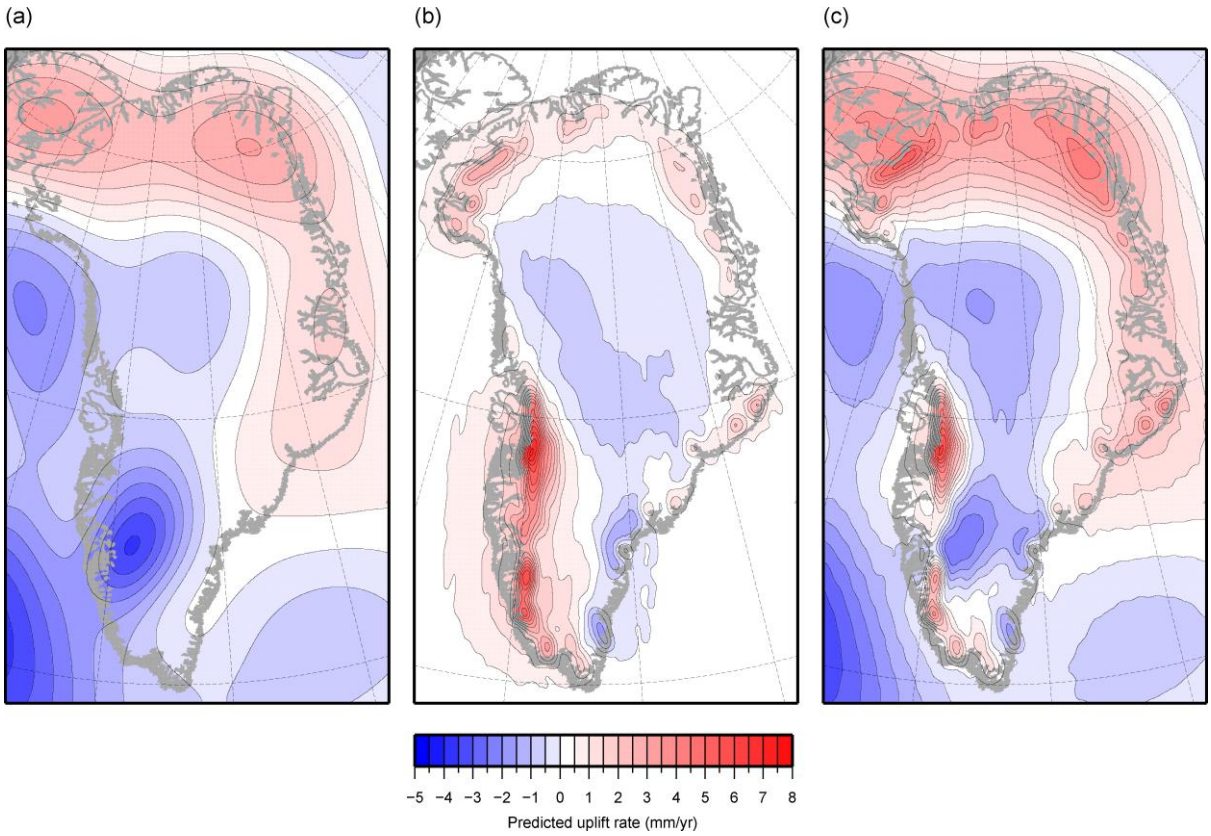

Fig. 33. Predicted present-day vertical crustal velocities showing: (a) the long-term viscous response generated using the Huy2 ice history (123 ka BP to 140 yrs BP); including non-Greenland (ICE-5G) ice evolution and ocean load changes (b) the combined elastic and viscous response generated using the surface mass balance model of Wake et al. (2009) – note that ocean load changes are not included. (c) is the resultant visco-elastic signal when (a) is added to (b). The Earth model is characterised by a 120 km lithosphere, an upper mantle viscosity of 5 x 10^{20} Pa s and a lower mantle viscosity of 10^{21} Pa s (our best-fit model; see Sub-Section 2.3.3.1).

The results suggest that SMB changes to the ice sheet over the period 1995 to 2005 play a significant role in determining the present-day uplift rate. For example, in ice-free areas in west and southwest Greenland we find that the solid Earth is mostly uplifting; this is largely due to the elastic response to contemporary ice mass changes (see also Figure. 32b). In central southern areas we find the Earth is subsiding; a consequence of both the longer-term response to the Holocene regrowth of the ice sheet and also accumulation in southeast Greenland over the last 140 years. The more recent ice mass changes in the southeast of Greenland cause subsidence rates of c. 4 mm/yr. The ice-free coast from north to east Greenland is uplifting; a consequence of both the long-term response to ice

margin retreat from the continental shelf (which is followed by continued Holocene retreat) and the short-term response to recent ice mass loss.

3.4.4. Comparison to the GPS data

In Table 3 we show the observed secular uplift rates of Khan et al. (2008). As opposed to the results shown in Table 2, the observed rates in Table 3 have not been corrected for the elastic response to contemporary ice mass changes (see Table 2 of Khan et al. (2008)). These observations, therefore, can be compared to uplift predictions generated using the Huy2-Wake hybrid model; in which modern ice mass changes largely reflect the variations in surface mass balance as described by Wake et al. (2009). We also show predictions from the Huy2 model to draw comparisons with the Huy2-Wake hybrid model. As discussed above, because the Wake et al. (2009) model does not resolve non-steady-state ice-dynamics, it will under estimate uplift in areas where outlet glaciers have been observed in retreat (e.g. Joughin et al., 2004; Howat et al., 2005; Rignot and Karagaratnam, 2006; Stearns and Hamilton, 2007). For example, at Kulusuk in southeast Greenland observations show the Earth is uplifting at a rate of 5.2 ± 1.1 mm/yr. The Huy2-Wake model predicts a rate of 1.5mm/yr and so under predicts uplift at this location (see Table 3). However, in comparison to the GPS data Khan et al. (2008) corrected for contemporary ice mass changes, we earlier showed that the Huy2 model provides fit to these observations from Kulusuk (see Table 2). The Huy2-Wake data-model discrepancy, therefore, can mostly be explained by the rapid ice mass loss from the nearby Helheim and Kangerlussuaq outlet glaciers (Khan et al., 2007). At Qaqortoq in the south, we similarly find that whilst the Huy2 model is able to provide fit to the observations presented in Table 2, the Huy2-Wake model under predicts uplift (see Table 3). We suggest that this Huy2-Wake data-model discrepancy can also be attributed to modern ice-dynamic mass loss in southeast Greenland (see Khan et al., 2007). We also note that for Qaqortoq there is very little difference between the predicted rates for the Huy2 and Huy2-Wake models.

In southwest Greenland the Huy2-Wake shows good agreement to the GPS data from both Kellyville and Nuuk. These results suggest that the Wake et al. (2009) model provides a reasonably accurate recent ice loading history for this region of the GrIS. There are few large glaciers in the southwest of Greenland as the ablation zone is broad and the slope of the ice sheet is shallow (Rignot and Kanagaratnam, 2006). Contemporary ice-dynamic changes, therefore, are less important in this area of the GrIS. At Thule, the Huy2-Wake under predicts the rate of uplift, although the data-model misfit here can be explained by insufficient ice thickness at the LGM (see Sub-Section 3.3.5). Satellite observations have shown that the glaciers in northwest Greenland have remained stable over the last c. 10 years (Rignot and Kanagaratnam, 2006).

GPS locations	Observed uplift rates (mm/yr) Khan et al., 2008	Predicted uplift rates (mm/yr)		
		Huy2 best-fit	Huy2 best-fit east	Huy2-Wake best-fit
Kellyville	0.2 ± 1.1	-0.94	N/A	0.42
Nuuk	-1.5 ± 1.3	-2.06	N/A	0.2
Qaqortoq	1.1 ± 1.1	-0.66	N/A	0.93
Kulusuk	5.2 ± 1.1	0.23	-1.72	1.50
Scoresby Sund	0.9 ± 1.1	1.17	-1.14	0.48
Thule	3.9 ± 1.1	0.02	N/A	-0.71

Table 3. Observed and predicted absolute rates of uplift at the GPS sites analysed by Khan et al. (2008). The observed values have not been corrected for contemporary ice mass changes. The best-fit Earth model of Huy2 is characterised by a 120 km thick lithosphere, upper mantle viscosity of 5×10^{20} Pa s and lower mantle viscosity of 10^{21} Pa s (see Sub-Section 2.3.3.1). The Huy2 best-fit Earth model for regions across east Greenland is characterised by a 120 km thick lithosphere, upper mantle viscosity of 3×10^{20} Pa s and lower mantle viscosity of 5×10^{22} Pa s (see Sub-Section 2.4.2.3).

Across the GPS network examined by Dietrich et al. (2005) the Huy2-Wake hybrid model offers no consistent improvement over the original results of the Huy2 model (Fig. 34). Most sites are affected at the sub-mm/yr level; except for MAN1-SIS0 and SIS0-KAN1 where the fit is worsened and improved, respectively. Results from the Wake et al. (2009) model demonstrate that recent ice mass

changes may influence present-day uplift rates in southwest Greenland significantly (see Fig. 32b). However, we note that past studies have argued that observed present-day uplift rates in this region largely reflect the readvance of the ice margin over the last 3 ka and not more recent centennial-scale ice mass changes (Wahr et al., 2001a; Dietrich et al., 2005; Khan et al., 2008).

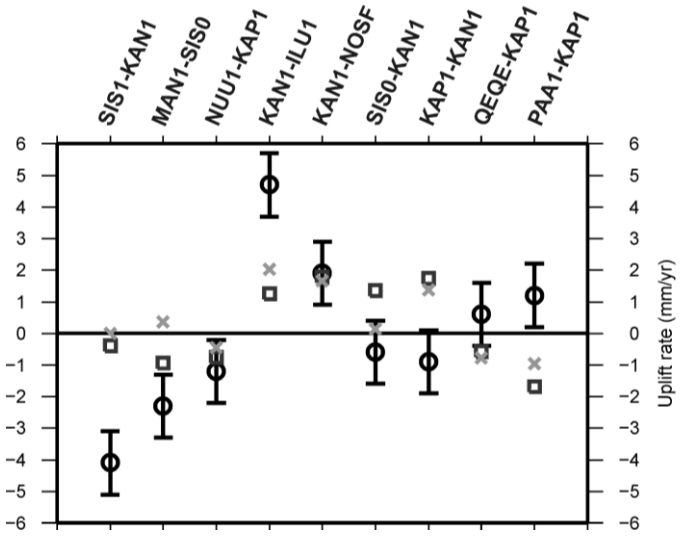

Fig. 34. Relative rates of uplift across southwest Greenland. The observations of Dietrich et al. (2005) are marked by open circles and have vertical error bars (which denote the rms error value). The predictions of the Huy2 best-fit Earth model are marked by dark grey squares. The predictions made for our hybrid Huy2-Wake model (using the Huy2 best-fit Earth model; see Sub-Section 2.3.3.1) are marked by the light grey crosses.

3.4.5. Summary and discussion; the last c. 100 years

The Huy2 modelled pattern of ice thickness change over the last century largely reflects the response of the GrIS to increased temperatures following Little Ice Age cooling (e.g. Huybrechts, 1994). To a lesser extent, changes in ice thickness can be attributed to the long-term reaction of the ice sheet to past (c. 10 ka BP) climate change (e.g. Abe-Ouchi et al., 1994; Huybrechts, 1994; Huybrechts and Le Meur, 1999). Uplift predictions show that Huy2 loading changes over the last century contribute around ± 0.2 mm/yr to the present-day viscous Earth response. In comparison to Huy2, the Wake et al. (2009) model shows high variability in time and exhibits changes in the spatial

pattern of melt and accumulation; this is because the model is forced by high temporal and spatial resolution climate data (Box et al., 2006, 2008; Hanna et al., 2008). However, despite these differences in ice mass changes, the uplift predictions generated using the 140 year Wake et al. (2009) reconstruction show that the present-day viscous response is similar in size and (to a lesser extent) pattern to that predicted using Huy2. This likely because the viscous Earth response is insensitive to the variability shown in the Wake et al. (2009) model (i.e. it only reflects the general trend of ice mass change over the 140 year period).

In contrast to Huy2, we note that the Wake et al. (2009) model has yet to be validated against RSL observations and so we are less confident of the accuracy of the uplift predictions, particularly in areas where the climate forcing is not well constrained. However, the model is consistent with a number of observed changes in the GrIS over the past century as well as the past decade. Several studies have detailed observed changes to the GrIS over the last 100 years, but these are limited to only a few regions of Greenland: In west Greenland, the frontal of recession of Jakobshavn Isbrae (c. 25 km) since 1900 is well recognised (Weidick and Bennike, 2007) and geomorphological evidence from southwest Greenland indicates that the ice front has retreated by c. 1-2 km over the last 100 years (Forman et al., 2007). Wake et al. (2009) find these observations agree well with their modelled ice thickness changes. An important finding from our analysis of the Wake et al. (2009) reconstruction is the suggestion that the present-day viscous signal is not significantly influenced by ice thickness changes over the last 100 years or so. However, it remains unclear what role ice mass variability over the last 500-1000 years, during which there were climate events such as the Little Ice Age and Medieval Warming Period, plays in determining the present-day viscous response. Clearly, future work should focus on improving the accuracy of ice sheet reconstructions of over this relatively recent period. In this regard, new high resolution relative sea-level records obtained from

salt marsh studies (Woodroffe and Long, 2009; Long et al., in press) can help constrain the behaviour of the GrIS over the last millennia.

The elastic Earth response to Huy2 modelled ice loading changes (over the last 100 years) is around ±2 mm/yr. The elastic component of Earth uplift generated using a Greenland millennial-scale ice sheet model has previously been examined by Le Meur and Huybrechts (1998). Using averaged ice thickness changes over the last 200 years they found the corresponding elastic term was no larger than ± 0.5 mm/yr and is dominated by the long-term viscous signal (see Fig. 3 of Le Meur and Huybrechts (1998)); although they acknowledged the elastic term is speculative. In terms of contemporary mass loss, the Wake et al. (2009) reconstruction shows the ice sheet is in negative mass balance and rates of peripheral thinning in west and southwest Greenland are as high as 5-10 m/yr over the period 1995-2005 (see their Fig. 5). Wake et al. (2009) find their modelling results compare favourably to recent repeated laser-altimetry studies (Krabill et al., 2004; Thomas et al., 2006). Unsurprisingly, in regions where there are high rates of thinning at the margin, we find corresponding uplift rates are also large (> 6 mm/yr in southwest Greenland). Khan et al. (2007) demonstrated that in areas close to major outlet glaciers, ice-dynamic mass loss has caused rapid rates of elastic rebound. These bull-eye's of local elastic uplift are presumably punctuated along the ice margin of the GrIS. In addition to this signal, our results show that there will also be a large elastic Earth response arising from surface mass balance changes. Uplift predictions generated using the reconstruction of Wake et al. (2009) suggest that this signal is significant; we therefore suggest that the elastic response to contemporary SMB changes is carefully considered when attempting to isolate the elastic and viscous contributions to present-day vertical land motion.

3.5. Conclusions

1. Predicted present-day uplift rates in Greenland are strongly dependent on the adopted Earth viscosity structure; the predictions are most sensitive to changes in upper mantle viscosity. It is important, therefore, that upper mantle viscosities are better constrained in future work (although, results from Chapter 2 (see Fig. 23) show that the current RSL data set is not able to place a useful bound on this parameter).

2. Analysis of post-LGM Greenland loading changes shows how different periods of ice mass variation dominate in particular regions of Greenland. These results will be a useful resource when interpreting existing and future observations of vertical land motion in Greenland. Of course, as pointed out in our first conclusion, these results are highly sensitive to changes in upper mantle viscosity.

3. The Huy2 model shows good agreement to the observed absolute uplift rates from southwest and south Greenland (Khan et al., 2008). This suggests that the timing and magnitude of the neoglacial readvance is reasonably well captured in these regions. However, the Huy2 model does not give fit to the relative rates presented by Dietrich et al. (2005), which suggests some aspect of the regrowth in the southwest is inaccurate.

4. Results from the Wake et al. (2009) model indicate that decadal-scale ice mass variability over the last c. 140 years plays an small role in determining the present-day viscous response. However, the Wake et al. (2009) model has yet to be validated against RSL observations and so we are not

confident of the accuracy of the uplift predictions, particularly in areas where the climate forcing is not well constrained.

5. Results from the Wake et al. (2009) model, over the period 1995 to 2005, show that contemporary ice mass changes generate high rates of elastic uplift (c. 6 mm/yr). This suggests that modern surface mass balance changes have a large influence on predicted present-day uplift rates in some areas of Greenland.

Chapter 4:

The influence of non-Greenland ice on the evolution of the Greenland ice sheet.

4.1. Introduction

In this Chapter we examine how non-Greenland ice mass loss influenced vertical land motion and sea-level change around Greenland over the last deglaciation and consider the implications for GrIS evolution. A previous modelling study has briefly described how the regional RSL history of Greenland was affected by the late North American Ice Sheets (NAIS) and, to a lesser extent, the Eurasian ice sheet (Fleming and Lambeck, 2004). Since the LGM (c. 21 ka BP), the melting of ice sheets predominantly in the northern hemisphere has caused a c. 120 m rise in global mean sea-level (e.g. Fairbanks, 1989; Yokoyama et al., 2000). Of this, the NAIS contributed 60-75 m ice-equivalent sea level (Tarasov and Peltier, 2004), which is approximately 50-62.5 % of the total melt. It is not surprising that this huge ice-ocean mass exchange produced a significant GIA-induced RSL signal across Greenland, given its close proximity to North America. It is important to note (and as shown in the analysis below) that the nature of this non-Greenland RSL signal departs significantly from eustatic sea level and is spatially non-uniform. In particular, this may have implications for our understanding of the post-LGM retreat of the GrIS from the continental shelf. Past studies have hypothesised that the marine retreat of the ice sheet was driven by sea-level rise (Funder, 1989; Funder and Hansen, 1996). If the marine retreat was sea-level controlled, we therefore require accurate knowledge of non-Greenland ice mass loss in order to understand the influence of sea-level change on the early phase of Greenland ice retreat.

The effect of non-Greenland ice on GrIS evolution can be thought about in two separate ways: Vertical land motion and RSL change (which includes the former). Firstly, we consider the deflection of the Earth's solid surface. Changes to the elevation of the solid Earth and therefore ice elevation will influence precipitation and melt rates, in turn affecting the mass balance of an ice sheet. Isostatic adjustment can have either a negative or positive feedback on ice volume change (e.g. Crucifix, 2001; Van den Berg, 2008). We showed in Chapter 2 that vertical solid Earth motion resulting from non-Greenland ice mass loss is particularly important over the Holocene period (see Sub-Section 2.4.2.1). We would expect, therefore, that the migration and collapse of non-Greenland forebulges would have influenced the evolution of the GrIS to some degree. The isostatic influence of 'neighbouring' ice sheets has not been considered in past modelling work. Indeed, studies that have addressed late Quaternary ice evolution in the northern hemisphere did not raise this issue (e.g. Tarasov and Peltier, 1997; Charbit et al., 2002; Zweck and Huybrechts, 2005).

GIA-induced RSL change can influence ice evolution if the ice sheet has a marine boundary, thus, changes in RSL (including solid Earth motion) will effect ice-ocean interactions and calving. The mechanism of calving at marine margins remains a poorly understood process and is difficult to implement in millennial-scale ice sheet models (Benn et al., 2007). The treatment of calving in northern hemisphere ice sheet models is, therefore, normally implemented as a simplistic paramaterisation. Typically in such schemes calving is a function of water depth (e.g. Siegert and Dowdeswell, 1995; Siegert et al., 1999, 2001; Huybrechts, 2002; Zweck and Huybrechts, 2003, 2005) and/or ice margin thickness if the buoyancy and floatation of ice is taken into account (e.g. Ritz et al., 1997; Charbit et al., 2002; Tarasov and Peltier, 2002). These parameterisations assume that water depth is the most important control on the position of the grounding line. This assumption is largely based on earlier results from the statistical analyses of tidewater glaciers (e.g. Brown et al., 1982; Pelto and Warren, 1991) which showed that the calving rate is linearly related to the water depth at

the ice terminus. It has since been noted that these empirical relationships may not reflect a causative correlation (e.g. Van der Veen, 1996; 2002, Warren et al., 2001).

Most Greenland and northern hemisphere ice sheet models use a sea-level forcing derived from either coral based observations (e.g. Fairbanks, 1989) or oxygen-isotope data; for example, the SPECMAP stack of Imbrie et al. (1984). The latter is often preferred if the ice model requires a sea-level record that spans several glacial cycles (e.g. Huybrechts, 2002). As mentioned, the component of RSL change around Greenland which is driven by non-Greenland ice mass variation departs significantly from such observations and records (see below). Perhaps because of the difficulties in modelling large-scale ice sheet response to changes in water depths, there has been almost no consideration of the spatial variability in past sea-level change when adopting a sea-level forcing - this is despite the existence of models which can accurately predict long-term sea-level change (e.g. Mitrovica and Milne, 2003; Kendall et al., 2005).

The primary aim of this Chapter is to present and analyse post-LGM predictions of vertical land motion and RSL change generated from non-Greenland ice load change and to consider the influence of these signals on a glaciological model of GrIS evolution. For this purpose, we use the global ice sheet reconstruction ICE-5G (Peltier, 2004) with the Greenland component removed. The reader should note that the NAIS component of the ICE-5G reconstruction is represented by the model of Peltier (2002). We begin, in Section 4.2, by examining the solid Earth motion component of non-Greenland RSL change. We go on to conduct an experiment with the Huy1 model to examine the influence of this RSL signal on the evolution of the GrIS. In Section 4.3 we show how the non-Greenland RSL signal departs from the eustatic signal and is spatially variable. We go on to examine the separate processes that cause this spatial variability. In our second modelling experiment, we

force the Huy2 model using a more realistic sea-level forcing, our results are discussed in Section 4.4 and summarised in Section 4.5.

4.2. The influence of non-Greenland solid Earth motion on the evolution of the GrIS

4.2.1 Nature of the non-Greenland solid Earth signal

As briefly described in Chapter 2 (see Sub-Section 2.4.2.1), non-Greenland solid Earth motion plays a significant role in the RSL history of Greenland. In particular, over the Holocene period, we found that in some areas solid Earth motion caused by Greenland and non-Greenland ice load change were approximately of the same magnitude (Fig. 21). As mentioned, in most regions the solid Earth is responding to the collapse and migration of peripheral forebulges (Fleming and Lambeck, 2004; Sub-Section 2.4.2.1). The exception is the northwest of Greenland, here the solid Earth component of non-Greenland RSL change records a net fall since the LGM. The response of the Earth in this region is characterised by post-glacial rebound due to the close proximity of Ellesmere Island ice. In areas outside of the northwest, however, our predictions of solid Earth deflection contribute to a net RSL rise. In general, this net RSL rise shows a pattern of RSL fall up until 14 ka BP and then a rise which continues up until present-day (see Fig. 40 below). Thus, the non-Greenland forebulges were highest around 14 ka BP – we therefore show a spatial plot of the vertical solid Earth component of RSL change at this time (Fig. 35a). This shows that the forebulge was around 30-60 m higher than at present in most areas of Greenland. A relatively small deflection of the solid surface when we consider local isostasy allows, if equilibrium is reached, the solid Earth to be depressed approximately 1/3 of the ice thickness. Note that predictions shown in Figure 35 were generated using our reference Earth model (the viscosity structure of which is characterised by a lithospheric thickness of 96 km and upper and lower mantle viscosities of 5×10^{20} Pa s and 10^{22} Pa s, respectively). Of course, to some degree, variations in mantle viscosity structure will influence the

size and dynamics of the non-Greenland forebulge (e.g. Peltier, 1974). Although this is likely unimportant as modelling results indicate that the post-LGM evolution of the GrIS shows little sensitivity to changes in the rate of isostatic uplift (and this is in response to changes in 'local' Greenland ice) (Huybrechts, 2002).

In Figure 35b we show the predicted size of the present-day non-Greenland deformation field. As shown in Chapter 3, there is continuing present-day Earth response to past non-Greenland ice load changes, which can be observed using GPS (see Sub-Section 3.3.3). Our predictions suggest the non-Greenland peripheral bulge results in a perturbation to land height elevation between 10-40 m today (relative to the equilibrium land height at the onset of surface loading - 123 ka BP).

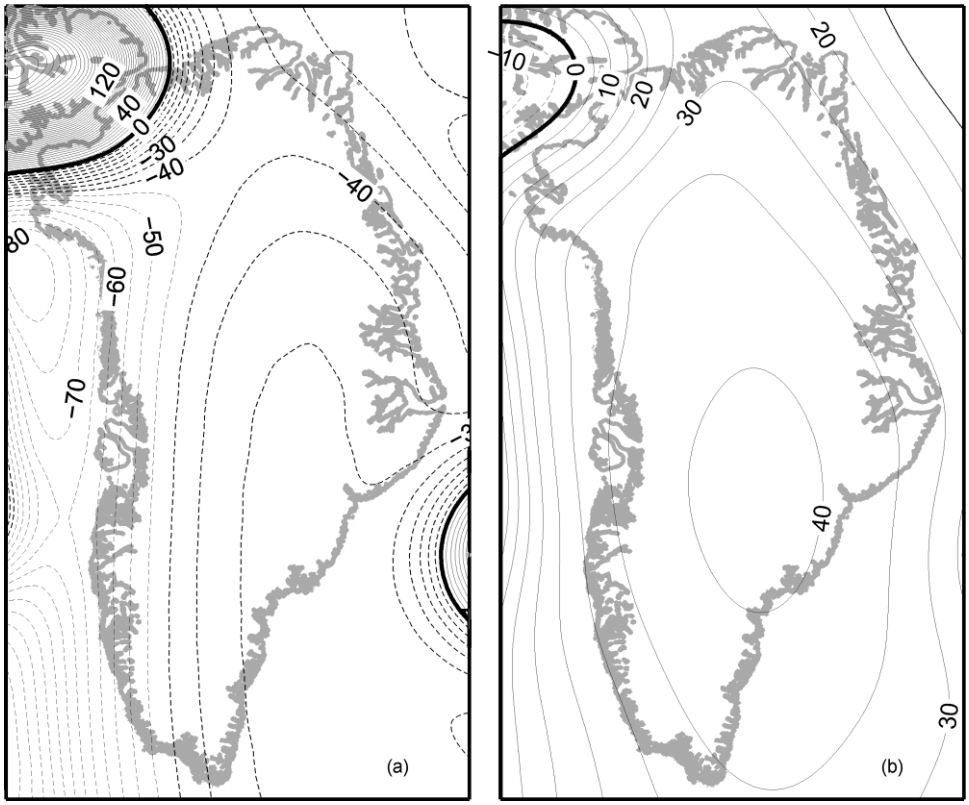

Fig. 35. Predicted land motion contribution to RSL change (metres) generated using non-Greenland ice (ICE-5G) and our reference Earth model. We show the vertical land motion component for (a) the relative change between 14 ka BP and present-day (b) the present-day deformation field (relative to the equilibrium land height at the onset of surface loading - 123 ka BP).

4.2.2 The influence of non-Greenland solid Earth motion: Modelling results

In this Sub-Section we conduct an experiment with the Huy1 model to consider how non-Greenland solid Earth motion might have influenced the evolution of the GrIS. As outlined in the description of Huy1 (see Sub-Section 1.4.1), the ice model contains its own isostasy treatment, which is commonly referred to as the elastic lithospheric relaxed asthenopshere (ELRA) model (see Huybrechts and de Wolde (1999) for a full description). This is a more simplified and less computationally expensive method than the spherically symmetric self-gravitating viscoelastic Earth model used to generate the sea-level predictions throughout this thesis. The ELRA model has an asthenopshere with a single relaxation time; for the Huy1 model this is assigned a value of 3000 years. This figure is based on results from an earlier study, which compared the ELRA model to more realistic isostasy treatments

(Le Meur and Huybrechts, 1996). The Huy1 model calculates isostatic adjustment every 20 years over the period 123 ka BP to present-day (i.e. since the last interglacial) and accounts for Greenland ice and ocean load changes. We generated predictions of non-Greenland solid Earth motion using our GIA model (see Sub-Section 1.4.1 for a description) over the same period and linearly interpolated the results so that they could be input to the Huy1 model using a 20 year time resolution.

Figure 36 shows the influence of non-Greenland solid Earth motion on modelled ice volume and extent changes of the GrIS. These results suggest that non-Greenland solid Earth deformation had little impact on the evolution ice sheet. This is not a particularly surprising finding given the relatively small size of the non-Greenland solid surface elevation changes (c. 30-60 m since 14 ka BP). However, we notice that the Holocene retreat of the ice sheet is somewhat slower and the model no longer evolves to reach its present-day reference state. During this period, the difference in the ice margin position between these two models runs is no larger than 20-40 km (figure not shown). The largest differences are in southwest Greenland where the non-Greenland forebulge is highest (see Fig. 35a) and where the Holocene retreat of the ice sheet was most prominent (e.g. Van Tatenhove et al., 1995, 1996). We interpret this result as being due to the presence of the non-Greenland forebulge which acts to raise the elevation of the ablation zone; at higher altitudes the temperature is lower and thus melting is reduced.

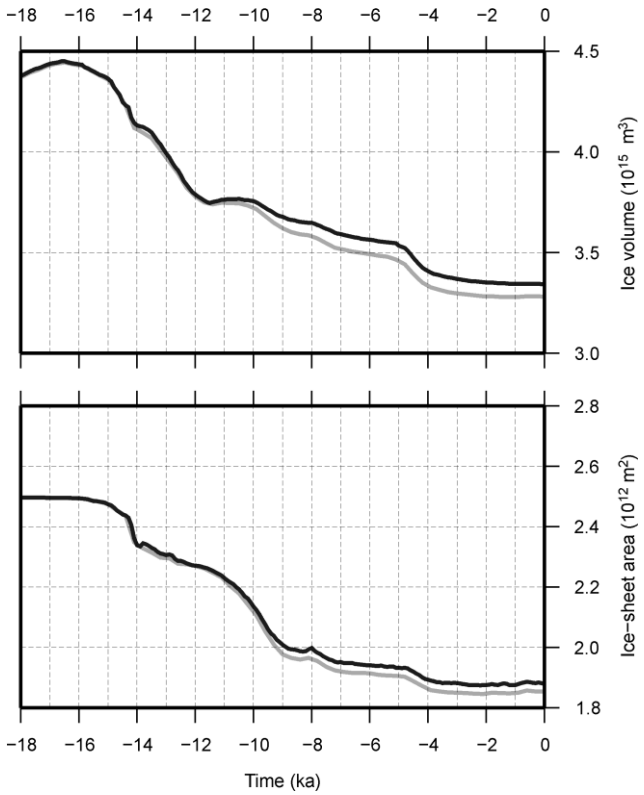

Fig. 36. Ice sheet volume and extent changes for the Huy1 model (grey line) and for an ice model run which includes non-Greenland solid Earth deformation (black line).

4.3. The influence of non-Greenland RSL change on the evolution of the GrIS

4.3.1 Nature of the non-Greenland RSL signal and eustatic sea level

In this Section, we examine the early period of post-LGM RSL change and the implications for the marine retreat of the GrIS. Figure 37 shows a location map of the 6 sites we have chosen to focus on for this purpose. They mark the locations of field investigations where past RSL changes have been measured (see Section 2.2) and their distribution represents a fairly evenly geographic spread around the coast of Greenland. For 5 of the coastal sites, we also mark a position that is seaward from each location (roughly perpendicular to the coast) and situated close to the edge of the continental shelf. This is done so we can examine how RSL change varied across the continental shelf.

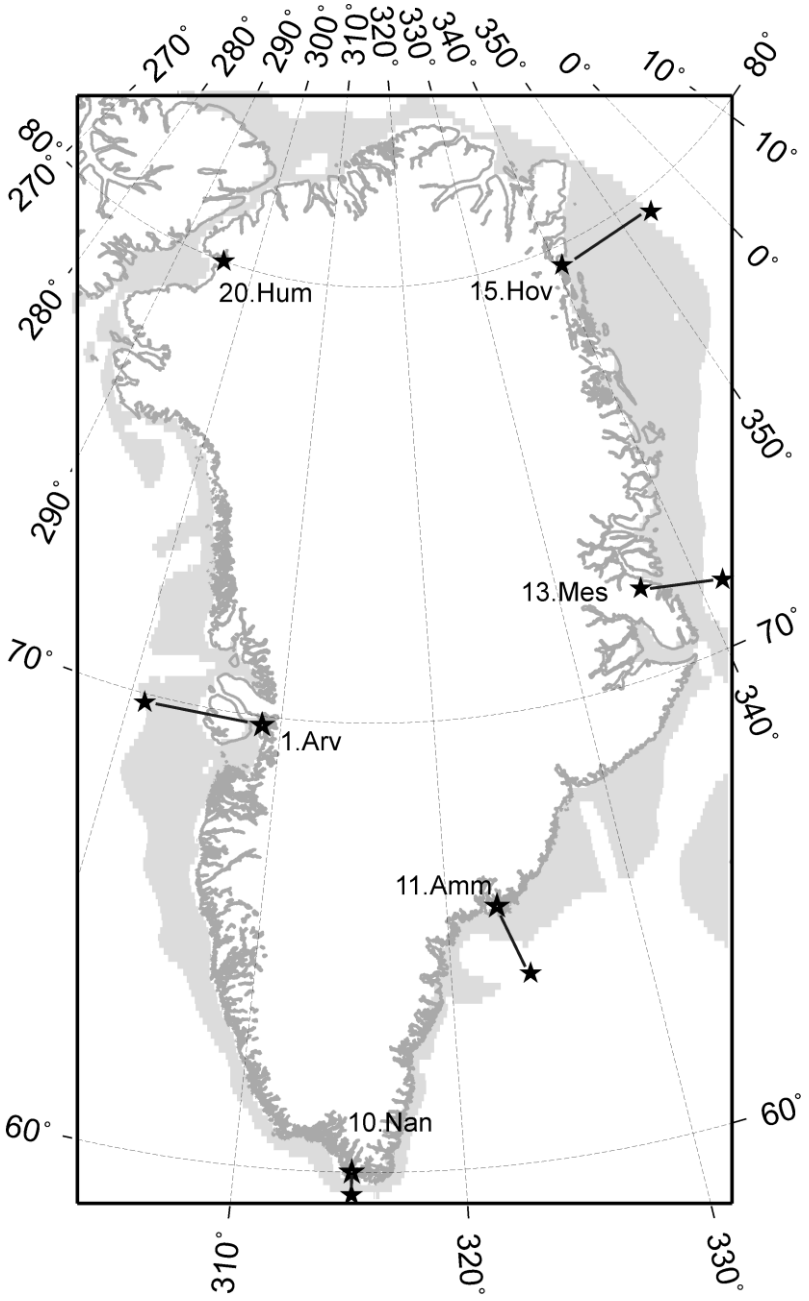

Fig. 37. Stars show the locations from around Greenland where we generated our sea-level predictions – they mark 6 coastal sites where RSL field investigations have been carried out (see Section 2.2) and adjacent locations (approximately perpendicular to the coastline) situated close to the edge of the continental shelf. The light grey shading defines bathymetric depths of < 400 m (i.e. the continental shelf).

Figure 38 shows non-Greenland RSL predictions for the locations shown in the above Figure 37. We also include plots of the eustatic signal from ICE-5G non-Greenland meltwater (Peltier, 2004) and the eustatic signal as derived from the $\delta 0^{18}$ SPECMAP stack (Imbrie et al., 1984). As mentioned, the sea-

level record used to force the Huybrechts (2002) model is derived from the SPECMAP data (a conversion of –34.83 m of sea-level per thousandth of a percentage change in the isotope values). It is worth noting that the Greenland component of the ICE-5G model contains an excess volume (relative to present) of 2.8 m ice-equivalent sea level at the LGM (Tarasov and Peltier, 2002; Peltier, 2004) – i.e. this is a small amount when compared to total eustatic signal. Comparing the eustatic contributions of the non-Greenland ICE-5G model and the SPECMAP record (which accounts for Greenland ice), therefore, seems reasonable.

At the LGM (21 ka BP), both of the eustatic signals record a value of c. -127.5 m. After this time, however, there are noticeable differences between the two curves (Fig. 38). The SPECMAP derived curve indicates a near constant rate of sea-level rise during deglaciation with present-day sea-levels reached by 4 ka BP. The rate of sea-level change is far more variable in time for the ICE-5G non-Greenland eustatic signal and the curve is punctuated by two periods of rapid sea-level rise; identified as meltwater pulses in the coral records (e.g. Fairbanks, 1989; Bard et al., 1990). Meltwater pulse 1A (mwp-1A) is dated to around 14.2 ka BP and the smaller amplitude meltwater pulse 1B (mwp-1B) follows the YD. Present-day sea levels are reached around 6-7 ka BP, this is in good agreement to studies which have compared RSL observations to model predictions for the mid-to-late Holocene period (Lambeck and Purcell, 2005; Milne et al., 2005). We assess the implications of the differences between the two eustatic signals in Sub-Section 4.3.4.

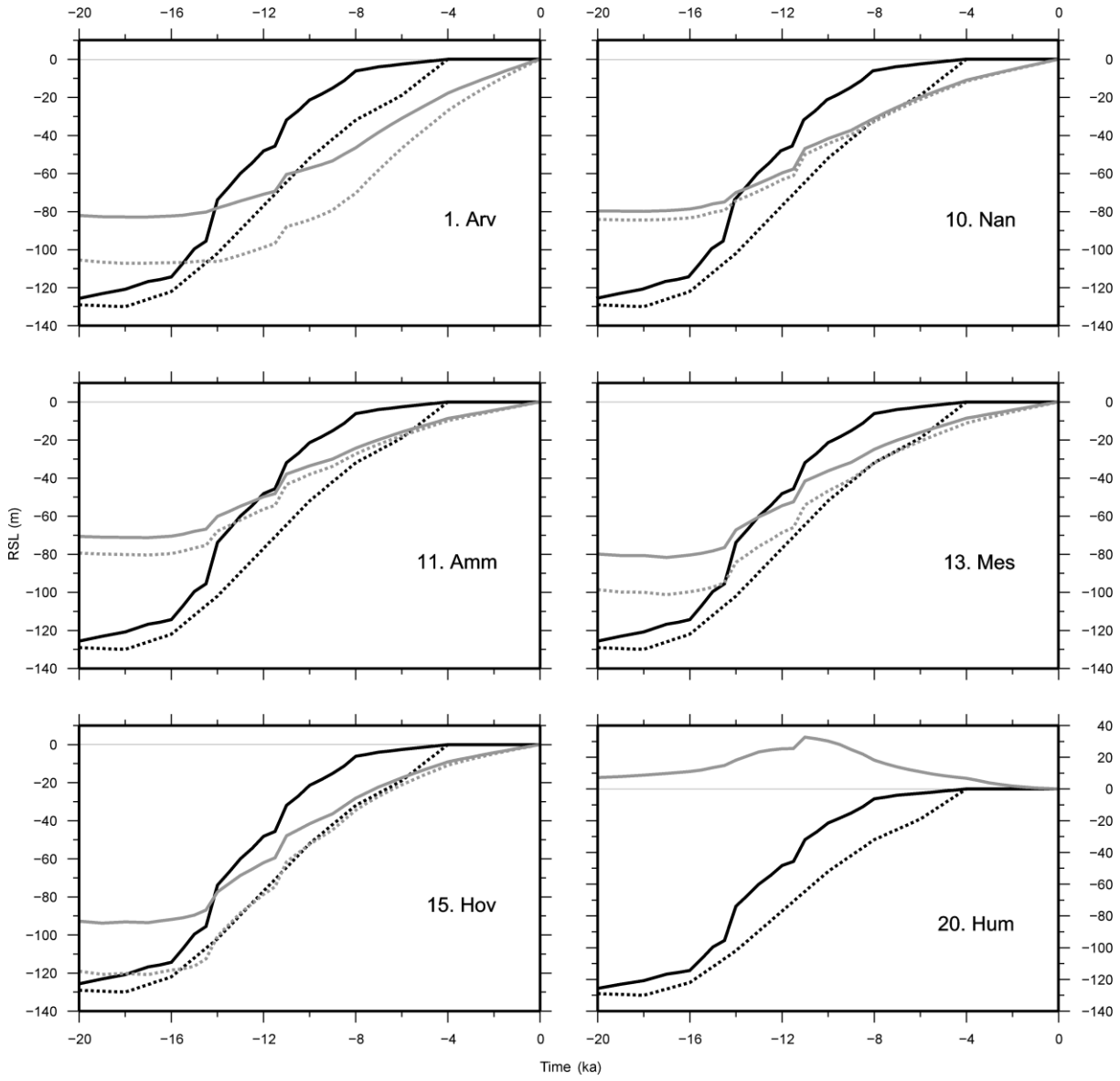

Fig. 38. Grey lines show predicted RSL generated using the non-Greenland ICE-5G (Peltier, 2004) ice history and our reference Earth model – the solid and dotted lines mark predictions for the coastal sites and their neighbouring shelf edge locations respectively (see Fig. 37). The black curves denote the eustatic meltwater contribution from the non-Greenland ICE-5G model (solid black line) and the eustatic signal as derived from the SPECMAP stack (Imbrie et al., 1984) which is used to force the Huy2 ice model (dotted black line).

Figure 38 also illustrates that non-Greenland RSL change has distinct regional variability and is significantly different from both eustatic signals. As discussed in the previous Sub-Section, non-Greenland RSL change in the northwest of Greenland is markedly different to other parts of

Greenland (it shows a net fall) due to its close proximity to Ellesmere Island ice (see Humbolt Gletcher – site 20, Fig. 38). Outside of the northwest, however, non-Greenland RSL change between the LGM and present-day shows a net rise. The size of this RSL rise varies across Greenland; for our locations shown in Figure 37 it is in the range 70-120 m. So in some areas, for example the southern sectors of Greenland, it is considerably less than the non-Greenland eustatic ICE-5G signal (an 80 m net rise is c. 63 % of the total eustatic contribution). Further, we note that the size of the RSL rise shows, in some cases, quite large differences between coastal and outer shelf locations. For example, in northeast Greenland (site 15, Fig. 38) where the continental shelf is wide (c. 270 km), the net RSL rise at the coastal site is c. 93 m and at the outer shelf location is c. 119 m. In all regions we find that the outer shelf position has experienced a larger RSL rise since the LGM than at the coastal location. Our predictions also indicate that in areas outside of northwest Greenland, RSL change during the early stages of deglaciation (20-15 ka BP) is much smaller than the 26 m rise embodied in the eustatic ICE-5G curve over the same period.

There are also considerable spatio-temporal differences in the non-Greenland RSL signal moving around the coast, particularly after 15 ka BP. At Arveprinsen (site 1, Fig. 38), for example, the RSL prediction shows no evidence of the rapid increase in sea-level rise associated with mwp-1A. In comparison, at other sites, the meltwater pulse is distinguishable in the predictions. In southern Greenland at Nanortalik (site 10, Fig. 38), the size of mwp-1A pulse is c. 5 m whilst in the east at Mesters Vig (site 13, Fig. 38) it is more pronounced and c. 9 m. Evidence from the Barbados coral record identifies mwp-1A as a sea level rise of c. 20 m in around 500 years (Fairbanks et al., 1989); there is a similar change in eustatic sea level for the ICE-5G model (see Peltier, 2004). After 14 ka BP sea-level change appears more uniform across Greenland; the rise in sea level associated with mwp-1B is of similar magnitude across all sites. These observations can be more clearly seen in Figure 39,

which shows predicted *rates* of non-Greenland RSL change for the 6 coastal locations and also the non-Greenland ICE-5G eustatic signal.

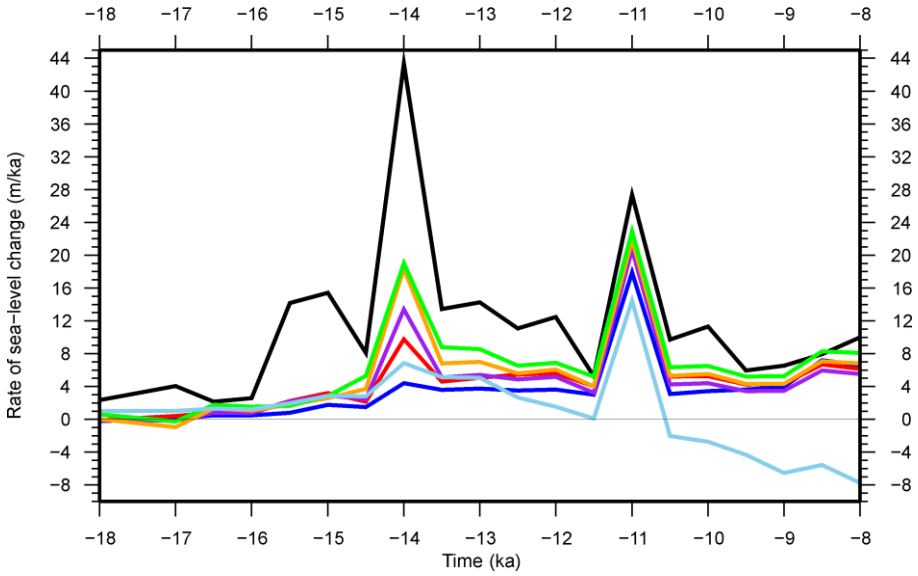

Fig. 39. Predicted rates of RSL change generated using the non-Greenland ICE-5G (Peltier, 2004) ice history and our reference Earth model: Arv (site1) – dark blue, Nan (site 10) – red, Amm (site 11) – purple, Mes (site 13) – orange, Hov (site 15) – green and Hum (site 20) – light blue. The black line denotes the eustatic meltwater contribution from the non-Greenland ICE-5G model.

4.3.2 Non-Greenland RSL change: The component signals

To better understand why regional differences in non-Greenland RSL change occur, we split the non-Greenland RSL predictions into their component signals (Fig. 40).

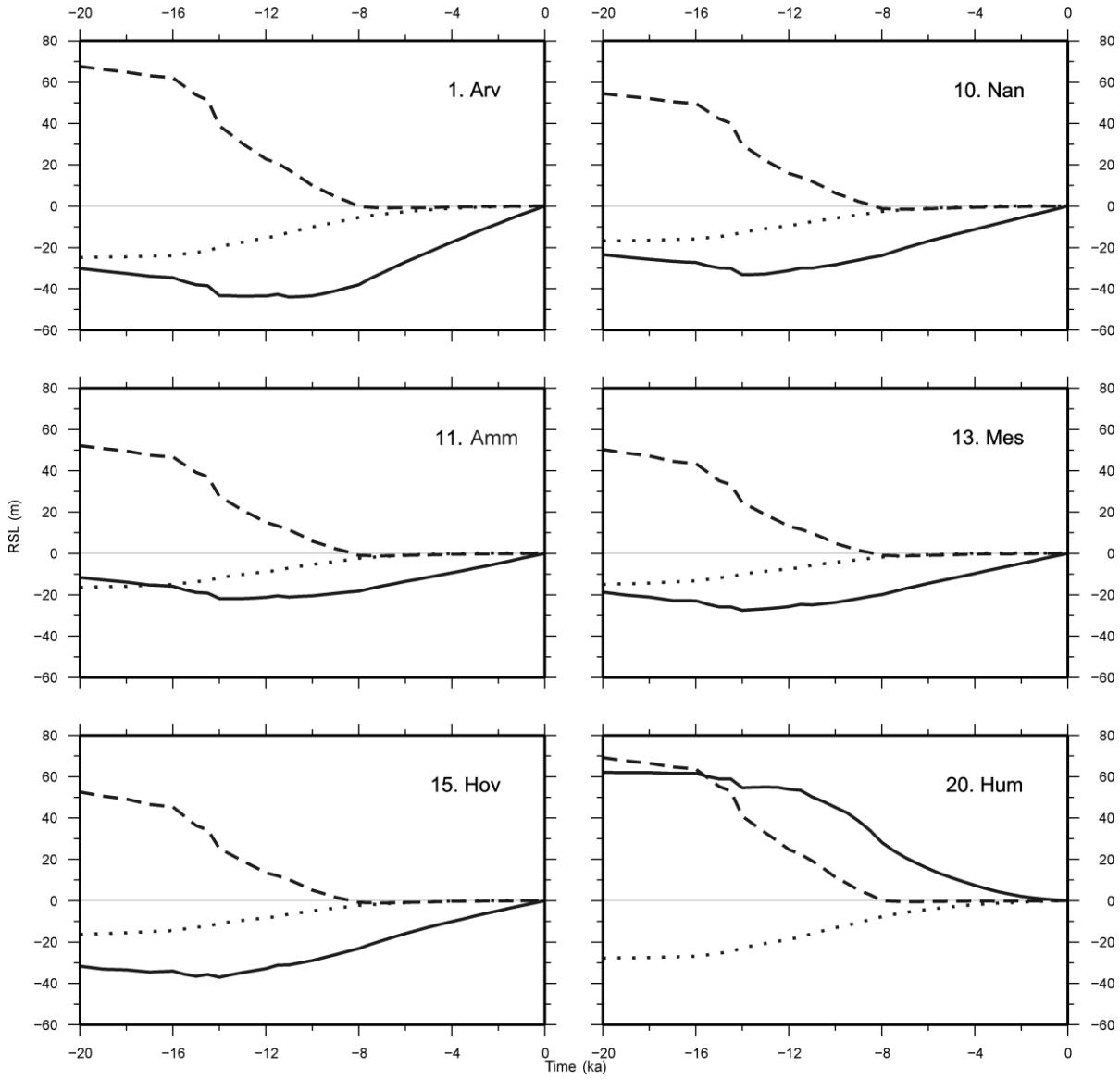

Fig. 40. RSL predictions for the 6 coastal locations shown in Fig. 37 and generated using the non-Greenland ICE-5G (Peltier, 2004) ice history and our reference Earth model. The solid line marks the RSL contribution due to deflection of the Earth's solid surface. The dashed and dotted lines denote, respectively, processes that perturb the ocean surface due to mass transfer between ice and ocean (direct effect) and the deformation of the solid Earth (indirect effect) (see also the description of the GIA model in Sub-Section 1.4.1).

We briefly examined the role of non-Greenland ice load change in Chapter 2 (Sub-Section 2.4.2.1) and found that, similar to the results of Fleming and Lambeck (2004), the direct effect dominates RSL change in most areas of Greenland during the early part of deglaciation and deformation of the

Earth's solid surface dominates during the Holocene period (see also above Sub-Section 4.2.1). It is well established that an ice sheet will exert a gravitational attraction on the neighbouring ocean and therefore water will be drawn towards it (e.g. Farrell and Clark, 1976) – the direct effect largely reflects this process. As the NAIS retreats from its maximum LGM extent and rapidly loses mass, therefore, the ice–ocean gravitational attraction becomes weaker. As a result, the area within c. 2000 km of the melting ice sheet will experience a fall in the height of the ocean surface (e.g. Mitrovica et al., 2001b, 2009); as illustrated by predictions of the direct effect (dashed lines, Fig. 40). This rapid RSL change occurs in concert with any ice mass variation; the other processes influencing RSL change (the indirect effect on the ocean surface and the influence of solid Earth deformation on vertical land motion) are governed by the viscoelastic response of the Earth, so will include both an immediate (elastic) component and a delayed (viscous) component to the loading changes. The indirect effect is the gravitational effect on the ocean surface which is caused by internal mass flux of the solid Earth. The predictions of the indirect effect (dotted lines, Fig. 40) show a pattern of post-LGM RSL rise before reaching and remaining at present-day sea levels at c. 8 ka BP. This rise is probably due to the dominant influence of post-glacial rebound in North America. It should be noted that predictions of the direct and indirect effects include sea-level changes associated with Earth's rotational feedback (Milne and Mitrovica, 1996), however, this effect is comparatively small in the near-field of Greenland. It is interesting to note that, over the early part of deglaciation (c. 20-15 ka BP), *rates* of predicted RSL change caused by the indirect effect and solid Earth motion are approximately opposite in most areas of Greenland – they effectively cancel out. For this reason, RSL change during this early period is dominated by the direct effect (Fleming and Lambeck, 2004; Sub-Section 2.4.2.1). As shown in Figure 38, the RSL fall associated with the direct effect acts to offset the eustatic sea-level rise, this results in predictions of relatively stable sea levels throughout most of Greenland from 20 to 15 ka BP.

4.3.3 The pattern of ice margin retreat and possible relation to the sea-level forcing

Figure 41 shows spatial plots of predicted rates of RSL change around Greenland up until 10 ka BP; after which time the ice sheet was inland of the present-day coastline (Bennike and Björck, 2002; Funder and Hansen, 1996). As discussed above, the early period of deglaciation (22-16 ka BP) is characterised by relatively stable sea-levels around Greenland - rates in most ice covered shelf areas less than ± 1 mm/yr (Fig. 41a, b and c). From 16 to 14 ka BP (Fig. 41d), rates of RSL change show a distinct east-west gradient: Rates of rise remain relatively low in the west, whereas, those in the east reach values between 6 and 8 m/ka. This spatial gradient is due to the diminishing gravitational signal of the NAIS. In the later periods (Fig. 41e and f), rates of rise generally increase but the east-west gradient becomes smaller. If the marine retreat of the ice sheet was driven by non-Greenland RSL rise; we would expect changes in the extent of the GrIS to reflect the RSL changes shown in Figure 41.

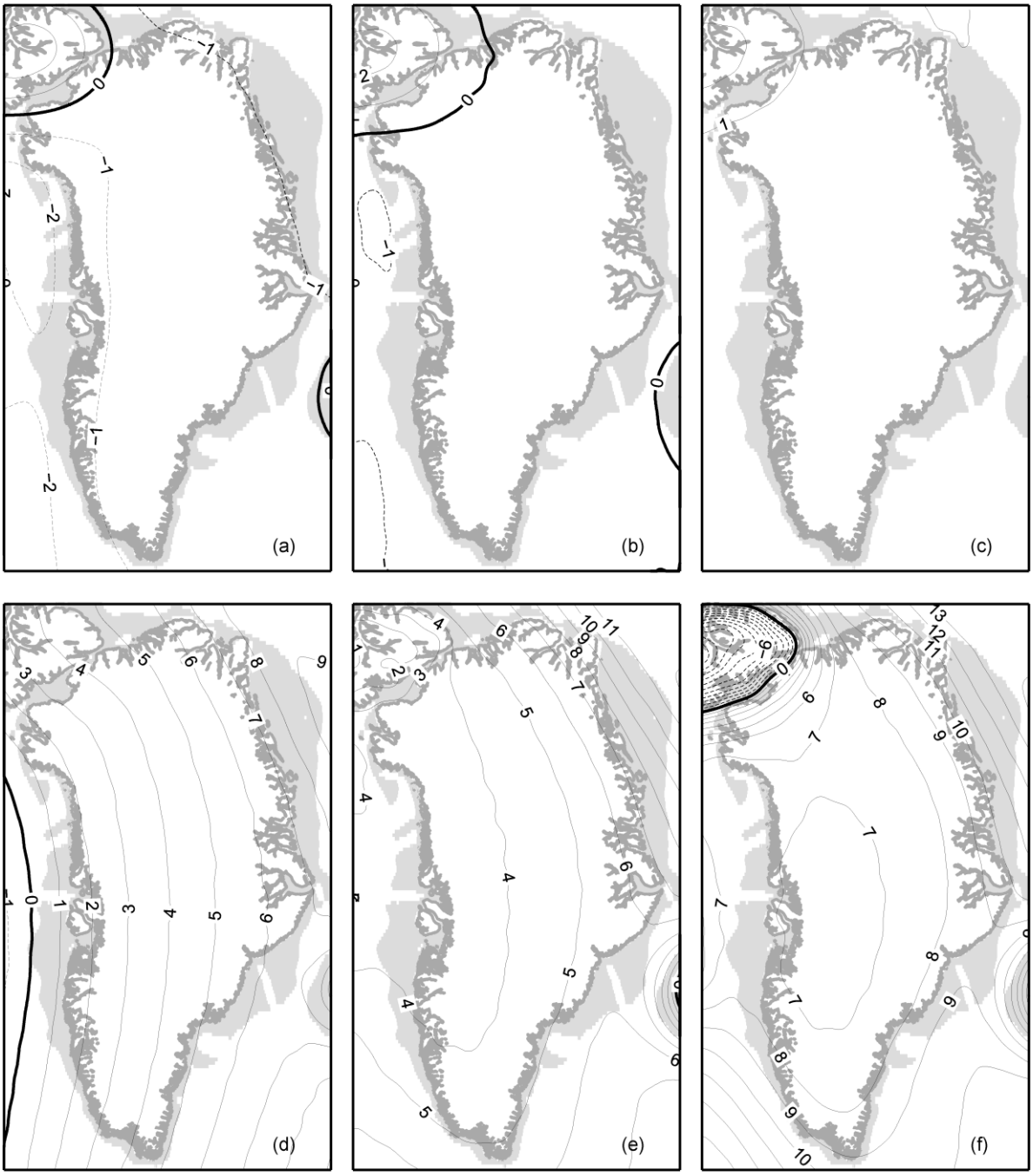

Fig. 41. Predicted mean rates of RSL change (m/ka) generated using the non-Greenland ICE-5G (Peltier, 2004) ice history and our reference Earth model; for the periods (a) 22-20 ka BP, (b) 20-18 ka BP, (c) 18-16 ka BP, (d) 16-14 ka BP, (e) 14-12 ka BP and (f) 12-10 ka BP. The light grey shading defines bathymetric depths of < 400 m (i.e. the continental shelf).

It has been generally assumed that the retreat of the GrIS occurred sometime after the LGM (c. 21 ka BP). Past studies that have used RSL data to constrain the evolution of the GrIS have suggested

different retreat scenarios; Tarasov and Peltier (2002) indicate retreat initiated as late as the early Holocene period whilst Fleming and Lambeck (2004) propose the retreat began c. 16 ka BP. The Huy2 model indicates the GrIS maintained its LGM extent up until 12 ka BP before undergoing a very rapid retreat (see Sub-Section 2.4.1.1 and Fig. 15). In Chapter 2, we explored several different marine retreat scenarios for the Huy2 model; the timing of the modelled marine retreat is controlled by varying the sea-level parameterisation. In our experiment (see Sub-Section 2.3.2.2), we found different sea-level parameterisations were favoured in different regions of Greenland: RSL data from eastern Greenland generally showed better agreement to sea-level predictions generated using an ice load history where the marine retreat began relatively early (c. 16 ka BP), whilst RSL data from western Greenland favoured a late retreat scenario (c. 12 ka BP). Observations of the marine deglacial chronology of the ice sheet generally support this finding (see below); although we note these data are sparse and often pertain to minimum ages (see Sub-Section 2.3.2.2 for initial discussion). It is therefore difficult to draw firm conclusions about the pattern of marine retreat.

Studies from the continental shelf in eastern regions of Greenland generally indicate that retreat began a few thousand years after the LGM (c. 21 ka BP) (e.g. Mienert et al., 1992; Nam et al., 1995; Andrews et al., 1997; Smith and Licht, 2000; Evans et al., 2002, 2009; Jennings 2002; 2006; Kuijpers et al., 2003). As mentioned, a GIA modelling study suggests the southern tip of the GrIS started to retreat from its LGM position at 22 ka BP (Sparrenbom, Ph.D. thesis). In southern Greenland evidence from lake sediments obtained on an island c. 10 km offshore indicate that the area was ice-free at or before 14.1 ka BP (Bennike and Björck, 2000; Bennike et al., 2002). This is in agreement with geochemical data obtained from a southern Greenland marine sediment core (Carlson et al., 2008).

Whilst evidence from eastern and southern Greenland indicates a relatively early retreat, data obtained in central west Greenland suggests retreat from the continental shelf occurred somewhat later. The deglaciation of the main part of Disko Bugt is dated to a minimum of 10.2 ka BP (Long et al., 2003; Lloyd et al., 2005) and recent cosmogenic studies from central southwest Greenland suggest that ice persisted on the inner continental shelf until the early Holocene (Rinterknecht et al., 2009; Roberts et al., 2009). The above observations and modelling results suggest the marine retreat of the ice sheet was asynchronous; with areas of the continental shelf becoming ice-free in the east and south before regions in the west. This is qualitatively consistent with the spatial variation in the sea-level forcing and we explore this possible connection further in the following Sub-Section.

4.3.4 The influence of non-Greenland RSL change: Modelling results

As briefly discussed in the Introduction, the treatment of calving in northern hemisphere ice sheet models is normally implemented as a simplistic paramaterisation. The sea-level forcing of Huy1/2 uses an empirical formulation that parameterises the maximum grounding depth of the ice sheet (H_c) as a function of eustatic sea-level change (ΔH_{sl}) (see Sub-Section 2.3.2.2). The marine-extent parameterisation is described by Huybrechts (2002) as a 'phenomenological relationship' as it allows grounded ice to advance into deeper water during low eustatic periods (times when the climate was colder). Conversely, during times of high eustatic sea level (i.e. when the climate was warmer) the ice margin is forced landward. The eustatic sea-level record (ΔH_{sl}) used is derived from the SPECMAP stack of marine oxygen-isotope values (Imbrie et al., 1984) and is shown in Fig. 38. Note that the Huy1/2 models account for solid Earth deflection arising from Greenland ice and ocean loading changes when calculating water depths (this creates a feedback between the marine extent of the ice sheet and grounding line migration). Eustatic sea-level changes are not included in the calculation of water depths (when determining the ocean load) as they were found to have a second-order effect when compared to Eq. 2 (see Zweck and Huybrechts, 2003).

In this Sub-Section we attempt to build a more realistic sea-level forcing for the Huy2 model; based upon our findings in the early parts of Section 4.3 and on the hypothesis that non-Greenland RSL change controlled the marine retreat of the GrIS (we address this assumption in the following Section). As discussed above, there are significant differences between the ICE-5G and SPECMAP eustatic sea level curves. Of these two datasets, the ICE-5G curve represents the more accurate record of eustatic sea-level change; it is in reasonable agreement with coral observations (e.g. Fairbanks, 1989; Bard et al, 1990; Yokoyama et al., 2000), which provide a direct measurement of past sea-level change (see Fig. 12a of Peltier (2004)). Whereas, the eustatic curve derived from the SPECMAP isotope values is a proxy record of eustatic sea-level change and thus has limited accuracy. To improve the accuracy of the sea-level record used to force the Huy1 model, therefore, we replace the SPECMAP curve with the predicted eustatic non-Greenland contribution of the ICE-5G model over the period 22 ka BP to present-day. We also introduce two spatially variable RSL changes to the sea-level forcing: (i) height shifts of the solid Earth, as detailed in the previous Sub-Section; (ii) height shifts of the ocean surface resulting from gravitational effects (the direct and indirect effect). We calculate non-Greenland RSL changes every 20 years over the period 123 ka BP to present-day (as with the previous experiment on land height changes) and input them to the Huy2 model. The LGM extent and sea-level parameterisation are as defined for the Huy2 model (see Sub-Sections 2.3.2.1 and 2.3.2.2 respectively).

Figure 42 shows the modelled maximum allowed extent of the ice sheet as defined by the sea-level parameterisation (note that ice extent changes due to variations in mass balance can occur within these bounds). In comparison to the Huy2 model, our new revised sea-level forcing produces a slightly smaller extent at the LGM and during the early part of the retreat (up until c. 10.5 ka BP). After this time, the new sea-level forcing allows a larger or as large an extent as the SPECMAP

oxygen isotope proxy. We do not place much importance on these results as the timing of the marine retreat is dependent on the formulation of the sea-level parameterisation.

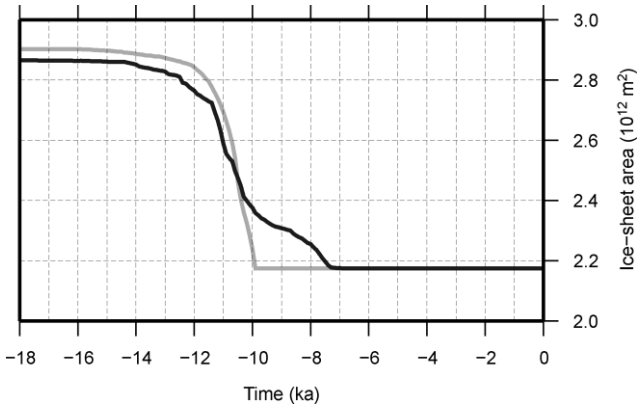

Fig. 42. Modelled maximum allowed ice sheet extent for Huy2 (grey line) and a model which has a sea-level forcing based on the non-Greenland RSL predictions of the ICE-5G model (black line).

In the Huy1/2 models, the pattern of marine retreat is essentially governed by the bathymetry of the continental shelf. However, making spatial changes to the sea-level forcing will also influence this pattern. Figure 43 shows the chronology of modelled maximum allowed extent for the Huy2 model and a model which includes spatial changes in non-Greenland RSL to the sea-level forcing. For the latter model, we find that the marine retreat was generally earlier in east Greenland and later in the west when compared to the results of Huy2. This finding is broadly consistent with the independent observations (see above Sub-Section 4.3.3.) and supports the hypothesis that the pattern of retreat was at least partly due to spatial variations in RSL change. A clear avenue for future work is to see whether the data-model misfits shown in Sub-Section 2.3.2.2 (where we found different sea-level parameterisations were favoured in different regions of Greenland) can be resolved by implementing a spatially variable sea-level forcing.

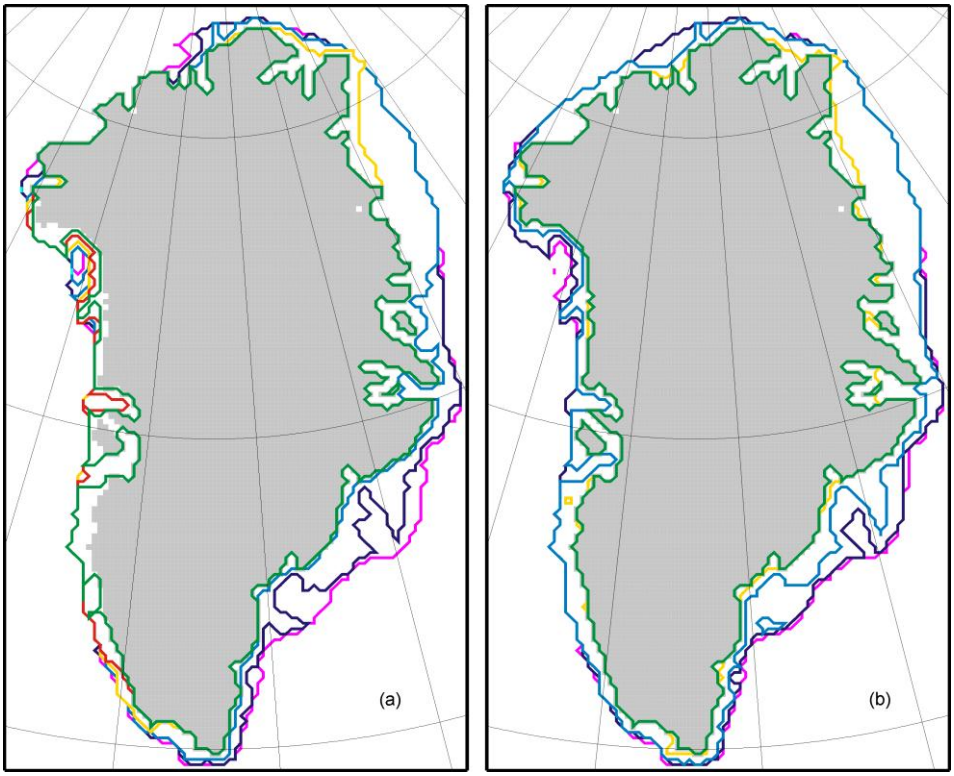

Fig. 43. Modelled maximum allowed ice sheet extent of a model which has a sea-level forcing based on the non-Greenland RSL predictions of the ICE-5G model (a) and Huy2 (b). The chronology is as follows; pink – 14 ka BP, dark blue – 12 ka BP, light blue – 11 ka BP, yellow – 10 ka BP, red – 9 ka BP and green – 8 ka BP. Modelled present-day land area is shaded dark grey.

4.4. Discussion

In the following discussion we focus on non-Greenland RSL change in relation to the marine retreat of the ice sheet. In the next Sub-Section (4.4.1) we examine the deglaciation of the NAIS and, in particular, uncertainty regarding the contribution of the NAIS to mwp-IA and the consequent implications for the above analysis. In Sub-Section (4.4.2) we discuss possible driving mechanisms of the marine breakup and in Sub-Section (4.4.3) limitations of the modelling approach adopted above. Issues to be explored in future work are to be highlighted in each Sub-Section.

4.4.1 The North American Ice Sheets and origin(s) of mwp-1A

As discussed above, sea-level predictions generated using the ICE-5G model indicate that the deglaciation of the NAIS had a strong control on post-LGM non-Greenland RSL change. The North American component of the ICE-5G global ice model is detailed by Peltier (2002); this analysis primarily uses observations of GIA-induced sea-level change to quantitatively infer the past behaviour of the NAIS. In contrast to other modelling efforts (e.g. Tushingham and Peltier, 1991; Peltier, 1998; Marshall et al., 2002), in which the LGM geometry of the NAIS has a monodomal structure, the ICE-5G reconstruction is characterised by a multidomal form. Peltier (2002) found that to reconcile modelling results with modern geophysical observations (Argus et al., 1999; Lambert et al., 2001), required a dome in the west (the so called "Keetawin dome") with a ridge of ice extending southeast and surrounding Hudson Bay. Such a multidomal structure has previously been proposed on the basis of geomorphological evidence (Dyke and Prest, 1987) and recent satellite gravity data further support this assertion (Tamisiea et al., 2007).

As represented in the ICE-5G model; the NAIS contains 74 m ice-equivalent sea-level at the LGM (see Fig. 10 of Peltier (2004)). Estimates from glaciological modelling suggest an LGM ice volume of this size is plausible (Marshall et al., 2002; Tarasov and Peltier, 2004). During the early period of deglaciation (21 to 15 ka BP), we showed that rates of non-Greenland RSL change remained low (< 2 m/ka), in contrast to the eustatic signal (Fig. 39). Over this same time, the ICE-5G reconstruction indicates that the NAIS is steadily losing mass; from 21 to 15 ka BP the modelled ice sheet reduces in volume by around 10 m ice-equivalent sea-level (see Fig. 10 of Peltier (2004)). Geomorphological observations show that the NAIS did not significantly change in extent during this early period (Dyke et al., 2003). If the ice sheet contributed to early sea-level rise, therefore, it was due to central thinning rather than peripheral retreat (Dyke et al., 2002).

One notable feature of the ICE-5G model is the large contribution of the NAIS to mwp-1A; the ice volume loss from 15 to 14 ka BP corresponds to a eustatic sea-level rise of c. 20 m (Peltier, 2004). As discussed above, this large ice-ocean mass exchange had a significant impact on the sea-level history of Greenland (see Fig. 38 and Fig. 39). The source distribution of mwp-1A, however, remains contested in the literature. Although traditionally assumed to be sourced from the NAIS, the work of Clark et al. (1996) first suggested that a significant amount of mwp-1A might have originated from the Antarctic Ice Sheets (AIS). This hypothesis was later directly tested using sea-level fingerprinting; which supported the assertion that the AIS were the most likely dominant source of mwp-1A (Clark et al., 2002; Bassett et al., 2005). However, Peltier (2005) argues that the sea-level data used in these fingerprint studies does not rule out the possibility that mwp-1A had an entirely northern hemisphere origin. Several studies have argued that a dominant Antarctic source of mwp-1A would have strengthened North Atlantic Deep Water formation, thereby causing a warming of the Northern hemisphere (e.g. Kienast et al., 2003; Weaver et al., 2003). This explanation is consistent with observed Bolling-Allerod warming in the northern hemisphere; the onset of which was concurrent with mwp-1A (Stuiver and Grootes, 2000). A recent study, which examined the geochemical constraints on the runoff of mwp-1A from North America, concluded that less than 30% of the meltwater pulse was sourced from Laurentide Ice Sheet (Carlson, 2009). Whilst glaciological modelling results suggests that the eustatic contribution of the NAIS to mwp-1A is in the range of 7.7 to 10.2 m (Tarasov and Peltier, 2004, 2006), around half the size of the meltwater pulse embodied in the ICE-5G model. We note that although a number of recent studies have argued for a large Antarctic component of mwp-1A, field observations of the AIS, along with ice sheet modelling results, indicate it made only a small contribution to mwp-1A (Licht, 2004; Price et al., 2007; Macintosh et al., 2007).

Given the uncertainty of the origin(s) of mwp-1A, we generate sea-level predictions using the global ice history presented by Bassett et al. (2005). This model is an adaption of the ICE-3G model (Tushingham and Peltier, 1991) and was revised to include a large (c. 15 m ice-equivalent sea level) contribution from the Antarctic Ice Sheets to mwp-1A. Figure 44 shows the corresponding non-Greenland RSL predictions at the 6 coastal sites we have examined – we also show predictions from the ICE-5G model for comparison. Over the early period of deglaciation (21-15 ka BP), we find that in areas outside of northwest Greenland predictions from the Bassett et al. (2005) model indicate a slightly larger rise in RSL than shown from the ICE-5G model. A key difference between the curves is the predicted RSL change during mwp-1A; the Bassett et al. (2005) model shows a uniform rapid rise in RSL which is similar in size to that shown in the eustatic curve. This is an unsurprising finding given that Greenland is in the far-field of Antarctica and suggests that in this scenario the corresponding pattern of ice margin retreat would be earlier and more symmetric than for a dominant North American source of mwp-1A. Unlike the ICE-5G model, the predictions from the Bassett et al. (2005) model show no rise in RSL associated with mwp-1B. After this time the predictions show generally similar changes in RSL up until present-day. These results show that the nature of sea-level change in Greenland during mwp-1A is very dependent on the source distribution of the meltwater. It is therefore important to better constrain the sources of mwp-1A in future work.

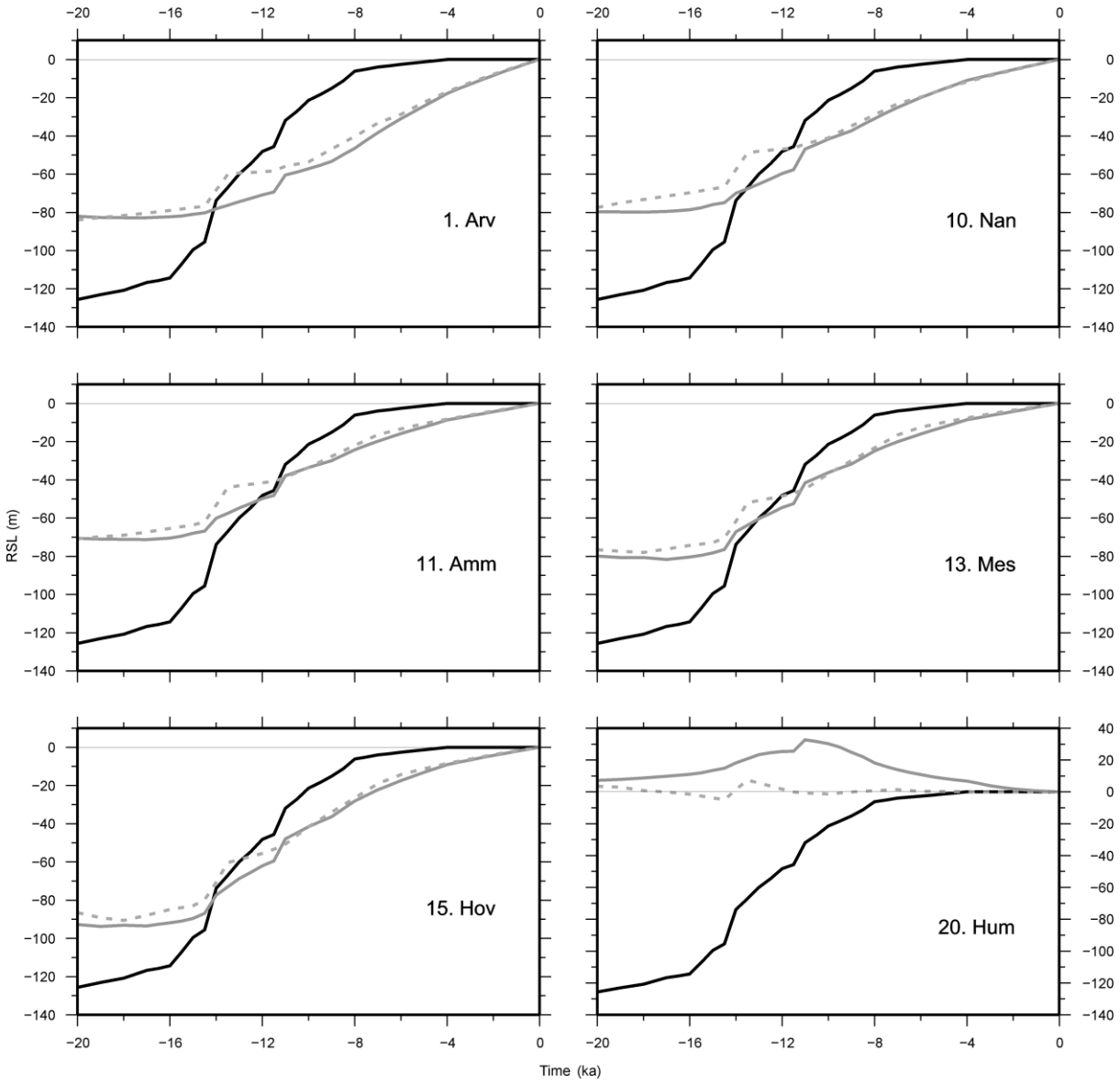

Fig. 44. The grey solid line shows predicted RSL generated using the non-Greenland ICE-5G (Peltier, 2004) ice history and our reference Earth model. The grey dashed line shows predicted RSL generated using the non-Greenland ice history of Bassett et al. (2005) – which includes a large contribution to mwp-1A from the Antarctic ice sheets. The black curve denotes the eustatic meltwater contribution from the non-Greenland ICE-5G model.

4.4.2. Possible driving mechanisms of the marine retreat

As discussed in the Introduction, past studies have hypothesised that the marine breakup of the GrIS was driven by sea-level rise (Funder, 1989; Funder and Hansen, 1996). Although post-LGM sea-level

change would have undoubtedly influenced calving, it is not yet clear to what extent it controlled the retreat of the ice sheet. Of course, as widely demonstrated in other modelling studies, the ice sheet is sensitive to changes in other climate parameters (e.g. Calov and Hutter, 1996; Greve, 1997; Huybrechts, 1994, 2002; Ritz et al., 1997; Zweck and Huybrechts, 2005). However, recent investigations have drawn attention to physical effects not normally considered in ice sheet modelling analyses. The work of Alley et al. (2007), for example, has shown that sedimentation at the grounding line of an ice shelf stabilises ice sheets against sea-level rises of at least several metres (<10 m) – and as pointed out by the authors, sedimentary stabilisation of tidewater glaciers is well recognised (e.g. Meier and Post, 1987). This would suggest that the GrIS may not have responded to smaller sea-level changes of this order. Clearly, other physical processes of climate change will have also influenced the marine breakup of the GrIS. Modelling studies of ice shelves, for example, show that the melt rate is highly sensitive to changes in ocean temperature (Holland et al., 2008a). Indeed, episodes of contemporary ocean warming in Greenland have been shown to correspond to the retreat of outlet glaciers (Hanna et al., 2009) and modern hydrological observations from the west coast of Greenland suggest that is the delivery of warm subsurface waters that initiated the acceleration of Jakobshavn Isbrae in 1997 (Holland et al., 2008b). Paleo-evidence shows there has been considerable post-LGM variability of the major oceanographic currents that circumnavigate Greenland (e.g. Lloyd et al., 2005), so it seems plausible that ocean warming played an important role in driving the marine retreat of the GrIS.

If the extent of the ice sheet was sea-level controlled, one assumption made in this work is that it was non-Greenland RSL change which drove the marine retreat. There are clear potential couplings between marine based ice sheet evolution and changes in relative sea levels – i.e. could there be a feedback mechanism between 'local' GrIS loading changes and associated variations in RSL that caused the marine retreat? Although not extensively studied, the few modelling works that have

addressed this problem suggest that the coupling is limited. This is mainly because once marine based ice retreats it is replaced by ocean water and so the surface load is not significantly changed (Le Meur and Hindmarsh, 2001). Zweck (1998) examined the sensitivity of marine ice sheet evolution to changes in Earth viscosity structure - he found that the ability of the ice sheet to advance varies with changes in lithospheric thickness. We note that neither of these studies account for the other processes that influence RSL change (i.e. the direct and indirect effect).

4.4.3. Limitations of the modelling and future work

In terms of our modelling work, an obvious limitation of the Huy1/2 models is that they do not contain a physically coherent treatment of calving. This is a long standing problem with ice sheet models, partly because some of the processes controlling grounding-line migration are not fully understood. Further, calving is sensitive to small-scale processes; these cannot easily be determined given that the horizontal grid resolution of millennial-scale ice sheet models is typically around 20 km. It is important to remember that the Huy1/2 models treat calving as a function of water depth (see introduction), although we note that there is considerable discussion surrounding the accuracy of this relationship (e.g. Van der Veen, 1996; 2002, Warren et al., 2001). As mentioned in Chapter 2, models of tidewater glaciers, supported by observations, have shown that it is *changes* in the bedrock topography that are the dominant control on episodes of rapid retreat (e.g. Vieli et al., 2001; Schoof, 2007).

As discussed in the previous Sub-Section, there are potential coupling between marine ice sheet evolution and changes in RSL. We note that the Huy1/2 models account for changes in Greenland ice and ocean load when calculating water depths (see Sub-Section 4.3.4) – however, the adopted formulation of the sea-level parameterisation clearly remains the control on ice sheets marine

extent (and are therefore a function of eustatic sea-level or, in the case of our second experiment, non-Greenland RSL change). Also as discussed above, changes in the height of the ocean surface (i.e. the direct and indirect effect) due to 'local' ice mass variations have not been considered before and should be investigated in future work.

Finally, we recommend that ice sheet modellers, when possible, adopt a sea-level forcing based on coral observations which provide a direct measure of past sea-level change (e.g. Fairbanks, 1989; Bard et al, 1990; Yokoyama et al., 2000). As mentioned, the eustatic curve derived from the SPECMAP isotope values (Imbrie et al., 1984) and used within the Huy1/2 ice models is a proxy record of sea-level change and thus has limited accuracy. Zweck and Huybrechts (2003) conduct a modelling study of the northern hemisphere and, similar to the Huy1 model (See Eqn. 2), find a hybridised sea-level parameterisation is needed to reproduce the correct timing of deglaciation. They suggest several reasons as to why the parameterisation requires a non-linear form – that it represents a switch from fast to slow calving, that is because the model does not account for the floatation of ice and/or it represents a climate signal not encapsulated in the ice sheet model. We suggest that, alternatively, the non-linearity may simply be related to the adopted sea-level forcing. As with the Huy1/2 models, Zweck and Huybrechts (2003) use the SPECMAP derived eustatic curve which is characterised by an almost linear rate of rise. Whereas, both observations of far-field sea levels (e.g. Fairbanks, 1989; Bard et al, 1990; Yokoyama et al., 2000) and predictions of non-Greenland RSL show the rate of change is variable with time.

4.5. Conclusions

Using the ICE-5G model, we have shown and analysed predictions of non-Greenland RSL change. We have also considered how this signal may have influenced the post-LGM evolution of the GrIS. Based on this work, we find the following:

1. The influence of non-Greenland ice on solid Earth motion in Greenland (i.e. the collapse and migration of peripheral forebulges) is relatively small. Our model predictions suggest that the forebulges, at their largest, increase land height by around 30-60 m in Greenland. Their influence on the evolution of the GrIS is small but possibly slowed the Holocene retreat in southwest Greenland.

2. RSL change around Greenland which is driven by non-Greenland ice mass loss departs from the associated eustatic signal; largely because of the close proximity of the late North American Ice Sheets. Observations indicate that eustatic sea-level began to rise shortly after the LGM (c. 21 ka BP) (e.g. Hanebuth et al., 2000; Yokoyama et al., 2000; Clark et al., 2004). In Greenland, however, our model predictions indicate that the early period of deglaciation (22-15 ka BP) was characterised by relatively stable sea-levels. After this period, specifically during the occurrence of mwp-1A, rates of RSL change around Greenland show a distinct east-west gradient: Rates of rise from 16 and 14 ka BP remained relatively low in the west, whereas, those in the east reach values between 6 and 8 m/ka. This pattern arises because in the ICE-5G model the North American Ice Sheet contains a large contribution (c. 20 m ice-equivalent sea level) to mwp-1A. If the meltwater pulse had a dominant Antarctic source, however, then RSL change at this time would more closely resemble the eustatic signal and be more uniform.

3. If the marine breakup of the GrIS was forced by non-Greenland RSL change then we would expect the retreat of the ice sheet to reflect the sea-level changes described in Conclusion 2. This suggests that the ice sheet would not have been driven from the continental shelf until after c. 16 ka BP, which is in agreement with the results of GIA modelling studies of the GrIS which are constrained by RSL data (Tarasov and Peltier, 2002; Fleming and Lambeck, 2004, Chapter 2). Our modelling results suggest that, assuming a conventional ice sheet model calving treatment, a more realistic sea-level

forcing results in a pattern of ice margin retreat which is at least partly due to spatial variations in RSL change. Thus, these results show that the marine retreat was generally earlier in east Greenland and later in the west when compared to the results of Huy2.

4. An earlier deglaciation of eastern Greenland, when compared to other regions, is generally consistent with observations from the continental shelf (see Sub-Section 3.3). In a past RSL field investigation Long and Roberts (2003) hypothesised that the Jakobshavn Isbrae (situated in west Greenland) was able to survive high rates of sea-level rise (including mwp-1A) and persist on the shelf west of Disko Bugt until the early Holocene because of its high ice discharge and the relatively shallow water depths. Our sea-level predictions indicate that there may not have been any sea-level rise associated with mwp-1A. Indeed, the deglaciation of Disko Bugt can be tentatively correlated with the later mwp-1B and/or rapid climate change following the YD.

Chapter 5:

Summary and future work.

In this thesis we have made use of GIA and glaciological models to investigate the behaviour of the GrIS from the LGM (21 ka BP) up until the present-day. We begin our final Chapter with a discussion of the methodology applied in Chapter 2 (i.e. the Earth and ice model sensitivity analysis and χ^2 test) to arrive at our resultant new ice history for Greenland (Huy2). Following this we readdress the implications of the research (see Section 1.3) and summarise our most important findings. Possible avenues of future work are detailed where appropriate. Given that summaries are provided at the end of each chapter, the main aim here is to bring together the content of each chapter summary and discuss the implications in terms of the main research aims and the implications for future work.

5.1. Review of methodology in arriving at Huy2 model

The primary aim of the work was to calibrate a glaciological model of GrIS evolution since the LGM using inferences of RSL and past ice extent from field data (Chapter 2). As part of this analysis we performed detailed ice and Earth model sensitivity tests with our GIA model - RSL predictions are sensitive to changes in both the ice loading history and the adopted Earth model. The sensitivity of our RSL predictions to variations in Earth structure (e.g. Sub-Section 2.3.1.1) is larger than previous studies of Greenland have indicated because we sampled a wider range of Earth model parameters (e.g. Tarasov and Peltier, 2002; Fleming and Lambeck, 2004; Long et al., 2008). We note there is little information on mantle viscosity structure beneath the GrIS. Observations of GIA-induced RSL change

that have previously been used to infer mantle viscosity structure (and determined the parameter values explored in this thesis) have largely focussed on postglacial uplift curves from Fennoscandia and/or from Hudson Bay in Canada (e.g. Mitrovica and Peltier, 1993; Mitrovica and Peltier, 1995; Peltier and Jiang, 1996; Mitrovica and Forte, 1997, 2004). However, the Earth parameter values derived from such investigations largely pertain to local viscosity structure (e.g. see Paulson et al., 2005) and so may not reflect the Earth viscosity structure of Greenland – we therefore require better constraints on these parameters for Greenland (see also Section 5.4).

In terms of the ice model, we performed a more limited sensitivity analysis; this is because there are many ice model parameters that can be varied (see Section 2.4). We therefore targeted parameters that were effective in addressing the large misfits between the RSL data and our sea level predictions (LGM extent, the calving parameterisation and Holocene temperature forcing). It would be interesting to extend our study with a more comprehensive test of climate parameters (i.e. those related to temperature and precipitation) as these have a strong control on ice sheet evolution and extent (see Zweck and Huybrechts, 2005). We also note that, unlike for the Earth model, there are a number of independent observations available which helped us to better constrain the ice history. While there a quite a few field observations which detail past changes in the position of ice margin (e.g. Funder, 1989; Mienert et al., 1992; Van Tatenhove et al., 1995, 1996; Bennike and Björck, 2002) there are relatively few that pertain to the past height extent of the ice sheet (e.g. Roberts et al., 2008). Changes to the parameters affecting ice flow (deformation and sliding law coefficients and geothermal heat flux) have the largest influence on ice thickness and the profile of the ice sheet (e.g. see Ritz et al., 1997), so it would be useful to examine these along with the climate parameters in future work.

Following our sensitivity analyses we determined an optimum Earth viscosity model for Huy2 using the χ^2 criterion. Determining a best-fit model in this manner is time consuming because of the wide search of parameter space that must be performed. In future analyses, therefore, we may adopt a probabilistic inversion method to reduce computation time (e.g. Cianetti et al., 2002). As discussed in Chapter 2, the χ^2 test has a bias toward fitting the west Greenland RSL dataset as: (1) there are numerous data from this region and (2) the data here are mostly from isolation basins which have good height precision and so the χ^2 values will increase quickly with an increasing misfit (see Sub-Section 2.3.1.2). Certainly, to better constrain our GIA model, we require more high quality RSL data that have a well constrained height relationship to former sea-level (e.g. Long et al.,1999; Bennike et al., 2002; Sparrenbom et al., 2006a) and which have better geographical coverage. In particular, this is the case for areas in the northern and eastern parts of Greenland, where the observations consist only of limiting dates (these data only provide a height limit on former sea level). An additional important finding from the χ^2 test was to show that the current RSL data set is not able to place a useful bound on upper mantle viscosity – this has implications for the uplift predictions (Section 5.3) and also indicates that we require additional data to better constrain this parameter.

5.2. GrIS ice history and palaeoclimate

An important motivation for our work was that our GIA model can provide insights into how the ice sheet reacted to past sea-level and climate change. In the following Sub-Sections we review the large-scale changes of the GrIS since the LGM and also its response to the HTM.

5.2.1. Large-scale changes since the LGM

At the LGM, the Huy2 model shows that the ice sheet contained c. 4 m excess ice-equivalent sea level, previous studies have indicated a excess volume closer to 3 m (e.g. see Clark and Mix, 2002; Tarasov and Peltier, 2002; Fleming and Lambeck, 2004). The Huy2 model has a larger LGM volume because the ice sheet grounds further out on the continental shelf in the east, which is in better agreement with evidence from marine geophysical surveys (e.g. Evans et al., 2002). The modelled post-LGM marine retreat of the GrIS begins later (c. 12 ka BP) and is far more rapid than the original glaciological predictions of Huybrechts (2002), this suggests that the ice model underestimates the response of the GrIS to sea-level rise and/or rapid climate change (see also Sub-Section 5.4 below). Results from the Huy2 model show that the retreat was largely driven by sea-level rise and misfits between our sea-level predictions and the RSL data suggest that the marine retreat may have initiated first in east Greenland and then later in the west (although this pattern is not well produced by the ice model). The east-west pattern of marine breakup is consistent with sparse field observations (e.g. see Sub-Section 4.3.3) and, as shown in Chapter 4, could be due to the non-uniform nature of sea-level change associated with non-Greenland ice mass variations. If sea-level change did play a significant role in the retreat of the GrIS then our findings in Chapter 4 suggest we require a good understanding of non-Greenland ice melt (i.e. the source of the meltwater). In particular, the origin(s) of mwp-1A need to be better constrained as sea-level change in Greenland is sensitive to the relative partitioning of the source of meltwater between the Laurentide and Antarctic ice sheets.

5.2.2. The retreat behind present-day ice margin and neoglacial regrowth

A key aim of the work was to analyse the reaction of the GrIS to warming during the Holocene. Our modelling results suggest the ice sheet retreated largely in the southwest (by up to 80 km) and

contributed 0.17 m ice-equivalent sea level in response to the HTM. This is a relatively moderate response to the millennial-scale warming that occurred during the Holocene (Dahl Jensen et al., 1998). The Huy2 model has an imposed warming of between 2 and 3.75 ^{o}C (all temperatures are relative to preindustrial times) with spatio-temporal variations to reproduce the observed pattern of warming (see Sub-Section 2.3.2.3). However, we note that the degree day factors (which govern how the melt rate increases with temperature) had to be reduced by 30 % over the Holocene period to ensure that the ice sheet model evolved to reach its present-day state. We also note a previous modelling study of Huybrechts (1991) showed that area averaged warming in Greenland needs to exceed 2.7 ^{o}C before the surface mass balance becomes negative. Given these results it is not surprising that the modelled ice volume change during the HTM is quite small (i.e. a rise of 0.17 m ice-equivalent sea level relative to present-day); such a sub-metre variation could not be resolved using current observations of far-field sea level change that date to the Holocene period (e.g. see Nakada and Lambeck, 1989; Fleming et al., 1998; Lambeck and Bard, 2000; Lambeck and Purcell, 2005; Milne et al., 2005).

Proxy climate records show mean summer temperatures in Greenland rose 1.7 ^{o}C between 1991 and 2006 (Hanna et al., 2008) and over the 21st century mean annual temperatures are predicted to rise by around 4 ^{o}C (see Huybrechts et al., 2004). If the current warming trend continues, therefore, then temperatures in Greenland will soon reach or exceed those observed for the HTM. If warming follows a similar pattern to the HTM, then we expect that the results of the Huy2 model can be used to some extent as a guide for the future long-term (i.e. millennial scale) behaviour of the GrIS. However, we are somewhat cautious on this issue, as although predictions of the Huy2 model provide good fit to the RSL data from west Greenland there remains considerable uncertainty on Earth viscosity structure (RSL predictions are clearly sensitive to changes in Earth model parameters) and also the influence of the non-Greenland GIA signal. These matters need to be more closely

examined before the magnitude of retreat and subsequent neoglacial regrowth can be more tightly constrained.

5.3. Predictions of present-day vertical land motion

One application of the Huy2 model is to predict the pattern of present-day solid Earth deformation in Greenland (Chapter 3). Contemporary geodetic and altimetry measurements require a correction for the ongoing vertical motion of the Earth which comes from GIA models such as the one developed in this thesis (e.g. Velicogna and Wahr, 2005; Thomas et al., 2006; Zwally et al., 2005). In this regard, we note that a recent study of Barletta et al. (2008) examined the sensitivity of such mass balance estimates derived from gravity data to changes in both Earth model parameters and the ice loading history. They found that the corresponding range of mass balance estimates for the GrIS was between -122 and -50 Gt/yr for the period 2003 to 2006; this is larger than commonly stated in the literature (see also Sub-Section 1.1.2).

Our analysis of post-LGM Greenland loading changes show how different periods of ice mass variation dominate in particular regions of Greenland. These findings will be a useful resource when interpreting existing and future observations of vertical land motion in Greenland. Furthermore, our modelling results show that present-day uplift rates are strongly dependent on the adopted Earth viscosity structure and particularly on the value of upper mantle viscosity. As discussed above, the current RSL data set is not able to place a useful bound on upper mantle viscosity structure. In future analyses, therefore, GPS observations could be used to address this problem and help constrain mantle viscosity structure in Greenland (note that the GNET project aims to establish around 50 new continuous GPS stations around the periphery of the ice sheet). Furthermore, we only examined vertical uplift rates in Chapter 3. Analysis of horizontal crustal velocities should be included in future

work; although we note that this component of motion appears far more sensitive to lateral variations in Earth structure (e.g. see Latychev et al., 2005 and also Section 5.4). Comparison of uplift predictions generated using the Huy2 model are generally in good agreement with the most recent absolute GPS observations from southwest Greenland (Khan et al., 2008). This finding corroborates our findings from Chapter 2 and suggests that broad features of the ice sheet's Holocene evolution in this region are well reproduced. However, our predictions do not agree with the relative rates recorded in southwest Greenland by Dietrich et al. (2005), which suggests that the pattern of the neoglacial readvance is not accurately reproduced.

Results from the Wake et al. (2009) model indicate that decadal-scale ice mass variability over the last c. 140 years plays a small role in determining the present-day viscous response but surface mass balance changes from 1995 to 2005 significantly influence present-day elastic uplift rates. Future studies should focus on improving the accuracy of ice sheet reconstructions over the last few hundred years, or even earlier - recent work has shown predicted present-day uplift rates are potentially very sensitive to ice mass changes over the last two millennia (Ivins and James, 2005). As mentioned, new high resolution relative sea-level records obtained from salt marsh studies (Woodroffe and Long, 2009; Long et al., in press) can help in this regard and be used to constrain the behaviour of the GrIS over the last millennia.

5.4. Limitations of ice sheet and Earth models

As mentioned above, the original Huy1 model of Huybrechts (2002) was found to underestimate the response of the ice sheet to past climate change. This point was previously discussed in Chapter 2 and could be due to uncertainties in the palaeoclimate forcing and/or because physical processes such as calving and ice stream dynamics are poorly represented in the current generation of ice

sheet models (see Section 2.4). Furthermore, we noted that the horizontal (20 x 20 km) of the ice model is too coarse (Van den Berg et al., 2006). These issues may mean that the ice model underestimates rates of change (especially ice-dynamic changes) (e.g. Alley et al., 2005). In particular, we note that it is the speed of the ice sheet's marine retreat that is underestimated by the original Huy1 model; this suggests that it is ice-ocean interactions which are not properly captured by the ice model (see Section 4.1 and Sub-Section 4.4.2). Three-dimensional ice sheet models which include higher-order stress gradients are available (e.g. Pattyn, 2003; Saito et al., 2003; Payne et al., 2004) - as a first step in addressing the above issues we therefore recommend the application of such models for the type of analysis presented in this thesis (although far longer computation times will restrict this work).

A particular limitation of the Earth model used in this study is the assumption of a 1-D depth dependent viscosity structure. As shown in Chapter 2 (see Sub-Section 2.4.2.3), misfits between the RSL data and our model predictions could possibly be explained by lateral variations in Earth viscosity structure. Indeed, as mentioned, there is good evidence from seismic studies that in Greenland lateral variations in Earth structure exist (e.g. Darbyshire et al., 2004). Such lateral variations can, to some extent, be detected using 1-D Earth models if the RSL data is divided into small geographical regions (see Kaufmann and Wu, 2002). We also note that predicted uplift rates are likely to be very sensitive to these lateral variations (see Chapter 3). Early work that addressed the issue of lateral variations in Earth viscosity structure made use of 2-D Earth models. These investigations showed that land motion close to the periphery of an ice load is extremely sensitive to lateral variations in upper mantle viscosities (e.g. Sabadini et al., 1986; Kaufmann et al., 1997). Furthermore, using observations of GIA-induced sea-level change to infer Earth viscosity structure will result in incorrect values if performed using a 1-D model that does not account for lateral variations (e.g. Martinec et al., 2001). These results have since been reproduced and confirmed

using more recent models that incorporate 3-D Earth viscosity structure (e.g. Kaufmann et al., 2000; Kaufmann and Wu, 2002; Steffen et al., 2006). Thus, there is increasing evidence that 3-D Earth structure needs to be considered in GIA modelling analyses. A clear target for future work is to apply a 3-D Earth model (e.g. Latychev et al., 2005) to Greenland and examine the influence on the RSL predictions; we note that this has not been done before.

Finally, we briefly discuss the limitations of the methodology employed to the modelling work in this thesis. As outlined in the model description (Sub-Section 1.4.1), the ice model contains its own treatment of isostasy (the ELRA model; see Chapter 4) and sea-level (see also Chapter 4). Thus, coupling the ice model to the Earth model and/or the sea level model employed in this thesis will allow us to explore several avenues in future work: Firstly, the influence of isostasy on ice sheet evolution. A recent case study of glacial cycles in Eurasia has illustrated that the ELRA model has limitations in comparison to more realistic treatments such as the spherically symmetric, visco-elastic, self-gravitating and compressible Earth model used throughout this thesis (Van den Berg et al., 2008). A similar study should be applied to the GrIS – an obvious further extension of the work would be to examine the influence of 3-D Earth structure on ice sheet evolution. Secondly, coupling the sea-level model will provide a more accurate sea-level forcing and also allow us to examine the potential coupling between marine ice sheet evolution and changes in RSL. Although, we note that this second objective somewhat relies on developing a physically coherent treatment of calving (see Chapter 4) - publications arising from the ice2sea project (www.ice2sea.eu) should help in this regard.

References

Abdalati, W., Steffen, K., 2001. Greenland ice sheet melt extent: 1979-1999. Journal of Geophysical Research – Atmospheres 106(D24), 33983-33988.

Abe-Ouchi, A., Blatter, H., Ohmura, A., 1994. How does the Greenland ice-sheet geometry remember the ice-age. Global and Planetary Change 9, 1-2, 133-142.

Alley, R.B., Anandakrishnan, S., Dupont, T.K., Parizek, B.R., Pollard, D., 2007. Effect of Sedimentation on Ice-Sheet Grounding-Line Stability. Science 315, 1838-1841.

Alley, R.B., Clark, P.U., Huybrechts, P., Joughin, I., 2005. Ice-sheet and sea-level changes. Science 310(5747), 456-460.

Andersen, K.K., Azuma, N., Barnola, J.-M., Bigler, M., Biscaye, P., Caillon, N., Chappellaz, J., Clausen, H.B., Dahl-Jensen, D., Fischer, H., Flückiger, J., Fritzsche, D., Fujii, Y., Goto-Azuma, K., Grønvold, K., Gundestrup, N.K., Hansson, M., Huber, C., Hvidberg, C.S., Johnsen, S.J., Jonsell, U., Jouzel, J., Kipfstuhl, J., Landais, A., Leuenberger, M., Lorrain, R., Masson-Delmotte, V., Miller, H., Motoyama, H., Narita, H., Popp, T., Rasmussen, S.O., Raynaud, D., Röthlisberger, R., Ruth, U., Samyn, D., Schwander, J., Shoji, H., Siggaard-Andersen, M.-L., Steffensen, J.P., Stocker, T., Sveinbjörnsdottir, A.E., Svensson, A., Takata, M., Tison, J.-L., Thortseinsson, Th., Watanabe, O., Wilhelms, F., White,

J.W.C., 2004. High-resolution record of Northern Hemisphere climate extending into the last interglacial period. Nature 431, 147-151.

Andrews, J.T., 2008. The role of the Iceland ice sheet in the north Atlantic during the late Quaternary: a review and evidence from Denmark Strait. Journal of Quaternary Science 23 (1), 3–20.

Andrews, J.T., Smith, L.M., Preston, R., Cooper, T., Jennings, A.E., 1997. Spatial and temporal patterns of iceberg rafting (IRD) along the East Greenland margin, ca. 68 °N, over the last 14 cal. ka. Journal of Quaternary Science 12, 1–13.

Argus, D.F., Peltier, W.R., Watkins, M.M., 1999. Glacial isostatic adjustment observed using very long baseline interferometry and satellite laser ranging geodesy. Journal of Geophysical Research – Solid Earth 104 (B12), 29077-29093.

Bamber, J.L., Layberry, R.L., Gogineni, S., 2001. A new ice thickness and bed data set for the Greenland ice sheet 1. Measurement, data reduction, and errors. Journal of Geophysical Research – Atmospheres 106 (D24), 33773–33780.

Baral, D.R., Hutter, K., Greve, R., 2001. Asymptotic theories of large-scale motion, temperature, and moisture distribution in land-based polythermal ice sheets: a critical review and new developments. Applied Mechanics Reviews 54 (3), 215–256.

Bard, E., Hamelin, B., Fairbanks, R.G., 1990. U-Th ages obtained by mass-spectometry in corals from Barbados – sea-level during the past 130,000 years. Nature 346 (6283), 456-458.

Barletta, V.R., Sabadini, R., Bordoni, A., 2008. Isolating the PGR signal in the GRACE data: impact on mass balance estimates in Antarctica and Greenland. Geophysical Journal International 172(1), 18-30.

Bartoli, G., Sarnthein, M., Weinelt, M., Erlenkeuser, D., Garbe-Schönberg, D., Lea, D.W., 2005. Final closure of Panama and the onset of northern hemisphere glaciation. Earth and Planetary Science Letters 237, 33–44.

Bassett, S.E., Milne, G.A., Mitrovica, J.X., Clark, P.U., 2005. Ice sheet and solid earth influences on far-field sea-level histories. Science 309, 925–928.

Benn, D.I., Warren, C.R., Mottram, R.H., 2007. Calving processes and the dynamics of calving glaciers. Earth-Science Reviews 82, 143-179.

Bennike, O., 1995. Paleoecology of 2 lake basins from Disko, west Greenland. Journal of Quaternary Science 10 (2), 149–155.

Bennike, O., 2002. Late Quaternary history of Washington Land, north Greenland. Boreas 31 (3), 260–272.

Bennike, O., 2008. An early Holocene Greenland whale from Melville Bugt, Greenland. Quaternary Research 69 (1), 72–76.

Bennike, O., Björck, S., 2000. Lake sediment coring in South Greenland in 1999. Geology of Greenland Survey Bulletin 186, 60–64.

Bennike, O., Björck, S., 2002. Chronology of the last recession of the Greenland ice sheet. Journal of Quaternary Science 17 (3), 211–219.

Bennike, O., Björck, S., Lambeck, K., 2002. Estimates of south Greenland late-glacial ice limits from a new relative sea level curve. Earth and Planetary Science Letters 197 (3–4), 171–186.

Bennike, O., Hansen, K.B., Knudsen, K.L., Penney, D.N., Rasmussen, K.L., 1994. Quaternary marine stratigraphy and geochronology in central west Greenland. Boreas 23 (2), 194–215.

Bennike, O., Weidick, A., 2001. Late Quaternary history around Nioghalvfjerdsfjorden and Jokelbugten, north-east Greenland. Boreas 30 (3), 205–227.

Bentley, M.J., Fogwill, C.J., Kubik, P.W., Sugden, D.E., 2006. Geomorphological evidence and cosmogenic Be-10/Al-26 exposure ages for the Last Glacial Maximum and deglaciation of the Antarctic Peninsula ice sheet. Geological Society of America Bulletin 118 (9–10), 1149–1159.

Berger, A., Loutre, M.F., 1991. Insolation values for the climate of the last 10 million years. Quaternary Science Reviews, 10, 297-317.

Bindschadler, R.A., 1984. Jakobshavn Glacier Drainage-Basin – a balance assessment. Journal of Geophysical Research – Oceans 89 (NC2), 2066–2072.

Box, J.E., Bromwich, D.H., Veenhuis, B.A., Bai, L.S., Stroeve, J.C., Rogers, J.C., Steffen, K., Haran, T., Wang, S.H., 2006. Greenland ice-sheet surface mass balance variability (1988-2004) from calibrated Polar MM5 output. Journal of Climate 19(12), 2783–2800.

Box, J.E., Yang, L., Bromwich, D.H., Bai, L., 2008. Greenland ice sheet surface air temperature and accumulation rate reconstruction (1840–2007) from in-situ data records. Eos., 89 (53), Fall Meeting Supplement, Abstract U22A-03.

Braithwaite, R.J., 1995. Positive degree-day factors for ablation on the Greenland ice-sheet studied by energy-balance modeling. Journal of Glaciology 41 (137), 153–160.

Brett, C.P., Zarudzki, E.F.K., 1979. Project Westmar, a shallow marine geophysical survey on the west Greenland shelf. Rapport Grønlands Geologiske Undersøgelse 87, 27.

Brown, C.S., Meier, M.F., Post, A., 1982. Calving speed of Alaska tidewater glaciers with applications to the Columbia Glacier, Alaska. U.S. Geological Survey Professional Paper, 1258-C. 13 pp.

Calov, R., Hutter, K., 1996. The thermomechanical response of the Greenland ice sheet to various climate scenarios. Climate Dynamics 12, 243–260.

Carlson, A.E., 2009. Geochemical constraints on the Laurentide Ice Sheet contribution to Meltwater Pulse 1A. Quaternary Science Reviews 28(17-18), 1625-1630.

Carlson, A.E., Stoner, J.S., Donnelly, J.P., Hillaire-Marcel, C., 2008. Response of the southern Greenland Ice Sheet during the last two deglaciations. Geology 36 (5), 359-362.

Charbit, S., Ritz, C., Ramstein, G., 2002. Simulations of Northern Hemisphere ice-sheet retreat: sensitivity to physical mechanisms involved during the Last Deglaciation. Quaternary Science Reviews 21, 243-265.

Cianetti, S., Giunchi, C., Spada, G., 2002. Mantle viscosity beneath the Hudson Bay: An inversion based on the Metropolis algorithm. Journal of Geophysical Research – Solid Earth 107 (B12), 2352.

Clark, P.U., Alley, R.B., Keigwin, L.D., Licciardi, L.D., Johnsen, J.M., Wang, S.J., 1996. Origin of the first global meltwater pulse following the last glacial maximum. Paleoceanography 11, 563–577.

Clark, P.U., McCabe, A.M., Mix, A.C., Weaver, A.J., 2004. Rapid rise of sea level 19,000 years ago and its global implications. Science 304 (5674), 1141-1144.

Clark, P.U., Mix, A.C., 2002. Ice sheets and sea level of the Last Glacial Maximum. Quaternary Science Reviews 21 (1–3), 1–7.

Clarke, P.U., Mitrovica, J.X., Milne, G.A., Tamisiea, M.E., 2002. Sea level finger printing as a direct test for the source of global meltwater pulse 1a. Science 295, 2438–2441.

Crucifix, M., Loutre, M., Lambeck, K., Berger, A., 2001. Effect of isostatic rebound on modelled ice volume variations during the last 200 kyr. Earth Planetary Science Letters 184, 623– 633.

Cuffey, K.M., 2000. Methodology for use of isotopic climate forcings in ice sheet models. Geophysical Research Letters 27 (19), 3065–3068.

Cuffey, K.M., Clow, G.D., 1997. Temperature, accumulation, and ice sheet elevation in central Greenland through the last deglacial transition. Journal of Geophysical Research – Oceans 102 (C12), 26383–26396.

Cuffey, K.M., Clow, G.D., Alley, R.B., Stuiver, M., Waddington, E.D., Saltus, R.W., 1995. Large arctic temperature-change at the Wisconsin-Holocene glacial transition. Science 270 (5235), 455–458.

Cuffey, K.M., Marshall, S.J., 2000. Substantial contribution to sea-level rise during the last interglacial from the Greenland ice sheet. Nature 404, 591-594.

Dahl Jensen, D., Mosegaard, K., Gundestrup, N., Clow, G.D., Johnsen, S.J., Hansen, A.W., Balling, N., 1998. Past temperatures directly from the Greenland ice sheet. Science 282 (5387), 268–271.

Dansgaard, W., Johnsen, S.J., Clausen, H.B., Dahl Jensen, D., Gundestrup, N.S., Hammer, C.U., Hvidberg, C.S., Steffensen, J.P., Sveinbjornsdottir, A.E., Jouzel, J., Bond, G., 1993. Evidence for general instability of past climate from a 250-Kyr ice-core record. Nature 364 (6434), 218–220.

Dansgaard, W., Johnsen, S.J., Clausen, H.B., Langway Jr., C.C., 1971. Climatic record revealed by the Camp Century ice core. In: Turekian, K.K. (Ed.), The Late Cenozoic Glacial Ages. Yale University Press, New Haven, CT, pp. 37–56.

Darbyshire, F.A., Larsen, T.B., Mosegaard, K., Dahl-Jensen, T., Gudmundsson, Ó., Bach, T., Gregersen, S., Pedersen, H.A., Hanka, W., 2004. A first detailed look at the Greenland lithosphere and upper mantle, using Rayleigh wave tomography. Geophysical Journal International 158 (1), 267–286.

Das, S.B., Joughin, I., Behn, M.D., Howat, I.M., King, M.A., Lizarralde, D., Bhatia, M.P., 2008. Fracture Propagation to the Base of the Greenland Ice Sheet During Supraglacial Lake Drainage. Science, 320(5877), 778-781.

Denton, G., Hughes, T., 1981. The Last Great Ice Sheets. Wiley, New York. Dowdeswell, J.A., Whittington, R.J., Marienfeld, P., 1994. The origin of massive diamicton facies by iceberg rafting and scouring, Scoresby-Sund, east Greenland. Sedimentology 41 (1), 21–35.

Dietrich, R., Rulke, A., Scheinert, M., 2005. Present-day vertical crustal deformations in West Greenland from repeated GPS observations. Geophysical Journal International 163 (3), 865-874.

Dyke, A.S., Andrews, J.T., Clark, P.U., England, J.H., Miller, G.H., Shaw, J., Veillette, J., 2002. The Laurentide and Innuitian ice sheets during the Last Glacial Maximum. Quaternary Science Reviews 21, 9–31.

Dyke, A.S., Moore, A., Robertson, L., 2003. Deglaciation of North America. Technical Report Open File 1574, Geological Survey of Canada, thirty-two maps at 1:7,000,000 scale with accompanying digital chronological database and one poster (in two sheets) with full map series.

Dyke, A.S., Prest, V.K., 1987. Late Wisconsinan and Holocene Retreat of the Laurentide Ice Sheet. Scale 1:5,000,000. Map 1702A. In: Geological Survey of Canada, Ottawa, Ontario, Canada.

Dziewonski, A.M., Anderson, D.L., 1981. Preliminary reference Earth model. Physics of the Earth and Planetary Interiors 25 (4), 297–356.

Ekholm, S., 1996. A full coverage, high-resolution, topographic model of Greenland computed from a variety of digital elevation data. Journal of Geophysical Research – Solid Earth 101 (B10), 21961–21972.

England, J., 1999. Coalescent Greenland and Innuitian ice during the Last Glacial Maximum: revising the Quaternary of the Canadian High Arctic. Quaternary Science Reviews 18 (3), 421–456.

Evans, J., Dowdeswell, J.A., Grobe, H., Niessen, F., Stein, R., Hubberten, H.W., Whittington, R.J., 2002. Late Quaternary sedimentation in Kejser Franz Joseph Fjord and the continental margin of east Greenland. In: Dowdeswell, J.A., O'Cofaigh, C. (Eds.), Glacier-Influenced Sedimentation on High-Latitude Continental Margins. Geological Society of London, London, United Kingdom.

Evans, J., O'Cofaigh, C., Dowdeswell, J.A., Wadhams, P., 2009. Marine geophysical evidence for former expansion and flow of the Greenland Ice Sheet across the north-east Greenland continental shelf. Journal of Quaternary Science 24 (3), 279-293.

Fairbanks, R.G., 1989. A 17,000-year glacio-eustatic sea-level record – influence of glacial melting rates on the Younger Dryas event and deep-ocean circulation. Nature 342 (6250), 637–642.

Farrell, W.E., Clark, J.A., 1976. Postglacial sea-level. Geophysical Journal of the Royal Astronomical Society 46 (3), 647–667.

Fleming, K., Johnston, P., Zwartz, D., Yokoyama, Y., Lambeck, K., Chappell, J., 1998. Refining the eustatic sea-level curve since the Last Glacial Maximum using far- and intermediate-field sites. Earth and Planetary Science Letters 163(1-4), 327-342.

Fleming, K., Lambeck, K., 2004. Constraints on the Greenland ice sheet since the Last Glacial Maximum from sea-level observations and glacial-rebound models. Quaternary Science Reviews 23 (9–10), 1053–1077.

Forman, S.L., Marín, L., van der Veen, C., Tremper, C., Csatho, B., 2007. Little Ice Age and neoglacial landforms at the Inland Ice margin, Isunguata Sermia, Kangerlussuaq, west Greenland. Boreas 36(4), 341–351.

Forsström, P.J., Greve, R., 2004. Simulations of the Eurasian ice sheet dynamics during the last glaciation. Global and Planetary Change 42, 59-81.

Funder, S., 1987. Quaternary Geology and Landforms of the Coast of Jameson Land, East Greenland. In: Geological Survey of Greenland, Copenhagen (map sheet).

Funder, S., Abrahamsen, N., 1988. Palynology in a polar desert, eastern north Greenland. Boreas 17 (2), 195–207.

Funder, S., 1989. Quaternary geology of the ice-free areas and adjacent shelves of Greenland. In: Fulton, R.J. (Ed.), Quaternary Geology of Canada and Greenland. Geological Survey of Canada, pp. 741–792.

Funder, S., Hansen, L., 1996. The Greenland ice sheet – a model for its culmination and decay during and after the Last Glacial Maximum. Bulletin of the Geological Society of Denmark 42, 137–152.

Funder, S., Hjort, C., Landvik, J.Y., Nam, S.I., Reeh, N., Stein, R., 1998. History of a stable ice margin east Greenland during the Middle and Upper Pleistocene. Quaternary Science Reviews 17 (1–3), 77–123.

Gotfredsen, A.B., Møberg, T., 2004. Nipisat – a Saqqaq culture site in Sisimiut, central west Greenland. Meddelelser om Grønland, Man and Society 31.

Grachev, A.M., Severinghaus, J.P., 2005. A revised +10 ± 4 degrees C magnitude of the abrupt change in Greenland temperature at the Younger Dryas termination using published GISP2 gas isotope data and air thermal diffusion constants. Quaternary Science Reviews 24 (5–6), 513–519.

Gregory, J.M., Huybrechts, P., 2006. Ice-sheet contributions to future sea-level change. Philiosophical transactions of the Royal Society A-Mathematical Physical and Engineering Sciences 364(1844), 1709-1731.

Greve, R., 1997. Application of a polythermal three-dimensional ice sheet model to the Greenland ice sheet: response to steady-state and transient climate scenarios. Journal of Climate 10 (5), 901–918.

Håkansson, L., Briner, J., Alexanderson, H., Aldahan, A., Possnert, G., 2007. Be-10 ages from central east Greenland constrain the extent of the Greenland ice sheet during the Last Glacial Maximum. Quaternary Science Reviews 26 (19–21), 2316–2321.

Hanebuth, T., Stattegger, K., Grootes, P.M., 2000. Rapid flooding of the Sunda Shelf: A late-glacial sea-level record. Science 288 (5468), 1033-1035.

Hanna, E., Cappelen, J., Fettweis, X., Huybrechts, P., Luckman, A., Ribergaard, M.H., 2009. Hydrologic response of the Greenland Ice Sheet: the role of oceanographic forcing. Hydrological Processes 23(1), 7-30.

Hanna, E., Huybrechts, P., Janssens, I., Cappelen, J., Steffen, K., Stephens, A., 2005. Runoff and mass balance of the Greenland Ice Sheet: 1958-2003. Journal of Geophysical Research - Atmospheres, 110(D13), D13108.

Hanna, E., Huybrechts, P., Mote, T., Thomas, L., 2002. Surface mass balance of the Greenland Ice Sheet from climate analysis data and accumulation/runoff models. Annals of Glaciology 35, 67-72.

Hanna, E., Huybrechts, P., Steffen, K., Cappelen, J., Huff, R., Shuman, C., Irvine-Fynn, T., Wise, S., Griffiths, M., 2008. Increased runoff from melt from the Greenland Ice Sheet: A response to global warming. Journal of Climate 21(2), 331-341.

Hays, J.D., Imbrie, J., Shackleton, N.J., 1976. Variations in the Earth's Orbit: Pacemaker of the Ice Ages. Science, 194(4270), 1121-1132.

Henriksen, N., Higgins, A.K., Kalsbeek, F., Pulvertaft, T.C.R., 2000. Greenland from Archaean to Quaternary. Geological Survey of Denmark and Greenland Bulletin 185.

Hjort, C., 1997. Glaciation, climate history, changing marine levels and the evolution of the northeast Water Polynya. Journal of Marine Systems 10 (1–4), 23–33.

Holland, P.R., Jenkins, A., Holland, D.M., 2008a. The response of Ice Shelf Basal Melting to Variations in Ocean Temperature. Journal of Climate 21(11), 2558-2572.

Holland, D.M., Thomas, R.H., De Young, B., Ribergaard, M.H., Lyberth, B., 2008b. Acceleration of Jakobshavn Isbrae triggered by warm subsurface ocean waters. Nature Geoscience 1(10), 659-664.

Howat, I.M., Joughin, I., Tulaczyk, S., Gogineni, S., 2005. Rapid retreat and acceleration of Helheim Glacier, east Greenland. Geophysical Research Letters 32, L22502.

Hutter, K., 1983. Theoretical Glaciology: Material Science of Ice and the Mechanics of Glaciers and Ice Sheets. Kluwer Academic, Norwell, Massachusetts.

Huybrechts, P., 1990. The Antarctic ice sheet during the last glacial–interglacial cycle: a three dimensional experiment. Annals of Glaciology 11, 52–59.

Huybrechts, P., 1994. The present evolution of the Greenland ice sheet: an assessment by modelling. Global and Planetary Change 9, 39–51.

Huybrechts, P., 1996. Basal temperature conditions of the Greenland ice sheet during the glacial cycles. Annals of Glaciology 23, 226–236.

Huybrechts, P., 2002. Sea-level changes at the LGM from ice-dynamic reconstructions of the Greenland and Antarctic ice sheets during the glacial cycles. Quaternary Science Reviews 21 (1–3), 203–231.

Huybrechts, P., de Wolde, J., 1999. The dynamic response of the Greenland and Antarctic ice sheets to multiple-century climatic warming. Journal of Climate 12 (8), 2169–2188.

Huybrechts, P., Gregory, J., Janssens, I., Wild, M., 2004. Modelling Antarctic and Greenland volume changes during the 20th and 21st centuries forced by GCM time slice integrations. Global and Planetery Change 42, 83–105.

Huybrechts, P., Le Meur, E., 1999. Predicted present-day evolution patterns of ice thickness and bedrock elevation over Greenland and Antarctica. Polar Research 18 (2), 299-306.

Huybrechts, P., Payne, A.J., Abe-Ouchi, A., Calov, R., Fabre, A., Fastook, J.L., Greve, R., Hindmarsh, R.C.A., Høydal, O., Jo´ hannesson, T., MacAyeal, D.R., Marsiat, I., Ritz, C., Verbitsky, M.Y., Waddington, E.D., Warner, R., 1996. The EISMINT benchmarks for testing ice-sheet models. Annals of Glaciology 23, 1–12.

Ingolfsson, O., Frich, P., Funder, S., Humlum, O., 1990. Paleoclimatic implications of an early Holocene glacier advance on Disko-Island, west Greenland. Boreas 19 (4), 297–311.

Imbrie, J.Z., Hays, J.D., Martinson, D.G., MacIntyre, A., Mix, A.C., Morley, J.J., Pisias, N.G., Prell, W.L., Shackleton, N.J., 1984. The orbital theory of Pleistocene climate: support from a revised chronology of the marine d18O record. In: Berger, A., Imbrie, J.Z., Hays, J.D., Kukla, G., Saltzman, B. (Eds.). Milankovitch and Climate. D. Reidel, Dordrecht, pp. 269–305.

Ivins, E.R., James, T.S., 2005. Antarctic glacial isostatic adjustment: a new assessment. Antarctic Science 17 (4), 541-553.

Janssens, I., Huybrechts, P., 2000. The treatment of meltwater retention in massbalance parameterizations of the Greenland ice sheet. Annals of Glaciology 31, 133–140.

Jennings, A.E., Hald, M., Smith, M., Andrews, J.T., 2006. Freshwater forcing from the Greenland ice sheet during the Younger Dryas: evidence from southeastern Greenland shelf cores. Quaternary Science Reviews 25 (3–4), 282–298.

Jennings, A.E., Knudsen, K.L., Hald, M., Hansen, C.V., Andrews, J.T., 2002. A mid-Holocene shift in Arctic sea-ice variability on the east Greenland Shelf. Holocene 12 (1), 49–58.

Johannessen, O.M., Khvorostovsky, K., Miles, M.W., Bobylev, L.P., 2005. Recent ice-sheet growth in the interior of Greenland. Science 310, 1013–1016.

Johnston, P., 1993. The effect of spatially nonuniform water loads on prediction of sea-level change. Geophysical Journal International 114 (3), 615–634.

Joughin, I., Abdalati, W., Fahnestock, M., 2004. Large fluctuations in speed on Greenland's Jakobshavn Isbræ glacier. Nature, 432, 608–610.

Joughin, I., Howat, I., Alley, R.B., Ekstrom, G., Fahnestock, M., Moon, T., Nettles, M., Truffer, M., Tsai, V.C., 2008. Ice-front variation and tidewater behavior on Helheim and Kangerdlugssuaq Glaciers, Greenland. Journal of Geophysical Research – Earth Surface 113(F1), F01004.

Kaplan, M.R., Wolfe, A.P., Miller, G.H., 2002. Holocene environmental variability in southern Greenland inferred from lake sediments. Quaternary Research 58 (2), 149–159.

Kaufman, D.S., Ager, T.A., Anderson, N.J., Anderson, P.M., Andrews, J.T., Bartlein, P.J., Brubaker, L.B., Coats, L.L., Cwynar, L.C., Duvall, M.L., Dyke, A.S., Edwards, M.E., Eisner, W.R., Gajewski, K., Geirsdottir, A., Hu, F.S., Jennings, A.E., Kaplan, M.R., Kerwin, M.N., Lozhkin, A.V., MacDonald, G.M., Miller, G.H., Mock, C.J., Oswald, W.W., Otto-Bliesner, B.L., Porinchu, D.F., Ruhland, K., Smol, J.P., Steig, E.J., Wolfe, B.B., 2004. Holocene thermal maximum in the western Arctic (0–180 degrees W). Quaternary Science Reviews 23 (5–6), 529–560.

Kaufmann, G., Lambeck, K., 2000. Mantle dynamics, postglacial rebound and the radial viscosity profile. Physics of the Earth and Planetary Interiors 121 (3–4), 301–324.

Kaufmann, G., Lambeck, K., 2002. Glacial isostatic adjustment and the radial viscosity profile from inverse modeling. Journal of Geophysical Research – Solid Earth 107 (B11), 2280.

Kaufmann, G., Wu, P., 2002. Glacial isostatic adjustment in Fennoscandia with a three-dimensional viscosity structure as an inverse problem. Earth and Planetary Science Letters 197, 1-10.

Kaufmann, G., Wu, P., Li, G., 2000. Glacial isostatic adjustment in Fennoscandia for a laterally heterogeneous Earth. Geophysical Journal International 143(1), 262–273.

Kaufmann, G., Wu, P., Wolf, D., 1997. Some effects of lateral heterogeneities in the upper mantle on postglacial land uplift close to continental margins. Geophysical Journal international 128 (1), 175-187.

Kelly, M., 1979. Comments on the implications of new radiocarbon datings from the Holsteinsborg region, central west Greenland. Rapport Grønlands Geologiske Undersøgelse 95, 35–42.

Kelly, M., 1980. The status of the neoglacial in western Greenland. Rapport Grønlands Geologiske Undersøgelse 96, 24.

Kelly, M., 1985. A review of the Quaternary geology of western Greenland. In: Andrews, J.T. (Ed.), Quaternary Environments Eastern Canadian Arctic, Baffin Bay and Western Greenland. Allen and Unwin, Boston, pp. 461–501.

Kendall, R.A., Mitroviva, J.X., Milne, G.A., 2005. On post-glacial sea level: II. Numerical formulation and comparative results on spherically symmetric models. Geophysical Journal International 161 (3), 679–706.

Khan, S.A., Wahr, J., Stearns, L.A., Hamilton, G.S., van Dam, T., Larson, K.M., Francis, O., 2007. Elastic uplift in southeast Greenland due to rapid ice mass loss. Geophysical Research Letters 34 (21), L21701.

Khan, S.A., Wahr, J., Leuliette, E., van Dam, T., Larson, K.M., Francis, O., 2008. Geodetic measurements of postglacial adjustments in Greenland. Journal of Geophysical Research – Solid Earth 113, B02402.

Kienast, M., Hanebuth, T.J.J., Pelejero, C., Steinke, S., 2003. Synchroneity of meltwater pulse 1a and the Bolling warming: New evidence from the South China Sea. Geology 31(1), 67-70.

Koerner, R.M., Fisher, D.A., 1990. A record of Holocene summer climate from a Canadian High-Arctic Ice Core. Nature 343 (6259), 630–631.

Krabill, W.B., Abdalati, W., Frederick, E., Manizade, S., Martin, C., Sonntag, J., Swift, R., Thomas, R., Wright, W., Yungel, J., 2000. Greenland Ice Sheet: High elevation balance and peripheral thinning. Science 289, 428–430.

Krabill, W., Hanna, E., Huybrechts, P., Abdalati, W., Cappelen, J., Csatho, B., Fredrick, E., Manizade, S., Martin, C., Sonntag, J., Swift, R., Thomas, R., Yungel, J., 2004. Greenland Ice Sheet: Increased coastal thinning. Geophysical Research Letters 31, L24402.

Kuijpers, A., Troelstra, S.R., Prins, M.A., Linthout, K., Akhmetzhanov, A., Bouryak, S., Bachmann, M.F., Lassen, S., Rasmussen, S., Jensen, J.B., 2003. Late Quaternary sedimentary processes and ocean circulation changes at the southeast Greenland margin. Marine Geology 195 (1–4), 109–129.

Kumar, P., Kind, R., Hanka, W., Wylegalla, K., Reigber, C., Yuan, X., Woelbern, I., Schwintzer, P., Fleming, K., Dahl-Jensen, T., Larsen, T.B., Schweitzer, J., Priestley, K., Gudmundsson, O., Wolf, D., 2005. The lithosphere–asthenopshere boundary in the north-west Atlantic region. Earth and Planetary Science Letters 236 (1–2), 249–257.

Lambeck, K., Bard, E., 2000. Sea-level change along the French Mediterranean coast since the time of the Last Glacial Maximum. Earth and Planetary Science Letters 175 (3-4), 203–222.

Lambeck, K., Purcell, A., 2005. Sea-level change in the Mediterranean Sea since the LGM: model predictions for tectonically stable areas. Quaternary Science Reviews 24 (18–19), 1969–1988.

Lambeck, K., Purcell, A., Funder, S., Kjaer, K.H., Larsen, E., Möller, P., 2006. Constraints on the Late Saalian to early Middle Weichselian ice sheet of Eurasia from field data and rebound modelling. Boreas 35, 539-575.

Lambeck, K., Smither, C., Johnston, P., 1998. Sea-level change, glacial rebound and mantle viscosity for northern Europe. Geophysical Journal International 134 (1), 102–144.

Lambert, A., Courtier, N., Sasagawa, G.S., Klopping, F., Winester, D., James, T.S., Liard, J.O., 2001. New constraints on Laurentide postglacial rebound from absolute gravity measurements. Geophysical Research Letters 28 (10), 2109-2112.

Landvik, J.Y., 1994. The last glaciation of Germania-land and adjacent areas, northeast Greenland. Journal of Quaternary Science 9 (1), 81–92.

Latychev, K., Mitrovica, J.X., Tromp, J., Tamisiea, M.E., Komatitsch, D., Christara, C.C., 2005. Glacial isostatic adjustment on 3-D Earth models: a finite-volume formulation. Geophysical Journal International 161(2), 421-444.

Le Meur, E., Hindmarsh, R.C.A., 2001. Coupled marine-ice-sheet/Earth dynamics using a dynamically consistent ice-sheet model and a self-gravitating viscous Earth model. Journal of Glaciology 47(157), 258-270.

Le Meur, E., Huybrechts, P., 1996. A comparison of different ways of dealing with isostasy: examples from modeling the Antarctic ice sheet during the last glacial cycle. Annals of Glaciology 23, 309-317.

Le Meur, E., Huybrechts, P., 1998. Present-day uplift patterns over Greenland from a coupled ice-sheet/ visco-elastic bedrock model. Geophysical Research Letters 25 (21), 3951-3954.

Lemke, P., Ren, J., Alley, R.B., Allison, I., Carrasco, J., Flato, G., Fujii, Y., Kaser, G., Mote, P., Thomas, R.H., Zhang, T., 2007. Observations: changes in snow, ice and frozen ground. In: Solomon, S., Qin, D., Manning, M., Chen, Z., Marquis, M., Averyt, K.B., Tignor, M., Miller, H.L. (Eds.), Climate Change 2007: The Physical Science Basis. Contribution of Working Group 1 to the Fourth Assessment Report of the Intergovernmental Panel on Climate Change. Cambridge University Press, Cambridge, United Kingdom and New York, NY, USA.

Letréguilly, A., Reeh, N., Huybrechts, P.,1991. The Greenland ice-sheet through the Last Glacial interglacial cycle. Global and Planetary Change 90 (4), 385–394.

Licht, K.L., 2004. The Ross Sea's contribution to eustatic sea-level during meltwater pulse IA. Sedimentary Geology 165, 343–353.

Lloyd, J.M., Park, L.A., Kuijpers, B., Moros, M., 2005. Early Holocene palaeoceanography and deglacial chronology of Disko Bugt, west Greenland. Quaternary Science Reviews 24 (14–15), 1741–1755.

Long, A.J., Woodroffe, S., Milne, G.A., Bryant, C.L., Wake, L.M., in press. Relative sea level change in west Greenland during the last millennium.

Long, A.J., Roberts, D.H., 2002. A revised chronology for the 'Fjord Stade' moraine in Disko Bugt, west Greenland. Journal of Quaternary Science 17 (5–6), 561–579.

Long, A.J., Roberts, D.H., 2003. LateWeichselian deglacial history of Disko Bugt, west Greenland, and the dynamics of the Jakobshavns Isbrae ice stream. Boreas 32 (1), 208–226.

Long, A.J., Roberts, D.H., Dawson, S., 2006. Early Holocene history of the west Greenland ice sheet and the GH-8.2 event. Quaternary Science Reviews 25 (9–10), 904–922.

Long, A.J., Roberts, D.H., Rasch, M., 2003. New observations on the relative sea level and deglacial history of Greenland from Innaarsuit, Disko Bug. Quaternary Research 60 (2), 162–171.

Long, A.J., Roberts, D.H., Simpson, M.J.R., Dawson, S., Milne, G.A., Huybrechts, P., 2008. Late Weichselian relative sea-level changes and ice sheet history in southeast Greenland. Earth and Planetary Science Letters 272 (1–2), 8–18.

Long, A.J., Roberts, D.H., Wright, M.R., 1999. Isolation basin stratigraphy and Holocene relative sea-level change on Arveprinsen Ejland, Disko Bugt, west Greenland. Journal of Quaternary Science 14 (4), 323–345.

Long, A.J., Woodroffe, S., Dawson, S., Roberts, D.H., Bryant, C., 2009. Late Holocene relative sea level rise and the Neoglacial history of the Greenland ice sheet. Journal of Quaternary Science 24(4), 345-359.

Lunt, D.J., Foster, G.L., Haywood, A.M., Stone, E.J., 2008. Late Pliocene Greenland glaciation controlled by a decline in atmospheric CO_2 levels. Nature 252, 1102-1105.

Mackintosh, A., White, D., Fink, D., Gore, D.B., Pickard, J., Fanning, P.C., 2007. Exposure ages from mountain dipsticks in Mac. Robertson Land, East Antarctic, indicate little change in ice-sheet thickness since the Last Glacial Maximum. Geology 35(6), 551-554.

Marshall, S.J., James, T.S., Clarke, G.K.C., 2002. North American ice sheet reconstructions at the Last Glacial Maximum. Quaternary Science Reviews 21 (1–3), 175–192.

Martinec, Z., Cadek, O., Fleitout, L., 2001. Can the 1D viscosity profiles inferred from postglacial rebound data be affected by lateral viscosity variations in the tectosphere? Geophysical Research Letters 28(23), 4403-4406.

Maslin, M. A., Li, X. S., Loutre, M.-F., Berger, A., 1998. The contribution of orbital forcing to the progressive intensification of Northern Hemisphere glaciation. Quaternary Science Reviews 17, 411–426.

Meehl, G.A., Stocker, T.F., Collins, W.D., Friedlingstein, P., Gaye, A.T., Gregory, J.M., Kitoh, A., Knutti, R., Murphy, J.M., Noda, A., Raper, S.C.B., Watterson, I.G., Weaver, A.J., Zhao, Z.-C., 2007. Global Climate Projections. In: Solomon, S., Qin, D., Manning, M., Chen, Z., Marquis, M., Averyt, K.B., Tignor, M., Miller, H.L. (Eds.), Climate Change 2007: The Physical Science Basis. Contribution of Working

Group 1 to the Fourth Assessment Report of the Intergovernmental Panel on Climate Change. Cambridge University Press, Cambridge, United Kingdom and New York, NY, USA.

Meier, M.F., Post, A., 1987. Fast tidewater glaciers. Journal of Geophysical Research 92 (B9), 9051–9058.

Mienert, J., Andrews, J.T., Milliman, J.D., 1992. The east Greenland continental margin (65-degrees-N) since the last deglaciation – changes in sea-floor properties and ocean circulation. Marine Geology 106 (3–4), 217–238.

Mikkelsen, N., Kuijpers, A., Arneborg, J., 2008. The Norse in Greenland and late Holocene sea-level change. Polar Record 44 (228), 45–50.

Milne, G.A., Davis, J.L., Mitrovica, J.X., Scherneck, H.G., Johansson, J.M., 2001. Space-geodetic constraints on glacial isostatic adjustment in Fennoscandia. Science 291 (5512), 3281-2385.

Milne, G.A., Long, A.J., Bassett, S.E., 2005. Modelling Holocene relative sea-level observations from the Caribbean and South America. Quaternary Science Reviews 24 (10-11), 1183-1202.

Milne, G.A., Mitrovica, J.X., 1996. Postglacial sea-level change on a rotating Earth: first results from a gravitationally self-consistent sea-level equation. Geophysical Journal International 126 (3), F13–F20.

Milne, G.A., Mitrovica, J.X., 1998. Postglacial Sea-Level Change on a Rotating Earth. Geophysical Journal International 133, 1-19.

Milne, G.A., Mitrovica, J.X., Davis, J.L., 1999. Near-field hydro-isostasy: the implementation of a revised sea-level equation. Geophysical Journal International 139 (2), 464–482.

Mitrovica, J.X., Davis, J.L., Shapiro, I.I., 1994. A spectral formalism for computing three-dimensional deformations due to surface loads 2. Present-day glacial isostatic adjustment. Journal of Geophysical Research 99 (B4), 7075-7101.

Mitrovica, J.X., Forte, A.M., 1997. Radial profile of mantle viscosity: results from the joint inversion of convection and postglacial rebound observables. Journal of Geophysical Research – Solid Earth 102 (B2), 2751–2769.

Mitrovica, J.X., Forte, A.M., 2004. A new inference of mantle viscosity based upon joint inversion of convection and glacial isostatic adjustment data. Earth and Planetary Science Letters 225 (1–2), 177–189.

Mitrovica, J.X., Gomez, N., Clark, P.U., 2009. The sea-level fingerprint of west Antarctic collapse. Science 323 (5915), 753.

Mitrovica, J.X., Milne, G.A., Davis, J.L., 2001a. Glacial Isostatic Adjustment on a Rotating Earth. Geophysical Journal International 147, 562-578.

Mitrovica, J.X., Milne, G.A., 2003. On post-glacial sea level: I. General theory. Geophysical Journal International 154 (2), 253–267.

Mitrovica, J.X., Peltier, W.R., 1991. On postglacial geoid subsidence over the equatorial oceans. Journal of Geophysical Research – Solid Earth 96 (B12), 20053–20071.

Mitrovica, J.X., Peltier, W.R., 1993. The inference of mantle viscosity from an inversion of the Fennoscandian relaxation spectrum. Geophysical Journal International 114 (1), 45–62.

Mitrovica, J.X., Peltier, W.R., 1995. Constraints on mantle viscosity based upon the inversion of postglacial uplift data from the Hudson-Bay Region. Geophysical Journal International 122 (2), 353–377.

Mitrovica, J.X., Tamisiea, M., Davis, J.L., Milne, G.A., 2001b. Recent Mass Balance of Polar Ice Sheets Inferred From Patterns of Global Sea-Level Change. Nature 409, 1026-1029.

Nakada, M., Lambeck, K., 1987. Glacial rebound and relative sea-level variations – a new appraisal. Geophysical Journal of the Royal Astronomical Society 90 (1), 171–224.

Nakada, M., Lambeck, K., 1989. Late Pleistocene and Holocene sea-level change in the Australian region and mantle rheology. Geophysical Journal - Oxford 96(3), 497-517.

Nam, S.I., Stein, R., Grobe, H., Hubberten, H., 1995. Late Quaternary glacial interglacial changes in sediment composition at the east Greenland continental margin and their paleoceanographic implications. Marine Geology 122 (3),243–262.

O'Cofaigh, C., Dowdeswell, J.A., Evans, J., Kenyon, N.H., Taylor, J., Mienert, A., Wilken, M., 2004. Timing and significance of glacially influenced mass-wasting in the submarine channels of the Greenland Basin. Marine Geology 207 (1–4), 39–54.

Paterson, W. S. B., 1994. The Physics of Glaciers. 480 pp. Butterworth-Heinemann, Oxford.

Paterson, W.S.B., Reeh, N., 2001. Thinning of the ice sheet in northwest Greenland over the past forty years. Nature 414, 60-62.

Pattyn, F., 2003. A new three-dimensional higher-order thermomechanical ice sheet model: basic sensitivity, ice stream development and ice flow across subglacial lakes. Journal of Geophysical Research – Solid Earth 108 (B8), 2382.

Paulson, A., Zhong, S.J., Wahr, J., 2005. Modelling post-glacial rebound with lateral viscosity variations. Geophysical Journal International 163(1), 357-371.

Payne, A.J., Vieli, A., Shepherd, A.P., Wingham, D.J., Rignot, E., 2004. Recent dramatic thinning of largest West Antarctic ice stream triggered by oceans. Geophysical Reserach Letters 31(23), L23401.

Peltier,W.R., 1974. The impulse response of a Maxwell Earth. Reviews of Geophysics and Space Physics 12, 649–669.

Peltier, W.R., 1994. Ice-age Paleotopography. Science 265 (5169), 195–201.

Peltier, W.R., 1996. Mantle viscosity and ice-age ice sheet topography. Science 273 (5280), 1359–1364.

Peltier, W.R., 1998. Postglacial variations in the level of the sea: Implications for climate dynamics and solid-earth geophysics. Reviews of Geophysics 36 (4), 603-689.

Peltier, W.R., 2002. Global glacial isostatic adjustment: paleogeodetic and spacegeodetic tests of the ICE-4G (VM2) model. Journal of Quaternary Science 17 (5–6), 491–510.

Peltier, W.R., 2004. Global glacial isostasy and the surface of the ice-age earth: the ICE-5G (VM2) model and grace. Annual Review of Earth and Planetary Sciences 32, 111–149.

Peltier, W.R., 2005. On the hemispheric origins of meltwater pulse 1a. Quaternary Science Reviews 24, 1655–1671.

Peltier, W.R., Jiang, X.H., 1996. Mantle viscosity from the simultaneous inversion of multiple data sets pertaining to postglacial rebound. Geophysical Research Letters 23 (5), 503–506.

Pelto, M.S., Warren, C.R., 1991. Relationship between tidewater glacier calving velocity and water depth at the calving front. Annals of Glaciology 15, 115-118.

Petit, J.R., Jouzel, J., Raynaud, D., Barkov, N.I., Barnola, J.M., Basile, I., Bender, M., Chappellaz, J., Davis, J., Delaygue, G., Delmotte, M., Kotlyakov, V.M., Legrand, M., Lipenkov, V., Lorius, C., Pépin, L., Ritz, C., Saltzman, E., Stievenard, M., 1999. Climate and Atmospheric History of the Past 420,000 years from the Vostok Ice Core, Antarctica. Nature 399(6735), 429-436.

Pfeffer, W.T., Harper, J.T., O'Neel, S., 2009. Kinematic Constraints on Glacier Contributions to 21st-Century Sea-Level Rise. Science 321, 1340-1343.

Price, S.F., Conway, H., Waddington, E.D., 2007. Evidence for late Pleistocene thinning of Siple Dome, West Antarctica. Journal of Geophysical Research 112, F03021.

Ramillien, G., Lombard, A., Cazenave, A., Ivins, E.R., Llubes, M., Remy, F., Biancale, R., 2006. Interannual variations of the mass balance of the Antarctica and Greenland ice sheets from GRACE. Global and Planetary Change 53, 198–208.

Rasch, M., 2000. Holocene relative sea level changes in Disko Bugt, west Greenland. Journal of Coastal Research 16 (2), 306–315.

Rasch, M., Jensen, J.F., 1997. Ancient Eskimo dwelling sites and Holocene relative sea level changes in southern Disko Bugt, central west Greenland. Polar Research 16 (2), 101–115.

Reimer, P.J., Baillie, M.G.L., Bard, E., Bayliss, A., Beck, J.W., Bertrand, C.J.H., Blackwell, P.G., Buck, C.E., Burr, G.S., Cutler, K.B., Damon, P.E., Edwards, R.L., Fairbanks, R.G., Friedrich, M., Guilderson, T.P., Hogg, A.G., Hughen, K.A., Kromer, B., McCormac, G., Manning, S., Ramsey, C.B., Reimer, R.W., Remmele, S., Southon, J.R., Stuiver, M., Talamo, S., Taylor, F.W., van der Plicht, J., Weyhenmeyer, C.E., 2004. IntCal04 terrestrial radiocarbon age calibration, 0–26 cal kyr BP. Radiocarbon 46 (3), 1029–1058.

Ridley, J.K., Huybrechts, P., Gregory, J.M., Lowe, J.A., 2005. Elimination of the Greenland ice sheet in a high CO2 climate. Journal of Climate 17, 3409-3427.

Rignot, E., Kanagaratnam, P., 2006. Changes in the velocity structure of the Greenland Ice Sheet. Science, 311, 986–990.

Rignot, E., Box, J.E., Burgess, E., Hanna, E., 2008. Mass balance of the Greenland ice sheet from 1958 to 2007. Geophysical Research Letters 35, L20502.

Rinterknecht, V., Gorokhovich, Y., Schaefer, J., Caffee, M., 2008. Preliminary ^{10}Be chronology for the last deglaciation of the western margin of the Greenland Ice Sheet. Journal Quaternary Science 24 (3), 270-278.

Ritz, C., Fabre, A., Letréguilly, A., 1997. Sensitivity of a Greenland ice sheet model to ice flow and ablation parameters: consequences for the evolution through the last climatic cycle. Climate Dynamics 13, 11–24.

Roberts, D.H., Long, A.J., Schnabel, C., Davies, B.J., Xu, S., Simpson, M.J.R., Huybrechts, P., 2009. Ice sheet extent and early deglacial history of the southwestern sector of the Greenland Ice Sheet. Quaternary Science Reviews, doi:10.1016/j.quascirev.2009.07.002.

Roberts, D.H., Long, A.J., Schnabel, C., Freeman, S., Simpson, M.J.R., 2008. The deglacial history of southeast sector of the Greenland ice sheet during the Last Glacial Maximum. Quaternary Science Reviews 27 (15–16), 1505–1516.

Sabadini, R., Yuen, D.A., Portney, M., 1986. The effects of upper mantle lateral heterogeneities on postglacial rebound. Geophysical Research Letters 13 (4), 337–340.

Saito, F., Abe-Ouchi, A., Blatter, H., 2003. Effects of first-order stress gradients in an ice sheet evaluated by a three-dimensional thermomechanical coupled model. Annals of Glaciology 37, 166–172.

Schoof, C., 2007. Ice sheet grounding line dynamics: steady states, stability, and hysteresis. Journal of Geophysical Research – Earth Surface 112, F3.

Sella, G.F., Stein, S., Dixon, T.H., Craymer, M., James, T.S., Mazzotti, S., Dokka, R.K., 2007. Observation of glacial isostatic adjustment in ‘‘stable’’ North America with GPS. Geophysical Research Letters 34(2), L02306.

Shennan, I., 1986. Flandrian sea-level changes in the Fenland. II: tendencies of sea level movement, altitudinal changes, and local and regional factors. Journal of Quaternary Science 1 (2), 155–179.

Sigert, M.J., Dowdeswell, J.A., 1995. Numerical Modelling of the Late Weichselian Svalbard-Barents Sea Ice Sheet. Quaternary Research 43, 1-13.

Siegert, M.J., Dowdeswell, J.A., Hald, M., Svendsen, J.I., 2001. Modelling the Eurasian Ice Sheet through a full (Weichselian) glacial cycle. Global and Planetary Change, 31, 367-385.

Siegert, M.J., Dowdeswell, J.A., Melles, M., 1999. Late Weichselian glaciation of the Eurasian High Arctic. Quaternary Research 52, 273-285.

Sigmundsson, F., 1991. Post-glacial rebound and asthenosphere viscosity in Iceland. Geophysical Research Letters 18 (6), 1131–1134.

Simpson, M.J.R, Milne, G.A., Huybrechts, P., Long, A.J., 2009. Calibrating a glaciological model of the Greenland ice sheet from the last glacial maximum to present-day using field observations of relative sea level and ice extent. Quaternary Science Reviews 28 (17-18), 1631-1657.

Smith, L.M., Licht, K.J., 2000. Radiocarbon Date List IX: Antarctica, Arctic Ocean, and the Northern North Atlantic. Institute of Arctic and Alpine Research, Occasional Paper, 54, pp. 138.

Solheim, A., Faleide, J.I., Andersen, E.S., Elverhoi, A., Forsberg, C.F., Vanneste, K., Uenzelmann-Neben, G., Channell, J.E.T., 1998. Late Cenozoic seismic stratigraphy and glacial geological development of the east Greenland and Svalbard Barents Sea continental margins. Quaternary Science Reviews 17 (1–3), 155–184.

Sparrenbom, C.J., 2006. Constraining the Southern Part of the Greenland Ice Sheet since the Last Glacial Maximum from Relative Sea-Level Changes, Cosmogenic Dates and Glacial-Isostatic Adjustment Models. Ph.D. thesis. Centre for Geo-Biosphere Science, Lund University.

Sparrenbom, C.J., Bennike, O., Björck, S., Lambeck, K., 2006a. Relative sea-level changes since 15 000 cal. yr BP in the Nanortalik area, southern Greenland. Journal of Quaternary Science 21 (1), 29–48.

Sparrenbom, C.J., Bennike, O., Bjorck, S., Lambeck, K., 2006b. Holocene relative sea level changes in the Qaqortoq area, southern Greenland. Boreas 35 (2), 171–187.

Stearns, L. A., Hamilton, G.S., 2007. Rapid volume loss from East Greenland outlet glaciers quantified using repeat stereo satellite imagery. Geophysical Research Letters 34 (5), L05503.

Steffen, H., Kaufmann, G., Wu, P., 2006. Three-dimensional finite-element modelling of the glacial isostatic adjustment in Fennoscandia. Earth and Planetary Science Letters 250 (1-2), 358-375.

Stirling, C.H., Esat, T.M., Lambeck, K., McCulloch, M.T., 1998. Timing and duration of the last Interglacial: evidence for a restricted interval of widespread coral reef growth. Earth and Planetary Science Letters 160, 745–762.

Storey, M., Pedersen, A.K., Stecher, O., Bernstein, S., Larsen, H.C., Larsen, L.M., Baker, J.A., Duncan, R.A., 2004. Long-lived postbreakup magmatism along the east Greenland margin: evidence for shallow-mantle metasomatism by the Iceland plume. Geology 32 (2), 173–176.

Stuiver, M., Grootes, P.M., 2000. GISP2 oxygen isotope ratios. Quaternary Research 53(3), 277-283.

Stuiver, M., Reimer, P.J., 1993. Extended C-14 revised calib 3.0 C-14 age calibration program. Radiocarbon 35 (1), 215–230.

Tamisiea, M.E., Mitrovica, J.X., Davis, J.L., 2007. GRACE gravity data constrain ancient ice geometries and continental dynamics over Laurentia. Science 316 (5826), 881-883.

Tarasov, L., Peltier, W.R., 1997. Terminating the 100 kyr ice age cycle. Journal of Geophysical Research – Atmospheres 102 (D18), 21665-21693.

Tarasov, L., Peltier, W.R., 2002. Greenland glacial history and local geodynamic consequences. Geophysical Journal International 150 (1), 198–229.

Tarasov, L., Peltier, W.R., 2003. Greenland glacial history, borehole constraints, and Eemian extent. Journal of Geophysical Research 108(B3), 2143.

Tarasov, L., Peltier, W.R., 2004. A geophysically constrained large ensemble analysis of the deglacial history of the North American ice-sheet complex. Quaternary Science Reviews 23 (3–4), 359–388.

Tarasov, L., Peltier, W.R., 2006. A calibrated deglacial drainage chronology for the North American continent: evidence of an Arctic trigger for the Younger Dryas. Quaternary Science Review 25, 659–688.

Ten Brink, N.W., Weidick, A., 1974. Greenland ice sheet history since the last glaciation. Quaternary Research 4, 429–440.

Thomas, R., Akins, T., Csatho, B., Fahnestock, M., Gogineni, P., Kim, C., Sonntag, J., 2000. Mass balance of the Greenland ice sheet at high elevations. Science 289 (5478), 426-428.

Thomas, R., Davis, C., Fredrick, E., Krabill, W., Li, Y.H., Manizade, S., Martin, C., 2008. A comparison of Greenland ice-sheet volume changes derived from altimetry measurements. Journal of Glaciology 54 (185), 203-212.

Thomas, R., Frederick, E., Krabill, W., Manizade, S., Martin, C., 2006. Progressive increase in ice loss from Greenland. Geophysical Research Letters 33 (10), L10503.

Trautman, M.A., Willis, E.H., 1963. Isotopes, Inc., radiocarbon measurements III. Radiocarbon 5, 62–79.

Tushingham, A.M., Peltier, W.R., 1991. ICE-3G – a new global-model of late Pleistocene deglaciation based upon geophysical predictions of postglacial relative sea-level change. Journal of Geophysical Research – Solid Earth and Planets 96 (B3), 4497–4523.

Van de Wal, R.S.W., 1999. The importance of thermodynamics formodeling the volume of the Greenland ice sheet. Journal of Geophysical Research 104, 3887–3898.

Van de Wal, R.S.W., Wild, M., de Wolde, J., 2001. Short-term volume change of the Greenland ice sheet in response to doubled CO2 conditions. Tellus, 53B, 94–102.

Van den Berg, J., van de Wal, R.S.W., Milne, G.A., Oerlemans, J., 2008. Effect of isostasy on dynamical ice sheet modelling: A case study for Eurasia. Journal of Geophysical Research 113 (B5), B05412.

Van den Berg, J., van de Wal, R.S.W., Oerlemans, J., 2006. Effects of spatial discretization in ice-sheet modelling using the shallow-ice approximation. Journal of Glaciology 52, 89–98.

Van der Veen, C.J., 1996. Tidewater calving. Journal of Glaciology 42, 375–385.

Van der Veen, C.J., 2002. Calving glaciers. Progress in Physical Geography 26, 96–122.

Van Tatenhove, F.G.M., van der Meer, J.J.M., Huybrechts, P., 1995. Glacial–geological geomorphological research in west Greenland used to test an ice-sheet. Quaternary Research 44 (3), 317–327.

Van Tatenhove, F.G.M., van der Meer, J.J.M., Koster, E.A., 1996. Implications for deglaciation chronology from new AMS age determinations in central west Greenland. Quaternary Research 45 (3), 245–253.

Velicogna, I., Wahr, J., 2005. Greenland mass balance from GRACE. Geophysical Research Letters 32, L18505.

Vieli, A., Funk, M., Blatter, H., 2001. Flow dynamics of tidewater glaciers: a numerical modelling approach. Journal of Glaciology 47 (159), 595–606.

Vieli, A., Payne, A.J., 2005. Assessing the ability of numerical ice sheet models to simulate grounding line migration. Journal of Geophysical Research – Earth Surface 110, F1.

Wahr, J., van Dam, T., Larson, K., Francis, O., 2001a. Geodetic measurements in Greenland and their implications. Journal of Geophysical Research – Solid Earth 106 (B8), 16567-16581.

Wahr, J., van Dam, T., Larson, K., Francis, O., 2001b. GPS measurements of vertical crustal motion in Greenland. Journal of Geophysical Research – Atmospheres 106 (D24), 33755-33759.

Wake, L.M., Huybrechts, P., Box, J.E., Hanna, E., Janssens, I., Milne, G.A., 2009. Surface mass-balance changes of the Greenland ice sheet since 1866. Annals of Glaciology 50, 178-184.

Warren, C.R., Benn, D.I., Winchester, V., Harrison, S., 2001. Buoyancy-driven lacustrine calving, Glaciar Nef, Chilean Patagonia. Journal of Glaciology 47, 135–146.

Washburn, A.L., Stuiver, M., 1962. Radiocarbon-dated post-glacial deleveling in northeast Greenland and its implications. Arctic 15, 66–73.

Weaver, A.J., Saenko, O.A., Clark, P.U., Mitrovica, J.X., 2003. Meltwater pulse 1a from Antarctica as a trigger of the Bølling-Allerød warm interval. Science 299, 1709–1713.

Weidick, A., 1972. Holocene shore-lines and glacial stages in Greenland – an attempt at correlation. Rapport Grønlands Geologiske Undersøgelse 41, 1–39.

Weidick, A., 1976. Glaciation and the Quaternary of Greenland. In: Escher, A., Watt, W.S. (Eds.), Geology of Greenland. Geological Survey of Greenland, Copenhagen, pp. 405–458.

Weidick, A., Oerter, H., Reeh, N., Thomsen, H.H., Thorning, L.S., 1990. The recession of the Inland Ice margin during the Holocene climatic optimum in the Jakobshavn Isfjord area of West Greenland. Palaeogeography, Palaeoclimatology, Palaeoecology 82, 389–399.

Weidick, A., 1993. Neoglacial change of ice cover and the related response of the Earth's crust in west Greenland. Rapport Grønlands Geologiske Undersøgelse 159, 121–126.

Weidick, A., Bennike, O., 2007. Quaternary glaciation history and glaciology of Jakobshavn Isbrae and the Disko Bugt region, west Greenland: a review. Geological Survey of Denmark and Greenland Bulletin 14.

Weidick, A., Kelly, M., Bennike, O., 2004. Late Quaternary development of the southern sector of the Greenland ice sheet, with particular reference to the Qassimiut lobe. Boreas 33 (4), 284–299.

Wilken, M., Mienert, J., 2006. Submarine glacigenic debris flows, deep-sea channels and past ice-stream behaviour of the east Greenland continental margin. Quaternary Science Reviews 25 (7–8), 784–810.

Woodroffe, S., Long, A.J., 2009. Salt marshes as archives of recent relative sea level change in West Greenland. Quaternary Science Reviews 28 (17-18), 1750-1761.

Wouters, B., Chambers, D., Schrama, E.J.O., 2008. GRACE observes small-scale mass loss in Greenland. Geophysical Research Letters 35, L034816.

Yokoyama, Y., Lambeck, K., De Dekker, P., Johnston, P., Fifield, L.K., 2000. Timing of the Last Glacial Maximum from observed sea-level minima. Nature 406 (6797), 713–716.

Zreda, M., England, J., Phillips, F., Elmore, D., Sharma, P., 1999. Unblocking of the Nares Strait by Greenland and Ellesmere ice-sheet retreat 10,000 years ago. Nature 398 (6723), 139–142.

Zwally, H.J., Abdalati, W., Herring, T., Larson, K., Saba, J., Steffen, K., 2002. Surface melt-induced acceleration of Greenland Ice-Sheet Flow. Science 297(5579), 218–222.

Zwally, H.J., Giovinetto, M.B., Li, J., Cornejo, H.G., Beckley, M.A., Brenner, A.C., Saba, J.L., Yi, D., 2005. Mass changes of the Greenland and Antarctic ice sheets and shelves and contributions to sea level rise: 1992-2002. Journal of Glaciology 51, 509–527.

Zweck, C., 1998. Glacial isostasy and the crustal structure of Antarctica. Annals of Glaciology 27, 321-326.

Zweck, C., Huybrechts, P., 2003. Modeling the marine extent of northern Hemisphere ice sheets during the last glacial cycle. Annals of Glaciology 37, 173–180.

Zweck, C., Huybrechts, P., 2005. Northern hemisphere ice sheet modeling of the last glacial cycle and glaciological sensitivity. Journal of Geophysical Research 110, D07103.